Extremum Seeking Maximum Power Point Tracking for a Stand-Alone and a Grid-Connected Photovoltaic Systems

By

Ali Abdalla Abushaiba

PhD, the University of Kansas, 2018

MS, Southern Illinois University, 2011

Submitted to the graduate degree program in the Department of Electrical Engineering and Computer Science and the Graduate Faculty of the University of Kansas in partial fulfillment of the requirements for the degree of Doctor of Philosophy.

_____

Chair: Dr. Ahmadi, Reza

_____

Dr. Prescott, Glenn

_____

Dr. Salandrino, Alessandro

_____

Dr. Demarest, Kenneth

_____

Dr. Dhar, Prajna*

Date Defended: April, 26, 2018

The dissertation committee for Ali Abdalla Abushaiba certifies that this is the approved version of the following dissertation:

Extremum Seeking Maximum Power Point Tracking for a Stand-Alone and a Grid-Connected Photovoltaic Systems

_____

Chair: Dr. Ahmadi, Reza

_____

Date Approved: May, 7, 2018

Abstract

Energy harvesting from solar sources in an attempt to increase efficiency has sparked interest in many communities to develop more energy harvesting applications for renewable energy topics. Advanced technical methods are required to ensure the maximum available power is harnessed from the photovoltaic (PV) system. This dissertation proposed a new discrete-in-time extremum-seeking (ES) based technique for tracking the maximum power point of a photovoltaic array. The proposed method is a true maximum power point tracker that can be implemented with reasonable processing effort on an expensive digital controller. The dissertation presented a stability analysis of the proposed method to guarantee the convergence of the algorithm.

Two-types of PV systems were designed and comprehensive framework of control design was considered for a stand-alone and a three-phase grid connected system.
Grid-tied systems commonly have a two-stage power electronics interface, which is necessary due to the inherent limitation of the DC-AC (Inverter) power converging stage. However, a one stage converter topology, denoted as Quasi-Z-source inverter (q-ZSI), was selected to interface the PV panel which overcomes the inverter limitations to harvest the maximum available power.

A powerful control scheme called Model Predictive Control with Finite Set (MPC-FS) was designed to control the grid connected system. The predictive control was selected to achieve a robust controller with superior dynamic response in conjunction with the extremum-seeking algorithm to enhance the system behavior.

The proposed method exhibited a better performance in comparison to conventional Maximum Power Point Tracking (MPPT) methods and required less computational effort than the complex mathematical methods.

Dedication

To

My parents; My wife; My children

Acknowledgements

I would like to thank my academic advisor, Dr Reza Ahmadi, for his great help and guidance and his continuous support. I would like also to thank my advisory committee members for their suggestions and comments throughout my pursuit of this degree.

Thanks also go to my friends and colleagues and the department faculty and staff for making my time at Southern Illinois University (SIU) and University of Kansas (KU) a great experience. Finally, thanks to my Mother, father, wife and children for their encouragement

Table of Contents

List of Figures

Chapter 1

1 Introduction

The growth and development in the area of alternative energy resources has been recently driven by numerous economic, environmental, and political issues. Distress caused by the economic and political complications of fossil fuel depletion, growing environmental concerns such as global warming, and the huge current increase of power demand are the vital stimuli for efforts toward harnessing renewable, inexpensive, abundant, and green energy resources. Two of the well-known alternative energy sources that almost perfectly fit the description are the solar and wind energy. Wind and solar energies are abundant; harvesting them has limited effect on the environment, and they are inherently renewable. However, currently the electrical energy from a Photovoltaic (PV) cell or a wind tower is not exactly inexpensive. The high cost of electrical energy from these sources is due to the high initial capital cost of the current energy harvesting systems. To pay off the high initial cost of the infrastructure, it is imperative that a solar or wind generation system always operates efficiently. This matter is predominantly important for PV systems due to the fact that besides the effects of solar irradiation and temperature on the generated power, the PV panel characteristic itself is nonlinear with a unique operating point where PV power is maximized. This makes the extraction of maximum power from a PV cell a hard task.

Aside from the unsafe contamination associated with conventional energy resources, fossil fuels reserves are diminishing rapidly, which leads to the continuous rise in their price. The renewable energy resources are on the other hand, permanent and free. In the past few years, renewable energy has taken on the way of replacing conventional fossil fuel energy production. Figure 1 shows the renewable energy share of global energy production in year 2017.

1.1 Renewable energy resources

1.1.1 Solar power

There are two key methods to harness the power from the sun, the first method is to collect the terminal solar energy with mirrors and focus it on pipes to interchange the heat of the sun with a certain fluid to drive traditional steam turbines or engines that generate electricity [2]. As shown in Figure 2.

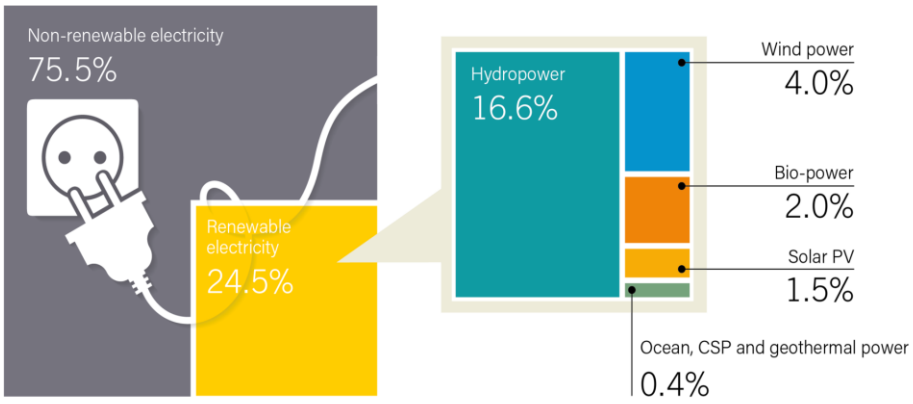

Figure 1. Estimated renewable global energy share of total final consumption [1].

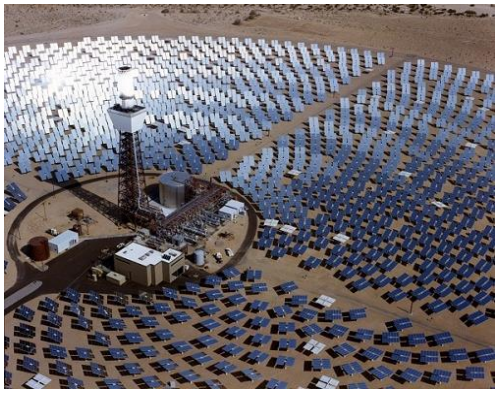

Figure 2.Concentrating Solar Power (Photo courtesy of Sandia National Laboratories)[2, 3].

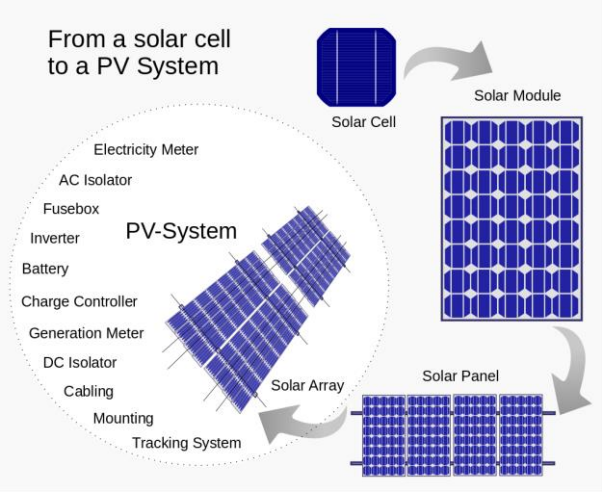

Figure 3. From Solar cell to PV system[4].

The second method is to generate electricity directly from sun light using static photovoltaic cells [4] as shown in Figure 3 [4].

1.1.2 Wind power

Wind turbines are used to extract the energy available in airflows, as illustrated in figure 4 [3]. Wind energy is one of the effective renewable forms of energy today to generate electricity, and it is an encouraging area of application for variable-speed generators functional on the constant grid frequency. The output power of a wind turbine rises with the increase of the wind speed; as a result, wind turbines are mounted in higher altitudes, particularly in places known for higher wind speeds [5]. There are different types of wind turbines for instant fixed speed, and variable speed wind turbine

Figure 4. Wind turbines near Lamar, Colorado[3].

[6].

1.1.3 Hydro power

Hydropower is using water stored in dams or falling water, to power electrical generators or turbines. There are different types of hydropower plants or facilities; however, they are driven by the flowing water's energy. The most common one is an impounded facility which uses a dam to store the water

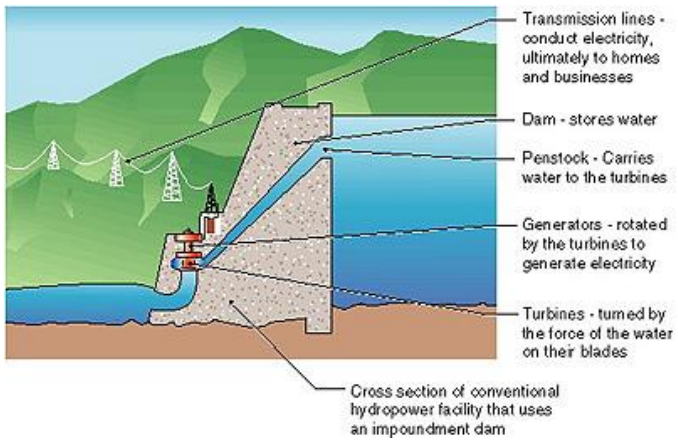

Figure 5. Hydroelectric power plant is an impoundment facility[7].

in a reservoir. Then the water can be released for meeting electricity demand or maintaining reservoir level which flows through the turbine that spins a generator to generate electricity [7]. Figure 5 illustrates an impounded hydro plant.

1.1.4 Introduction to Photovoltaic Energy Conversion

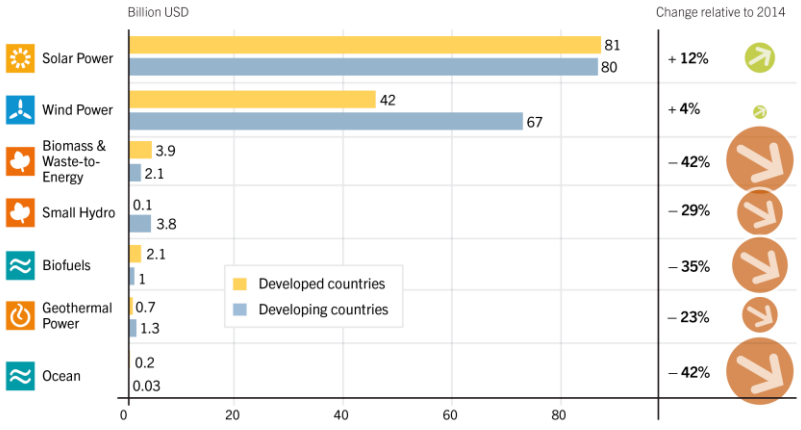

Figure 6. Global new investments in renewable energy in developed and developing countries [1].

According to the Renewable global status report, the recent three years were extraordinary for renewable energy. The cost of renewable sources is competitive with fossil fuels in many markets as mainstream sources of energy. However, wind and hydropower are limited to specific geographic locations and conditions. On the other hand, solar power took the leading sector in terms of new investments during the last two years, accounting for more than 56% of total new investments in the renewables sources and fuels. Figure 6 shows the global new investments in renewable energy.

1.1.5 Advantages of photovoltaic systems

Photovoltaic systems have many advantages and few disadvantages as any systems do:

1- PV cells convert sunlight directly into electricity.

2- A PV module has no moving mechanical parts so it's a low maintenance energy source.

3- PV systems are pollution free not causing carbon emissions.

4- PV systems can stand rugged weather and environment condition.

5- PV systems are manufactured in a wide range of sizes and power ratings making them suitable for many different applications.

6- PV systems can be cost effective energy sources for remote places.

Photovoltaic systems disadvantages are:

1- PV electricity is expensive due to initial Capital cost.

2- PV systems generate electricity during the daylight only.

3- PV systems are low efficiency resource (maximum power point problem).

4- PV systems require some cleaning on occasion.

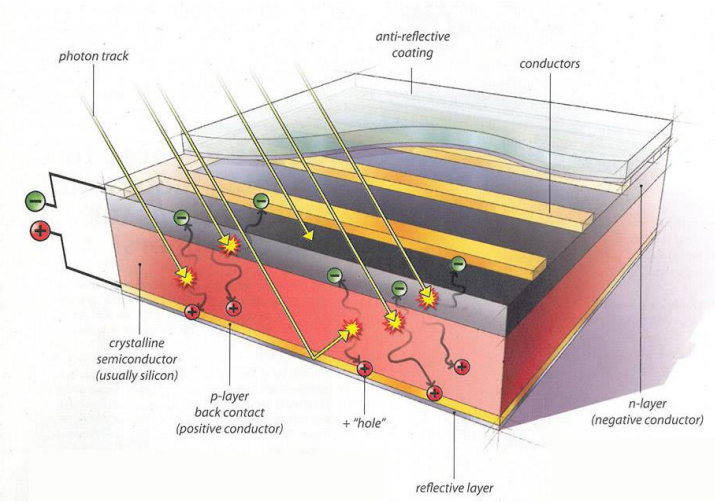

Figure 7. Diagram of a typical crystalline silicon solar cell [7].

1.1.6 PV cell description.

PV which stand for Photovoltaics is the most straight way to transform solar radiation into electrical energy, and it's built on the photovoltaic impact, that was determined first by Henri Becquerel in 1839 [8]. It's pretty much described as the development of a voltage between two electrodes connected to a solid or liquid. Basically, all solar devices include a p-n junction in a semiconductor that develop the photovoltage. These are recognized also as photovoltaic cells. Light absorption happens in a semiconductor material. The semiconductor material has to be able to soak up a large section of the photovoltaic spectrum. Depending on the material property, the absorbed light in a neighborhood is more or less adjacent to the surface. This is a result of a flow of electrons and holes. Even for a weak absorption, silicon semiconductor, the most carriers are produced near the surface. This leads to the typical solar cell structure in Figure 7 [2].

The p-n junction between the transmitter and the base layer is very close to the surface to have a high probability of photo generation Chargers. The thin layer of the emitter on the tie has a relatively high resistance, that requires a well-designed contact grid [8].

For a practical use, solar cells are packaged in contained modules in which a number of crystalline cells are connected in series or in a thin layer of film material also internally connected in series. The module serves two objectives: protecting solar cells from the environment and offering a greater voltage than a single cell, which only develops a voltage less than 1 volt. The conversion efficiencies of current production cells are in the range of 13-16%, but the efficiency of the module is a bit lower. The best crystalline silicon efficiency obtained so far is 24.7%, which is the theoretical limit for this kind of solar cells.

1.2 Power Electronics integration in PV systems

The power electronic interfaces are used to convert DC into AC in order to feed AC loads or to control the photovoltaic module terminal to track the MPP to maximize the extracted power as explained in this work. They also offer extensive operation range, ability to operate under different daily and regular environmental conditions, and ability to reach the highest potential productivity. There are many ways to classify power electronics Interfaces for solar systems. In this section, power electronic interfaces are classified for stand-alone photovoltaic systems and grid-connected photovoltaic systems [9].

1.2.1 Power Electronics Interfaces for Stand-Alone PV Systems

A Stand-Alone photovoltaic system is the simplest type with one power stage directly interfacing the PV module to the DC load or a battery. There are several types of Stand-Alone PV systems, Figure 8 shows the most common types. For more information about these systems refer

to [9]. In the illustrated system, the PV module and storage device are provided with their separate DC/DC converters. A DC/AC conversion stage is employed to offer power for local AC loads. The converter of the PV panel can only be a unidirectional power converter, whereas the battery pack converter can be a bidirectional converter to charge/discharge the battery [9].

1.2.2 Power Electronics Interfaces for Grid-Connected PV Systems

The electronic power interfaces for photovoltaic systems connected to the grid can be categorized

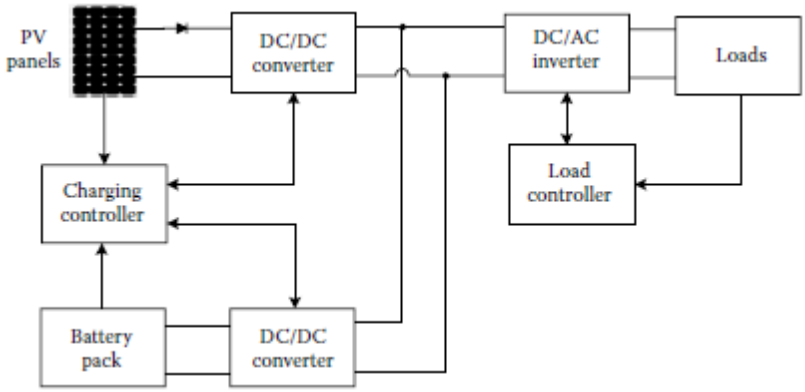

Figure 8. PV/ battery connection type 4 [9].

two ways either based on the usage of the inverter or based on the number of stages of the system and the configurations of the PV modules. Based on the usage of the inverter, the categories are,

- Centralized inverter
- String inverter
- Multistring inverter.

Based on the number of the converter stages and topologies, the categories are

- Two-stage single module

- Two stage multimodule
- Single-stage multimodule
- Single-stage multilevel.

In Figure 9 a string inverter topology is shown, in which a single string of the modules is connected to an individual inverter for the entire system.

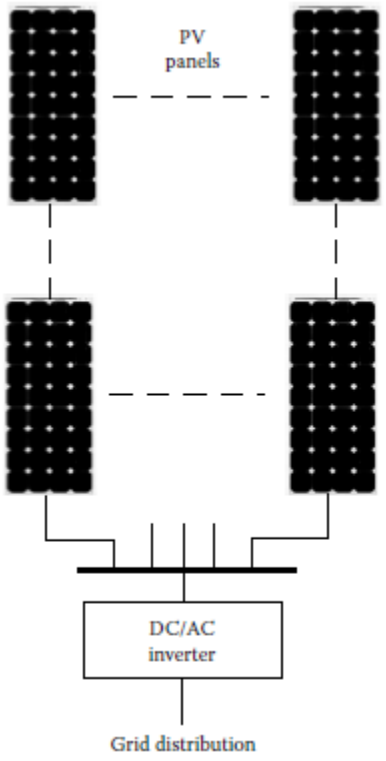

Figure 9. Conventional PV system using centralized inverter system topology [9].

1.3 Dissertation Objective [1]

Maximum Power Point Tracking (MPPT) techniques are described as real-time optimization algorithms that can identify the Maximum Power Point (MPP) of a PV panel. These techniques are used to maximize the PV power generation in various temperature and irradiance conditions [10]. Currently, it's conventional to have a power electronic converter transfer the electrical energy from the PV panel to a load, energy storage element, or the power grid [11]. The MPPT algorithm can be implemented as a high-level supervisory controller for this power electronic converter. The MPPT algorithm attempts to continuously direct the operating point of the power electronic converter to the MPP of the PV panel.

The major challenge in tracking the MPP of a PV panel is posed by the panel's nonlinear and variable current-voltage (I-V) characteristics [12]. The I-V characteristic of a PV panel is not only nonlinear but also a function of the inherent and ambient changes
such as temperature or irradiance variations.

1.3.1 Problem Statement

The difficulty of tracking the MPP of a PV array occurs because of the nonlinear and variable current-voltage (I-V) characteristics of PV cells. Figure 10 depicts the I-V characteristic curves of a typical PV panel (BP365) for different temperature and insolation levels [13]. According to this

[1] Part of this section is reprinted with permission from A. A. Abushaiba, S. M. M. Eshtaiwi, and R. Ahmadi, "Comparative analysis of dynamic performance of four prominent Maximum Power Point Tracking algorithms in photovoltaic systems using realistic experimental implementation," in 2016 IEEE International Conference on Electro Information Technology (EIT), 2016, pp. 0576-0579.

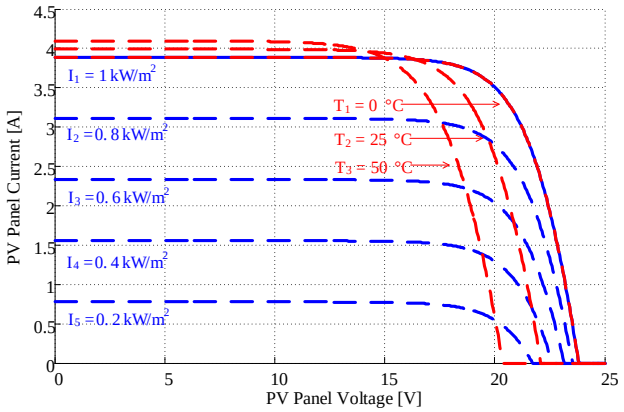

Figure 10 The I-V characteristic curves of BP 365 for different irradiance levels (I1 to I5) and temperatures (T1 to T3).

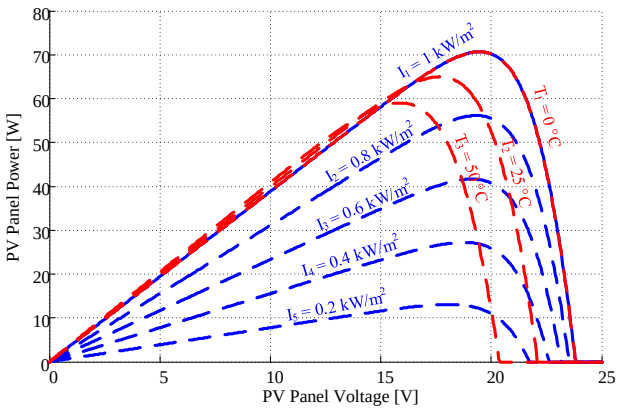

Figure 11. The P-V characteristic curves of BP 365 for different irradiance levels (I1 to I5) and temperatures (T1 to T3).

figure, the I-V characteristics of a typical PV array are not linear, and are also highly dependent on the panel temperature and local irradiation.

The power and voltage (P-V) characteristic curves of a BP 365 for different insolation levels and temperatures are plotted in Figure 11. As shown in this figure, for any given irradiation level and temperature, the maximum power can be drawn from the PV panel at a certain voltage (MPP voltage). However, due to issues such as uncertainties in the PV panel modeling, aging effects, and parameter nonlinearity, it's generally impractical to formulate and predict the MPP of a PV panel under different temperature and insolation conditions. As a result, the MPP voltage should be adaptively identified, and continuously tracked in real-time. The PV panels are typically interfaced to the main DC/AC bus via a power electronic converter. The power converter can be controlled to regulate the PV voltage to the desired MPP.

The MPP voltage can be tracked either directly by the controller algorithm through controlling the duty cycle of the active switches of the converter, or indirectly by generating reference voltage

set points by an outer MPP tracker loop and regulating the PV voltage to the generated reference points by an inner controller loop.

Problem Statement

The amount of power generated by the PV panel is a function of many parameters, most notably the local insolation, the panel temperature, and the panel voltage. The power-voltage (P-V) characteristic of a BP365 solar panel for different insolation levels and temperatures is illustrated in Figure 11. Typically, the power converter is responsible for regulating the panel voltage (equivalent to its input terminal voltage) to the appropriate value to achieve the maximum power output through use of an MPPT algorithm. The dynamic behavior of the converter depends on both the converter topology and the converter's operating point dictated by the I-V characteristic curve of the solar panel. The two-types of PV systems, a stand-alone system and a three-phase grid connected system that are studied in this work are illustrated in Figure 12 and Figure 13 respectfully.

In this matter, chapter 2 presents in great detail both systems regarding the power electronic stage design.

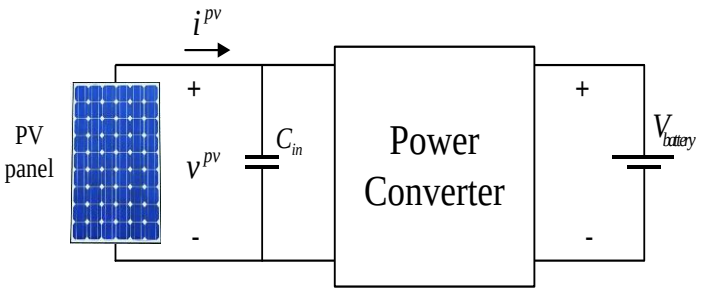

Figure 12. A typical PV energy system based on a power converter.

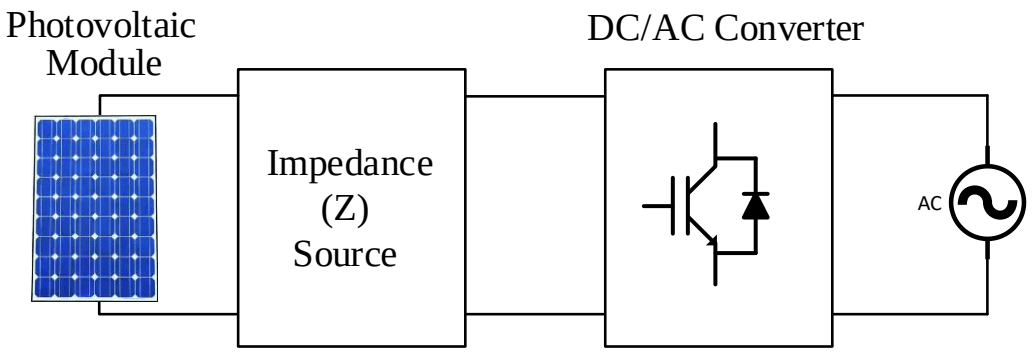

Figure 13. A three-phase grid connected PV system.

1.4 Dissertation Overview

As stated in section 1.3 the dissertation address two main criteria which are design and control of PV system for a stand-alone system as well as for a grid-connected system for the proposed MPPT algorithm. The remainder of the dissertation is organized as follows.

In section 2, the photovoltaic systems that are a subject of study in this dissertation are introduced. Three DC/DC converters are studied and a dynamic performance analysis is conducted to propose a selection of one power converter to interface the PV module to battery for a stand-alone system. This dissertation also presents a comprehensive frame work based on the latest literature reviews for three phase grid-tie PV systems, for selecting, designing and control of a power converter to interface the PV modules to the power grid. A new novel power converter topology called the impedance source converter is selected for the mentioned PV system.

In section 3, controller design for power converters that were introduced in section 2 is carried out. A classical linear control is designed for the stand-alone system. A state of the art model

predictive controller for power electronics converter application for the grid-tied PV system is presented as well.

In section 4, a new MPPT algorithm based on discreet in time extremum seeking is proposed which is highly effective in steady state and provides fast dynamic response to change in environmental conditions. A comparison of the proposed MPPT with conventional well known MPPT algorithms is presented to validate the effectiveness of the proposed method. Both experimental and simulation results using a powerful computer based simulation tool named PLECS are conducted and presented.

In section 5, a conclusion and discussion of future work is presented.

Chapter 2

2 PV Systems

2.1 PV system for a stand-alone system[2]

The first objective of this section is to select a power converter to interface with the PV system for a stand-alone system. It compares the dynamic performance of a PV charger system designed using three different power electronic converters and to study the dynamic performance of three power electronic converters suitable for a PV charger system.

2.2 Motivation

Real time identification of the Maximum Power Point (MPP) of a PV panel and forcing the panel to operate near this point is called Maximum Power Point Tracking (MPPT). Typically the MPPT algorithm is a high level controller implemented on a power electronic converter. To function properly the MPPT algorithm requires the internal voltage or current controller loops of the converter to regulate a voltage or current value to some desired value generated by the algorithm. As a result, it is fundamental to the operation of the MPPT controller that the converter's transient response to the generated MPPT commands be fast and well damped. The transient behavior of power converters has been subject to extensive research and study in the literature over the years [14-16]. However study of the transient behavior of power converters in Photovoltaic (PV) energy systems is a relatively new concept [17]. The major challenge in

[2] Part of this section is reprinted with permission from A. A. Abushaiba, S. M. M. Eshtaiwi, and R. Ahmadi, "Comparative analysis of dynamic performance of four prominent Maximum Power Point Tracking algorithms in photovoltaic systems using realistic experimental implementation," in 2016 IEEE International Conference on Electro Information Technology (EIT), 2016, pp. 0576-0579. A. A. Abushaiba, S. M. M. Eshtaiwi, and R. Ahmadi, "Dynamic performance analysis of a PV charger system," in IECON 2014 - 40th Annual Conference of the IEEE Industrial Electronics Society, 2014, pp. 2069-2074.

dynamic performance analysis of PV energy systems is posed by the current-voltage (I-V) characteristic of the solar panels being both nonlinear and a function of ambient changes

2.3 Dynamic Performance Analysis of a stand-alone PV Charger System

The three converters under study shown in Figure 14 are the Single-Ended Primary-Inductor (SEPIC), Positive Buck-Boost, and Flyback. These converters are chosen for this study because of their flexible voltage transfer ratio and other intrinsic qualities. The I-V characteristic of photovoltaic modules are nonlinear and dependent on the ambient conditions. The authors in [18] compare these three converters in terms of their output voltage polarity, input current continuity, required gate drive circuitry, efficiency, and cost. However, a comprehensive comparison of the three converters in terms of the transient response remains untouched.

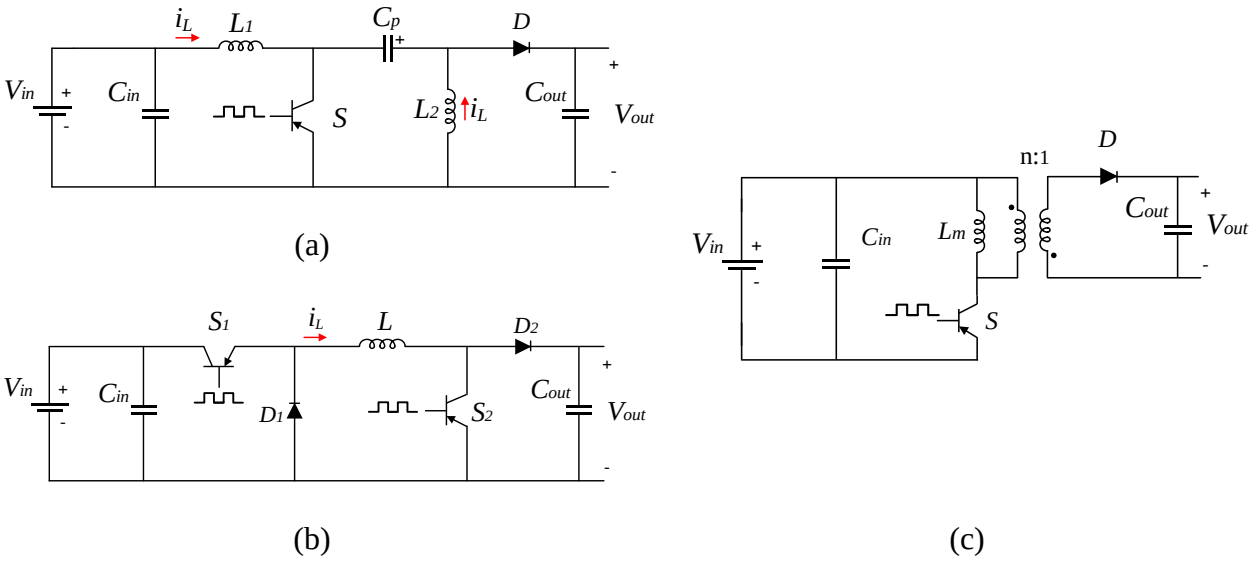

Figure 14. The three converters under study: (a) SEPIC (b) Positive Buck-Boost (c) Flyback.

The I-V characteristic curve of a BP365 for a specific insolation level and temperature is illustrated in Figure 10. According to that figure, the slope of the I-V curve and thus the dynamic resistance of the solar panel depends on the panel voltage and current. The dynamic resistance of the solar panel appears in the dynamic model of the converter and thus affects the dynamic behavior of the converter. The I-V curve of the solar panel can be divided into four regions: the current-source region, the power region I, the power region II, and the voltage-source region.

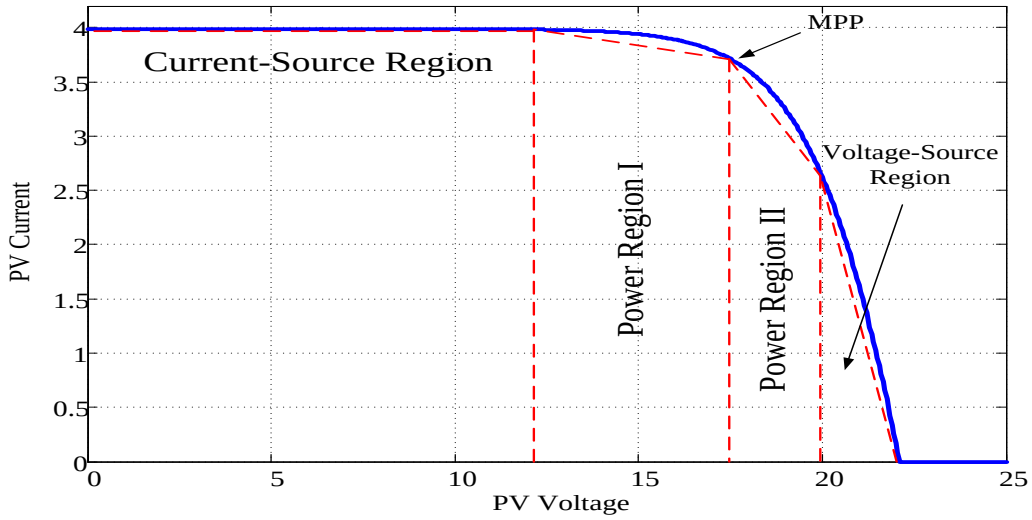

Figure 15. The I-V characteristic of BP365 for a certain insolation level and temperature.

It's safe to assume that the dynamic resistance of the panel for each region is approximately constant and thus, rather than studying a whole range of operating points, one must study a point inside each region. The objective of this work is to compare the transient behavior of each converter in the four power regions.

2.3.1 Verification of Results

In this section we compare the time domain simulations of the three converters. In the first case, the transient response of the three converters to a small step change of the duty ratio is compared while the converters are operating near the MPP. Figure 18 shows the resulting waveforms. This experiment corresponds to the frequency response comparison provided in Section III and verifies the relative merit of the Positive Buck-Boost and the Flyback over SEPIC in terms of the transient performance.

TABLE I. Five Operating Points on the I-V Curve of the PV panel

Point Characteristics	OP 1	OP 2	OP 3	OP 4	OP 5
PV voltage	10.013V	15.51V	17.6V	18.5V	20.5V
Dynamic Resistance $R_{pv}(\Omega)$	-776.0	-19.652	-4.35	-2.78	-0.99
PV Power (Watt)	39.9	60.8	65.0	63.8	45.1

In the next case, the transient response of each converter in the five operating points listed in Table I is compared. The resulting waveforms for SEPIC, Positive Buck-Boost and Flyback are illustrated in Figure 16 to Figure 19 respectively. This experiment corresponds to the comparison provided in Section IV and verifies the dependence of the transient behavior of the three converters to the operating point listed in Table I.

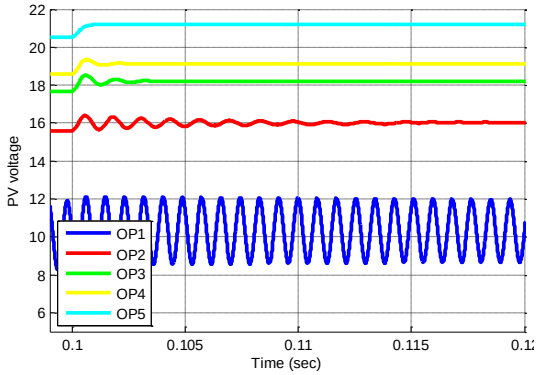

Figure 16. Response of Positive Buck-Boost to a step change of duty cycle in the four power regions and MPP.

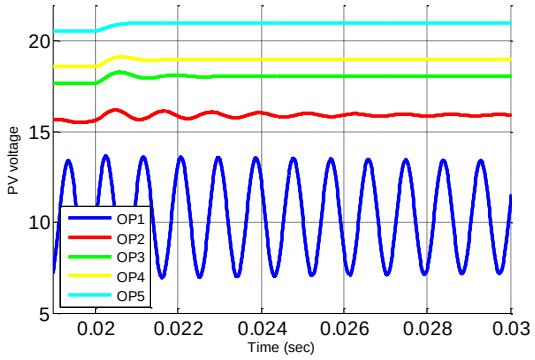

Figure 17. Response of Flyback to a step change of duty cycle in the four power regions and MPP.

The dynamic performance of a PV charger system designed based on three power electronic converters was analyzed in this study. Based on the provided results, the SEPIC converter seems to be the least favorite converter among the three for the design of the PV charger system. Per the outcome results, the Positive Buck-Boost was adopted for the proposed controller.

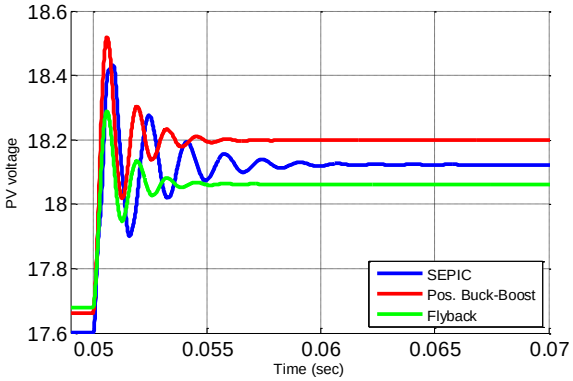

Figure 18. Response of the three converters to a step change of duty cycle at MPP.

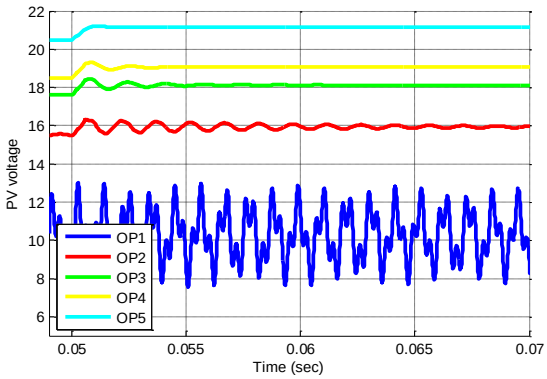

Figure 19. Response of SEPIC to a step change of duty cycle in the four power regions and MPP.

2.4 Grid-Connected PV systems

The second objective now is for Grid-tie systems. PV systems connected to the grid always have a connection with the utility grid network through an appropriate inverter since a photovoltaic cell generates only DC. The so called Inverters convert the DC output of a PV or storage battery to alternating current, either to feed power through the grid or to power a stand-alone system. There are many kinds of power electronic topologies used in the market. As it was explained in chapter 2 section 1.2, the grid-connected PV systems can be either a two stage converging system or a single stage system which is considered in this section.

2.4.1 Conventional Power Convertors

There are two conventional converters which are voltage-source and current-source converters. A DC input voltage source is parallel by a huge capacitor which delivers the power to the converter circuit, a three-phase inverter for grid-tie systems. The input voltage source could be used as a battery, solar-cell, or capacitor. Two switches are used in each leg; for each switch there is typically a power transistor and an antiparallel diode to offer a bidirectional current flow and unidirectional voltage blocking capability. The Voltage source converter has a wide application. Figure 20 shows the traditional three phase voltage source convertor. Yet, it has the some barriers and limitations [19]. Voltage-Source Inverters (VSI) can only step-down (a Buck Converter) the voltage whereas the Current-Source Inverters (CSI) can only step-up (a Boost Converter) the voltage. This is due the fact that the DC input voltage is set to be higher or equal the peak of AC output voltage [19]. As result, an additional power converter stage is necessary for some power application in a PV system as an example. Another shortcoming for a conventional DC/AC inverter is that two switches in the same leg cannot be turned on the same time. Otherwise, it will short out the input source and can damage the switches. The third issue is the boost factor of the voltage source

inverters do not exceed 1.2 which is not practical for PV systems [20, 21]. Recently a novel power converter topology called the impedance source convertor (referred as Z Source convertor) that overcomes the shortcomings of the typical VSIs and CSIs convertors.

In [19] the Z source was presented which is composed of z impedance network that includes two inductors and two capacitors between the DC input source and a normal H-bridge invertor. Figure 22 illustrated the z source invertor. The impedance circuit that

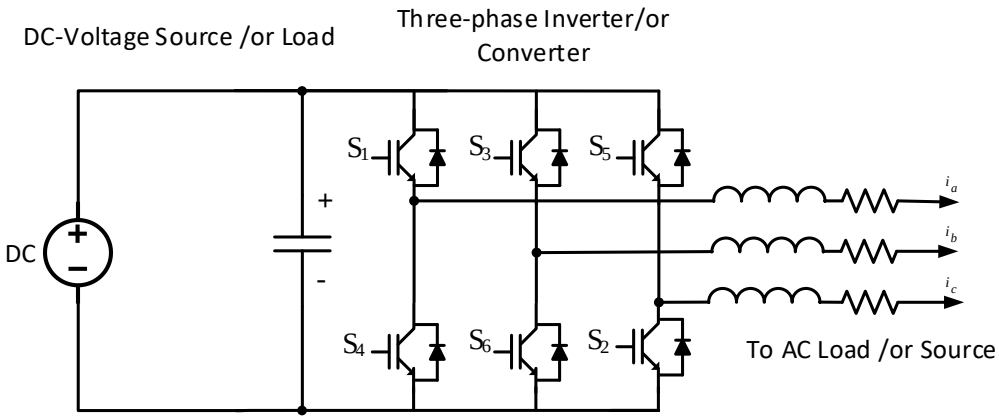

Figure 20. The traditional Three phase Invertor / Convertor (VSI).

couples the three phase invertor to a power source or another convertor or PV panel. As in this work to be as DC source input which features cannot be observed in the traditional voltage or current source convertors. The two inductors L_1 *and* L_2 can be a split- inductor or two separate ones. The conception of Z-source is valid to all types of power conversion devices from DC-to-AC or vice versa. The emphasis in this work is for the inverter DC/AC type since our DC input source is a PV system.

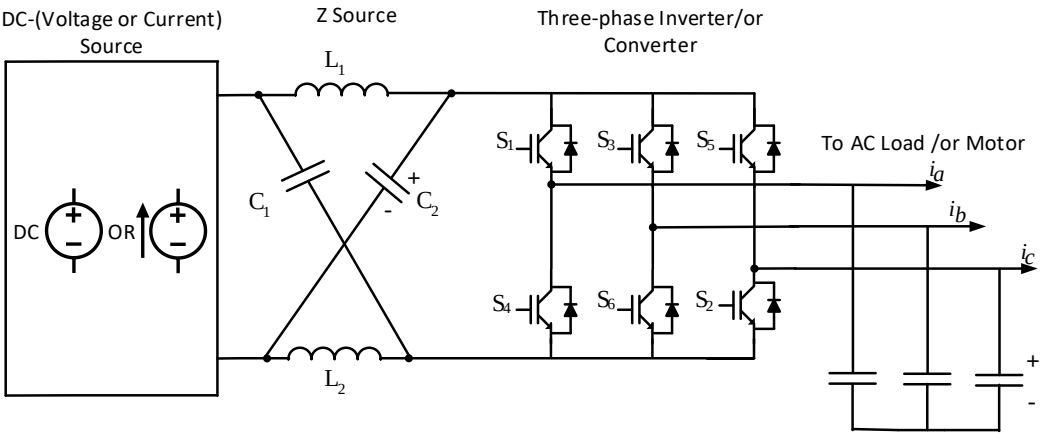

Figure 22. The impedance Source Convertor (Z-Source Invertor).

With a set of new configurations of the Z-source convertors, a new class of quasi-Z-source was proposed in [22] for PV systems since the input current is continues unlike the traditional Z-source invertor which its input current is discontinue.in addition to this, its passive components are reduces which reduces manufacture cost. Figure 23 shows the q-ZSI inverter. In this dissertation, a PV system with QZSI topology for grid connected application will studied and investigated with the proposed MMPT algorithm.

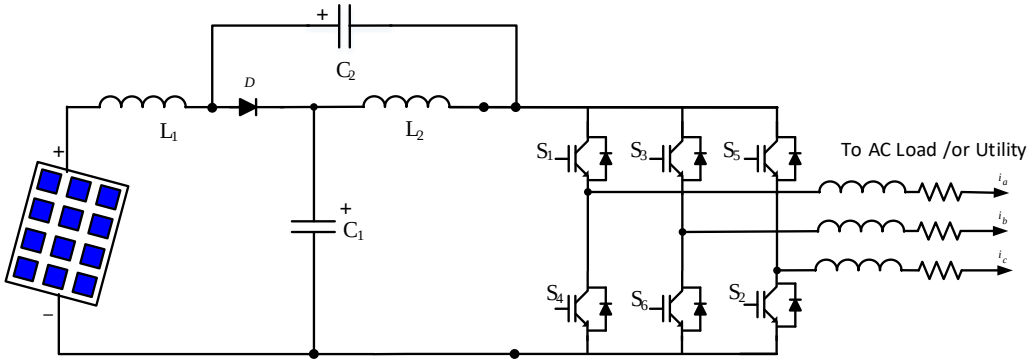

Figure 21. Voltage fed q-ZSI for PV application

2.4.2 QUASI-Z-Source Inverter

The QZSI has three main states, the active state in which the convertor works as a standard voltage source invertor, the null state in which all three upper switches or all lower switches of the invertor turned on, in the shoot through state in which the upper and lower switches can be turned on at the same time. This shoot through state is prohibited in the conventional convertor [23].

In the active state as shown in Figure 23 for an interval of T_1 , during a switching cycle of T. The voltage cross inductor and the current through the capacitor can be as follows:

$$C_1 \frac{dV_{c_1}}{dt} = i_{L_1} - i_{inv} \tag{2.1}$$

$$L_1 \frac{di_{L_1}}{dt} = V_{in} - V_{C_1} \tag{2.2}$$

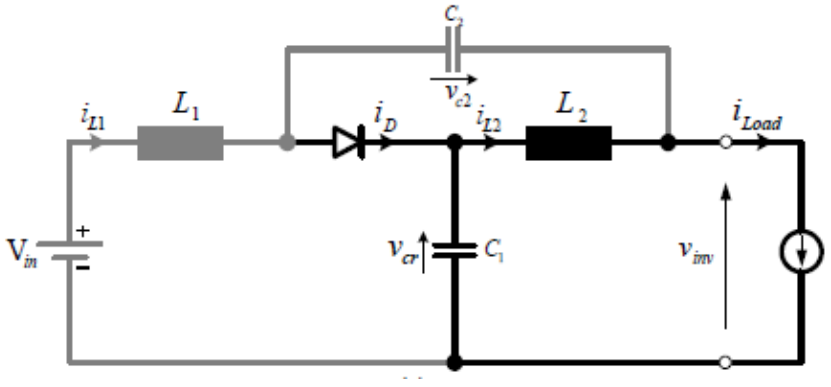

Figure 23. Equivalent circuit of QZSI in Non-shoot-through state

Where V_{in} is the input DC source voltage, r_{L_1} the inductor resistance, V_d the diode voltage, and i_{inv} is the inverter current.

In null state as shown in Figure 24, the inductor voltage is as given in equation (2.2). However, the capacitor current is as in equation (2.3).

$$C_1 \frac{dV_{c_1}}{dt} = i_{L_1} \tag{2.3}$$

In shoot-through state as shown in Figure 25, the inductor voltage and the capacitor current are:

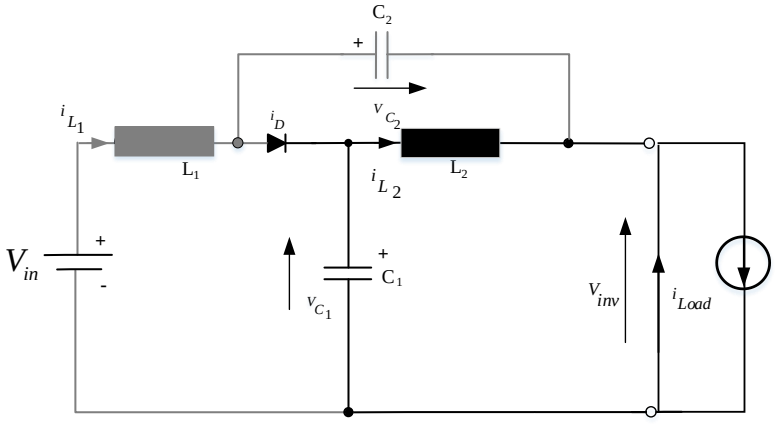

Figure 24. Equivalent circuit of QZSI in null state

$$C_1 \frac{dV_{c_1}}{dt} = -i_{L_1} \tag{2.4}$$

$$L_1 \frac{di_{L_1}}{dt} = V_{C_2} + V_{in} \tag{2.5}$$

In addition, in the above mentioned state, the inverter works in unique modes that it can be in a buck mode or in a boost mode. As it can be seen from the figure below, the inverter bridge is a short-circuit so the voltage across the inverter's terminal is zero. The shoot-through mode can be generated by up to seven unique ways. It can be via one arm or two and all of the threes arms in three phase application. Given that the inverter circuit in the shoot mode for an interval of T_0, during one period switching cycle, T, The shoot-through duty ratio is denoted as $D = \frac{T_0}{T}$.

In steady state condition, the inductor average voltage for an interval for one period is zero

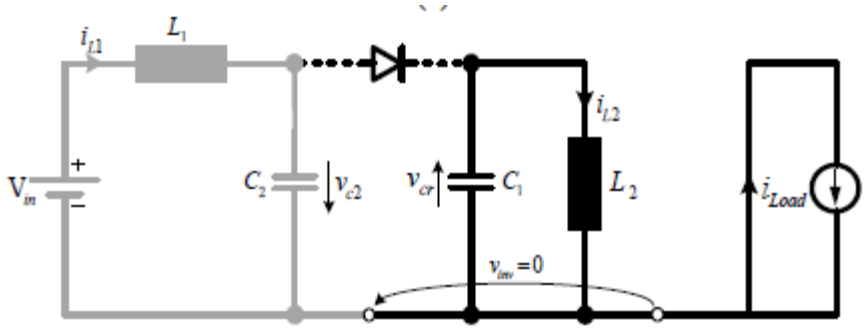

Figure 25. Equivalent circuit of QZSI in shoot-through state

$$V_{C1} = \frac{1-D}{1-2D} V_{in} \tag{2.6}$$

$$V_{C2} = \frac{D}{1-2D} V_{in} \tag{2.7}$$

From the equations in both non-shoot-through state the peak dc-link voltage at the input terminal of the inverter is:

$$V_{PN} = V_{C1} + V_{C1} = \frac{1}{1-2D} V_{in} = BV_{in} \tag{2.8}$$

Where B is the boost factor of the qZSI [24].

2.4.3 qZ-Source Grid connected application in Photovoltaic Power Systems

Z-source/quasi-Z-source inverters have a promising future in photovoltaic power generation due to their flexible power conversion in one single stage, and to be cable of working with a wide

range of DC input variations, thus reducing the overall system cost. It's worth to be mentioned, there are several configurations of Z-source topology that has been derived from the original topology in [19]. However, a voltage-Fed qZ-source inverter with continuous input current will be considered in this work in favor of PV application which was presented in [24]. A typical three phase configuration q-QZSI-based PV system for grid-connection shown in Figure 26 will be investigated.

Furthermore, the grid connected PV systems have more application than the stand-alone because they have immediate and more efficient utilization [25].

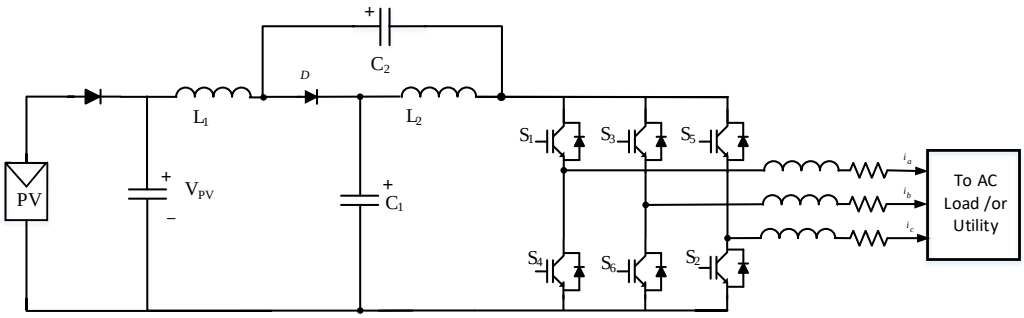

Figure 26. Three phase q-ZSI for PV application

2.4.4 Control and Operation of q-ZSI

A very common control method that has a wide range of application is Pulse-width modulation (PWM) control. The PWM method has been applied for the conventional power convertor as well as has been proposed for ZSI/q-ZSI to achieve better performance and reasonable real time implementation. As it was stated early that impedance power converter has a shoot-through state that is not possible for the standard power converters. As shown in Figure 27, when the triangle (carrier) waveform is greater than lower than the peak of the reference waveform, all top switches or all bottom switched turned on respectively as illustrated in the shadowed area. In the zero state,

the input short circuit, the output voltage of the inverter is zero. However, for the Z-source inverter, the idea of the control is to make all or some of the zero states into shoot-through states [26].

The Z-source inverter has three common PWM control techniques which are summarized as: simple boost control (SBC), maximum boost control (MBC) and constant boost control (CBC). An important control factor is defined as the ratio of amplitude of the sine waveform to the amplitude of the triangle wave.

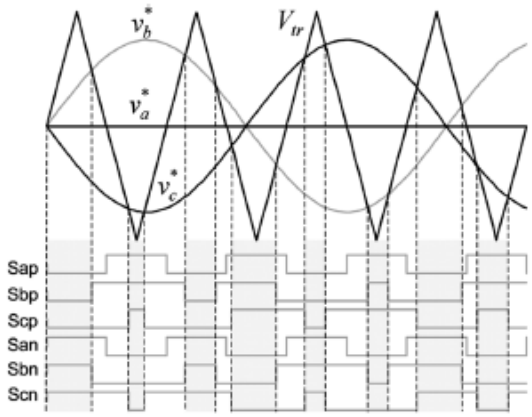

Figure 27. Three phase inverter control scheme

Chapter 3

3 Control of Power Electronics interface in PV systems[3]

3.1 Introduction

The vital role of power converters in renewable energy conversion systems has been persistently growing in the past few years, primarily in the interest of rising energy demands and ecologically aware alarms one of which, solar photovoltaic systems are a very attractive subject of power converter applications because it is not practical to utilize power from the PV panel to the grid without the use of a converter.

Power converters can improve the quality and stability of the PV system. Control schemes for power converters have been continuously developing according to the development of semiconductors and digital control platforms.

Several control methods have been proposed in literature and by researchers for the control of power convertors. The most well-known methods are being used illustrated in Figure 28 [27].

Implementation of these types of method varies from simple as PI-based control to very complex as Fuzzy logic control. In the recent few decades, the emerging development of digital platforms as digital signal processors (DSP) with high computational processors made the implementation of the high complex control schemes possible.

[3] Part of this section is reprinted with permission from A. A. Abushaiba, S. M. M. Eshtaiwi, and R. Ahmadi, "Comparative analysis of dynamic performance of four prominent Maximum Power Point Tracking algorithms in photovoltaic systems using realistic experimental implementation," in 2016 IEEE International Conference on Electro Information Technology (EIT), 2016, pp. 0576-0579. A. A. Abushaiba, S. M. M. Eshtaiwi, and R. Ahmadi, "Dynamic performance analysis of a PV charger system," in IECON 2014 - 40th Annual Conference of the IEEE Industrial Electronics Society, 2014, pp. 2069-2074.

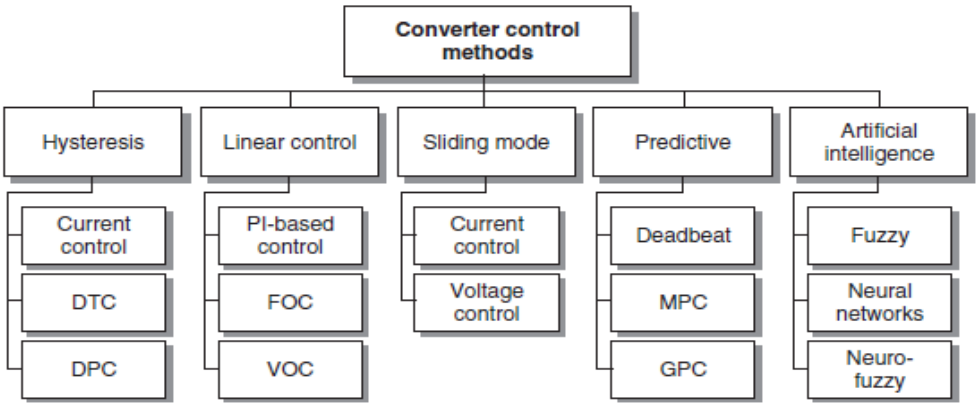

Figure 28. Different types of Converter control methods

3.2 Control challenges

Typically, the dynamic performance and transient stability of the system is a key role in control requirements. Now days, the code requirements and the regulations rules require more technical specifications and constraints. The design of a power converter for market and industrial application can be as an optimization problem rather than just regulating output or input signal. A few control challenges are important in power electronics as following [27]:

- The error signal should be as small as possible with faster dynamics for the following of the reference control signal.
- Minimizing the switching and conducting losses in the power switches.
- Meeting the industrial standard in the harmonics content
- Improved performance under various operating conditions.
- Some converters topology have prohibited switching state as we have seen in the previous section.

3.3 Controller Design for the Stand-alone PV system.

Typically the MPPT algorithm is a high level controller implemented on a power electronic converter. It is fundamental to the operation of the MPPT controller that the converter's transient response to the generated MPPT commands be fast and well damped. The transient behavior of power converters has been subject to extensive research and study in the literature over the years [17]. However, study of the transient behavior of power converters in Photovoltaic (PV) energy systems is a relatively new concept [28]. The authors in [18] compare converters in terms of their output voltage polarity, input current continuity, required gate drive circuitry, efficiency, and cost. However, a comprehensive comparison of the DC/DC converters in terms of the transient response remains untouched. The dynamic behavior of various power converters has been studied in the literature extensively [29]. However, the dynamic behavior of a power converter operating in a PV system is distinctive from what have been largely studied due to the fact that in proposed system one of the dynamic states is the input voltage of the converter rather than the output voltage Figure 29, illustrates a typical positive buck-boost type power converter interfacing a PV panel to a dc bus. The results of this study will be based on the use of a positive buck-boost converter for MPPT.

As pictured in Figure 29, the panel voltage is equal to input voltage of the converter; as a result, by controlling the input voltage of the converter, the panel voltage can be controlled easily. The goal of the converter control algorithm, then, will be to regulate the panel voltage to the MPP. By tracking the MPP in real-time, the maximum power can be delivered by the PV panel continuously.

The positive buck-boost converter of Figure 29, with the two mentioned controller loops are illustrated in Figure 54.The inner PI controller in Figure 54 will be designed based on the dynamic model of the converter using classical control design methods. This loop regulates the input voltage of the converter to the reference points generated by the outer MPP tracker loop [30].

The positive buck-boost converter in Figure 29 has two modes of operation. In mode 1, both switches are ON and both diodes are OFF, while in mode 2, both switches are OFF and both diodes are ON. The two modes of operation of the converter are shown in Figure 30. The state-space model of the converter in mode 1 can be derived from Figure 30 (a) by writing simple KVL and

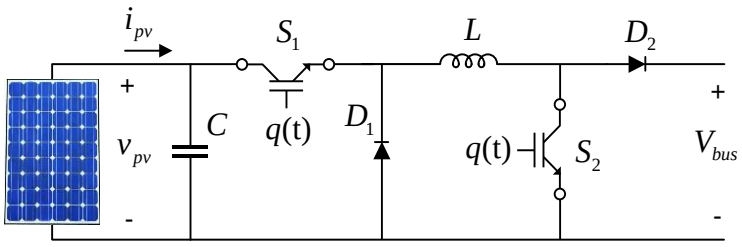

Figure 29. A positive buck-boost converter interfacing the PV panel to the dc bus.

KCL equations,

$$\begin{cases} L\dfrac{di_L(t)}{dt} = v_{pv}(t) \\ C\dfrac{dv_{pv}(t)}{dt} = i_{pv}(v_{pv}) - i_L(t) \end{cases} \qquad \textbf{(3.1)}$$

Where $v_{pv(t)}$ is the panel voltage, which is equal to the input voltage of the converter, $i_L(t)$ is the converter's inductor current, and i_{pv} is the current delivered by the PV panel at a certain voltage. Similarly, the state-space model of the converter in mode 2 can be derived from Figure 30

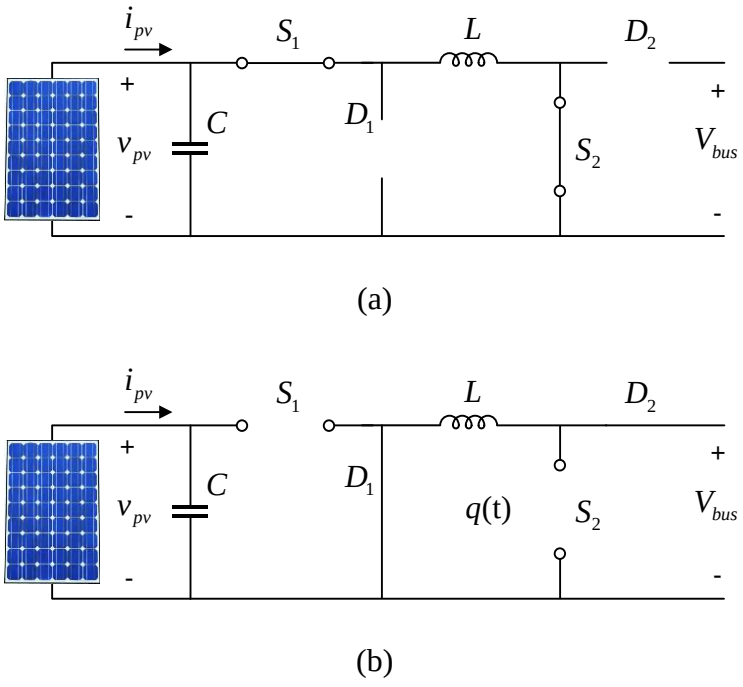

Figure 30. Two modes of operation of the buck-boost converter (a) Mode 1 where active switches are turned ON (b) Mode 2 where active switches are turned OFF

$$\begin{cases} L\dfrac{di_L(t)}{dt} = -V_{bus} \\ C\dfrac{dv_{pv}(t)}{dt} = i_{pv}(v_{pv}) \end{cases} \tag{3.2}$$

Where V_{bus} is the voltage of the dc bus at the output port of the converter. This voltage is maintained at a fixed value by an external power electronic system. The averaged state space model of the converter can be found by averaging (1) and (2) over one switching period using state-space averaging method [31],

$$\begin{cases} L\dfrac{di_L(t)}{dt} = dv_{pv}(t) - V_{bus}(1-d) \\ C\dfrac{dv_{pv}(t)}{dt} = i_{pv}(v_{pv}) - di_L(t) \end{cases} \tag{3.3}$$

Where d (duty cycle) is the control input and $v_{pv}(t)$ is the control variable.

The converter model in (3) is both nonlinear and, due to the presence of $i_{pv}(v_{pv})$, dependent on the I-V characteristics of the PV panel. This model can be linearized around the MPP of the panel in Standard Test Condition (STC) to obtain the duty cycle to input voltage transfer function. Denoting the MPP current and voltage of the panel in STC as I I_{MPP} and V_{MPP}, the linearized state-space model is where D is the equilibrium point value of duty cycle at the MPP and R_{MPP} is the equivalent resistance of the PV array at MPP.

$$\frac{d}{dt}\begin{bmatrix} i_L(t) \\ v_{pv}(t) \end{bmatrix} = \begin{bmatrix} 0 & \frac{D}{L} \\ -\frac{D}{C} & -\frac{1}{R_{MPP}C} \end{bmatrix} \begin{bmatrix} i_L(t) \\ v_{pv}(t) \end{bmatrix} + \begin{bmatrix} \frac{R_{MPP}+V_{bus}}{L} \\ -\frac{I_L}{C} \end{bmatrix} [d] \tag{3.4}$$

The equivalent resistance of the array is obtained from

$$R_{MPP} = -\left(\frac{di_{pv}(v_{pv})}{dv_{pv}} \right)^{-1} \tag{3.5}$$

Using (4). the duty cycle to input voltage transfer function can be derived:

$$\frac{v_{pv}(s)}{d(s)} = \frac{V_{bus} + I_L LS}{LCS^2 + \frac{L}{R_{MPP}} S + D^2} \tag{3.6}$$

This transfer function can be used to design the PI controller of the inner loop.

3.3.1 Controller Design Method for Buck-Boost Convertor

There are two main methods for designing a closed loop controller for power convertors. Time domain methods which are based on root locus diagram and the design criteria expressed in terms of time domain properties (settling time, overshoot, etc.). The second method is based on Bode diagram which are more frequently used for power electronics converters. The design criteria is expressed in terms of frequency response properties (phase margin and bandwidth). The latter one of will be used for designing controller for the selected Buck-Boost converter illustrated in Figure 31. It's worth to be mentioned that the input DC source for Buck-Boost converter PV panel. For the sake of simplicity, for oriented voltage control, the PV panel can be represented as voltage source V_{PV} in series with a resistance R_{pv} .

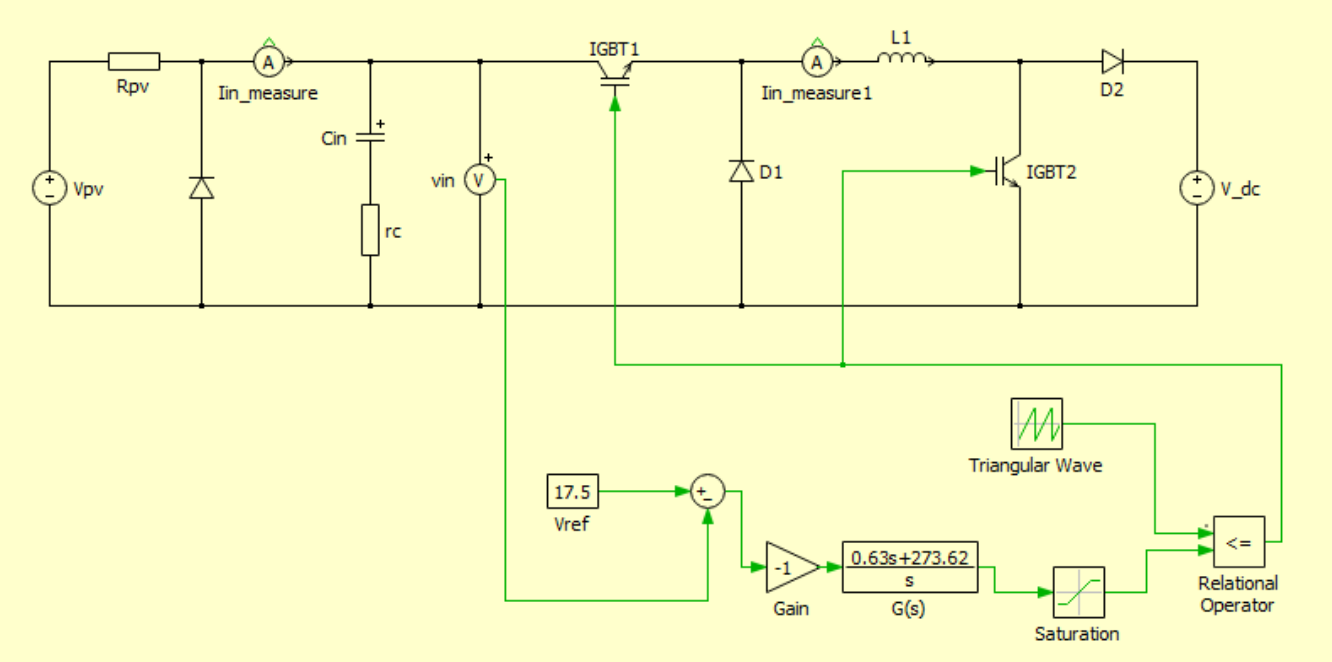

Figure 31. Buck-Boost simulation in PLECS.

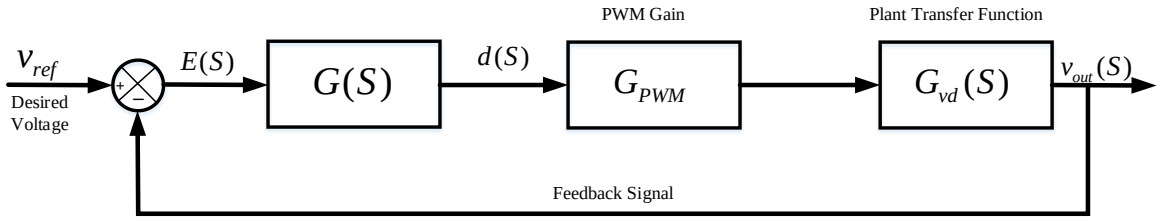

Figure 32. Closed-loop feedback control system.

Figure 32 shows the closed-loop feedback controller system. Considering proportional, Integral (PI) controller.

Where, $G_{vd}(s) = \frac{\hat{v}_{pv}(s)}{\hat{d}(s)}$, $G(s) = K_p + \frac{K_i}{S}$ and $G_{PWM} = 1$

The transient response of the closed-loop system depends on the place of the poles of the closed-loop transfer function,

$$1 + G(s)G_{PWM}G_{vd}(s) = 0 \qquad (3.7)$$

As mentioned early, for frequency response properties, phase margin and bandwidth, usually for practical system controller design at least 55 degree of phase margin is require and for a bandwidth at least 2kHz. In our case, MATLAB SISOTOOL is used for designing the PI controller. This tool is a powerful tool to design controllers for linear systems. Figure 33 shows SISIOTOOL in MATLAB before starting the design.

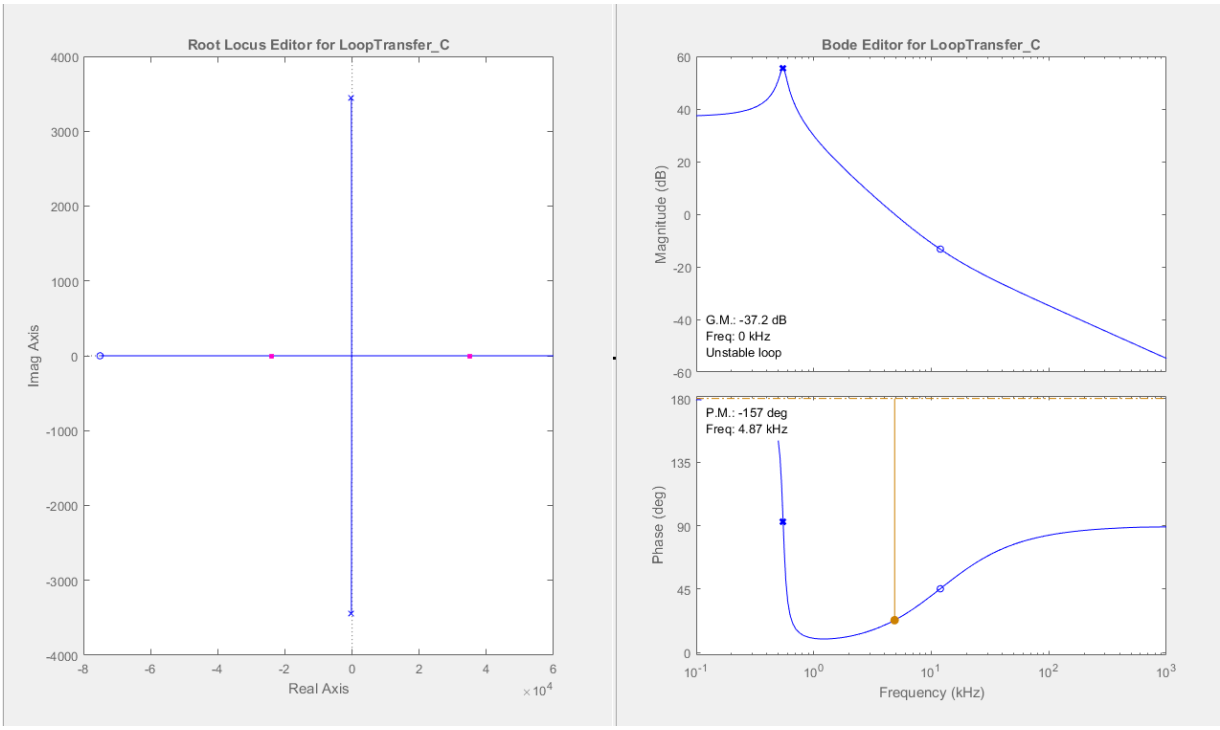

Figure 33. SISOTool MATLAB for Controller Design.

The design specifications for our convertor as follows:

$$L = 50\mu H, C_{in} = 560\mu F, V_{out} = 24volt, R_{pv_{MPP}} = 4.35\Omega, V_{c_{in}} = 17.6volt$$

From the developed transfer function, the duty cycle to input voltage, earlier in this section, we can create MATLAB script file and using the command $sisotool(G_{vd})$ in MATLAB command window. For the controller design, you can add poles and zeros then adjust their place according to the specified design criteria that was mentioned above. Figure 34 shows the final results for the designed PI controller of the Buck-Boost converter.

The resulted controller is as follows:

$$G(s) = K_p + \frac{K_i}{S} = 272.35 + \frac{0.63}{S} \tag{3.8}$$

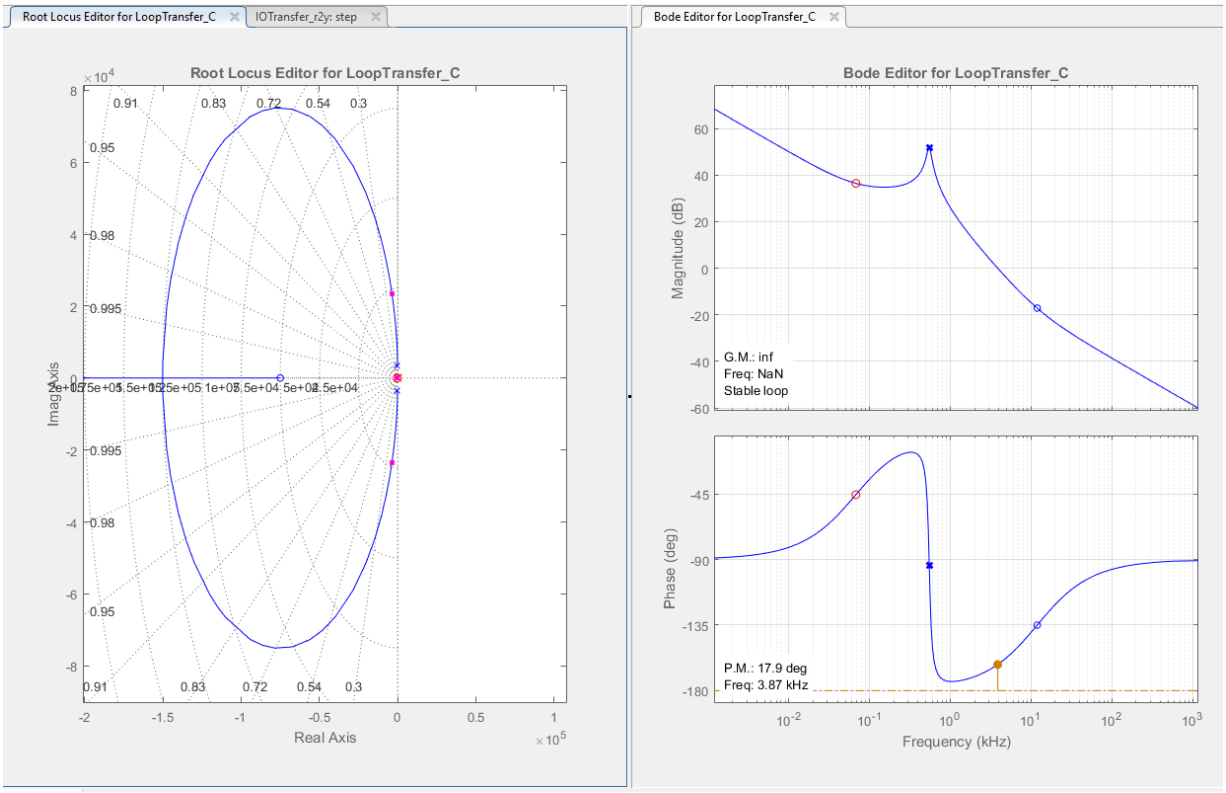

Figure 34. The Resulted Controller for Buck-Boost Convertor.

3.4 Controller Design for Grid-Connected PV system

The code requirements, current standers and regulations imposed on grid-connected power converging systems has to be met which are enforced by each power supplies that different by country. It worth to be mentioned, key factor of those standard, the injected current quality, voltage fluctuating, frequency synchronization and power factor.

The design of inverter of the PV system must be capable to meet the code standards in order to operate safely and provide high quality current to be fed to the utility grid.

The development of powerful digital platforms made implementation of powerful control algorithms and techniques promising in the field of power electronics converter and drivers. One of these promising control schemes is model predictive control. This powerful control method can be applied to various applications and multi objective optimization problems. It well known that controlling systems of power electronics converters have server constraints and nonlinearities. Model predictive control (MPC) made the implementation of those type of complex systems true.

As mentioned in the introduction of this section, Feeding ac power to the grid requires synchronization mechanism in which amplitude and phase angle are required in this process.

This section explores the proposed maximum power point tracking algorithm (MPPT) for grid connected PV system using a single stage power inverter controlled by model predictive controller.

3.4.1 Predictive control techniques

Power electronics converters are nonlinear system with finite number of switching states. The nature of power converters such as nonlinearity, finite number of switching states, and constraints inspire the application of model predictive controls.

There are four main methods in predictive controllers. Figure 35 illustrated four kinds of predictive methods. These methods their difference in using modulator with fixed frequency as in deadbeat control or not using modulator with variable frequency as in trajectory based predicate controller [27].

The highlighted model predictive controller with finite control set is the subject of focus in this dissertation for three phase PV grid connected system.

It worth to be mentioned, the main concept of predictive control is predicting the behavior of controlled actions by utilizing the model of the system for predefined time horizon. The concept of predicate control is to be simple for implementation and intuitive since you do not need to linearize nonlinear system and you can include constrains on the system for predefined boundaries [27].

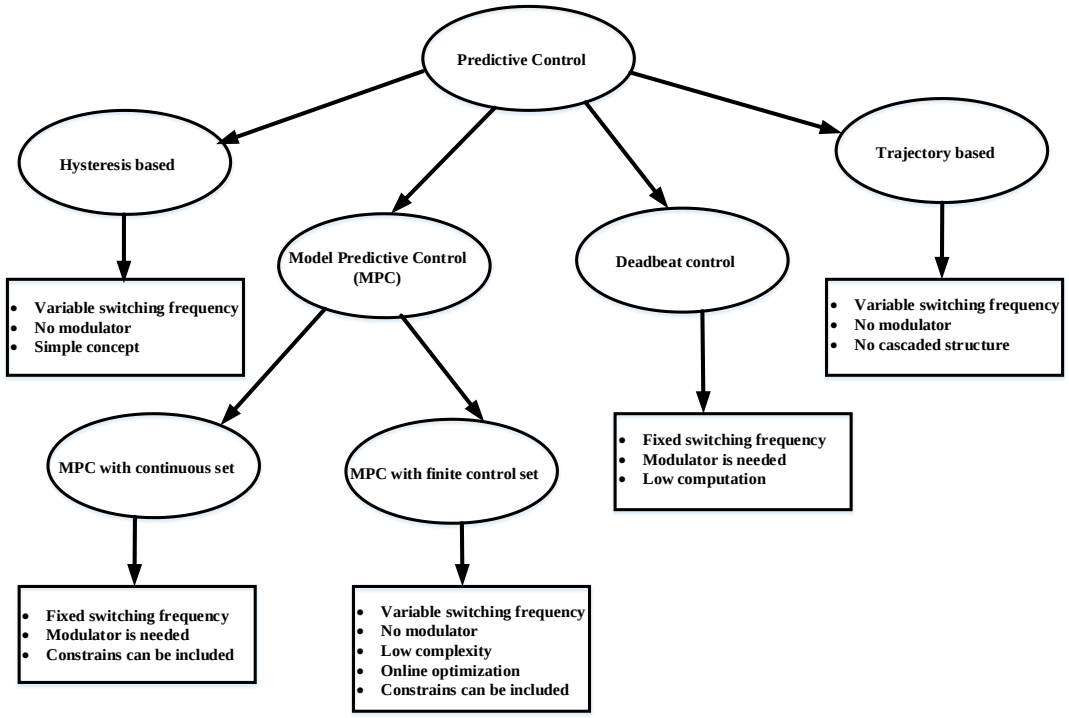

Figure 35. Classifications of predictive controllers

3.4.2 Principle of Model Predictive Control

MPC is gaining much intentions for being successfully applied in many industrial application for the last few decades. Thanks for the developments of a powerful digital platforms to handle high switching frequencies and can process large calculations today. However, the above mentioned are some disadvantages if compared to classic controllers. Nevertheless, MPC has several more important advantages that made it to be applied for a wide range of applications of which power electronics converters:

- Simple and initiative conception.
- A multi objective controller.
- Nonlinearities can be included in the model.
- Constraints on some controlled variables can be treated.

- Modifications and extensions can be included for some applications.

A discrete-time model of the system is needed and can be as a state space model as follows:

$$x(k+1) = Ax(k) + Bu(k)$$
$$y(k) = Cx(k) + Du(k) \quad (3.9)$$

Where $x(k)$ and $u(k)$ are the state and control variable at time, k and $x(k+1)$ is the predicted state.

A cost function g that defines the desired behavior of the system needs to be considered which represents the future states, references and future actuations:

$$g = f\big(x(k), u(k), \dots\dots, u(k+N)\big) \qquad for\ k\ \in \quad (3.10)$$

The cost function g is to be minimized for over the predefined time horizon. N optimal actuations will be the results that only the first element will be applied by the controller

$$u(k) = [1\ 0\ \dots\dots\ 0] arg\ \min_{u} J \quad (3.11)$$

This process is repeated for every sampling instant using the new measured data and obtaining the optimal solution so the optimization problem is solved.

The working principle of MPC is illustrated in Figure 36.

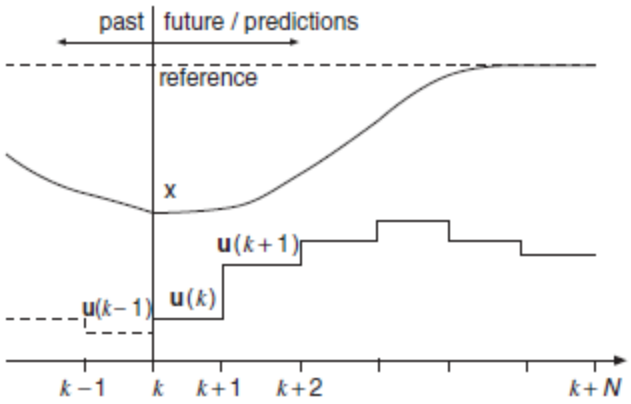

Figure 36. MPC working principle

3.4.3 MPC Controller design for power electronics converters

For a power converter, a finite set MPC is most explicit controller that suits the power converters [27].In case a converter, the fundamental element is the power switch which in ideal case has two states "ON" and "OFF". Thus, the possible number of different switching states is the total number minus the forbidden states. A general rule is given by:

$$N = x^y \tag{3.12}$$

Where x the number of is possible states of each arm of the converter, and y is the number of arms of the converter. So, three phase, two level converter has $2^3 = 8$ states.

However, in some multilevel converters the number of possible switching states can be very high since it depends on the number of levels. Figure 37 shows the relationship between the voltage vectors and the possible switching states.

As mentioned early, a system constraints or requirements for some applications can be included in the cost function that to be minimized for optimal control actions.

Those constraints can have different units, each of these in the cost function should be multiplied by weighting factors depends on their important [27].

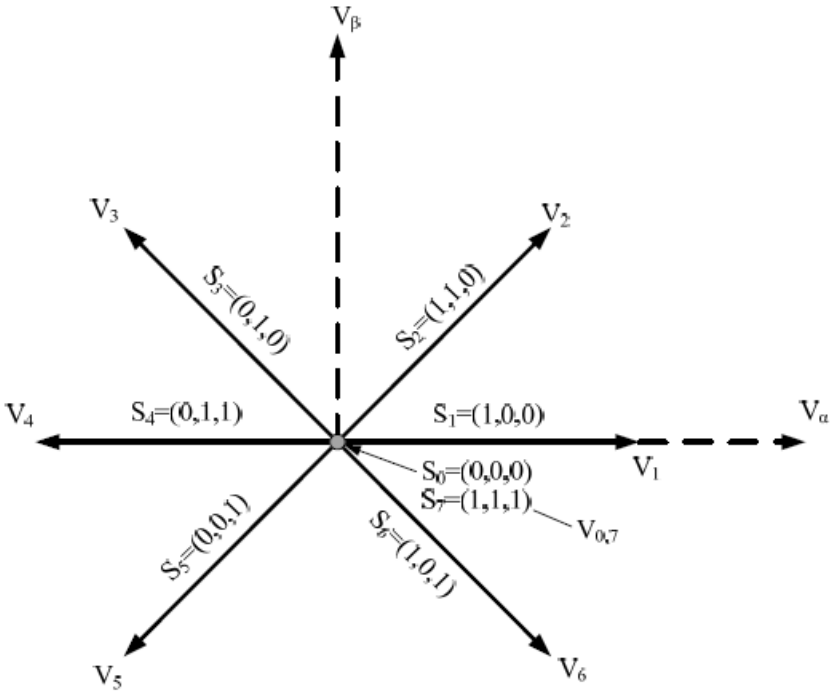

Figure 37. Voltage vectors for conventional three phase two level converter.

It is worth to mentioned, to determine the predicted future values of the controlled variables of the system, a discrete model is to be taken into account for the system. There some various discretization methods exit. However, for simple first order, Euler forward method can be valid to use.

$$\frac{dx}{dt} = \frac{x(k+1) - x(k)}{T_s} \tag{3.13}$$

Where T_s is the sampling time.

The general predictive control for MPC which for power converters is depicts in Figure 38 Where $x(k)$ the measured value is used for predicting $x(k+1)$ of controlled variable for each possible control action. Now, the cost function which is the difference between measured value and the reference multiplied by the weighting factor in our application to be evaluated for optimal actuations S to be selected and applied.

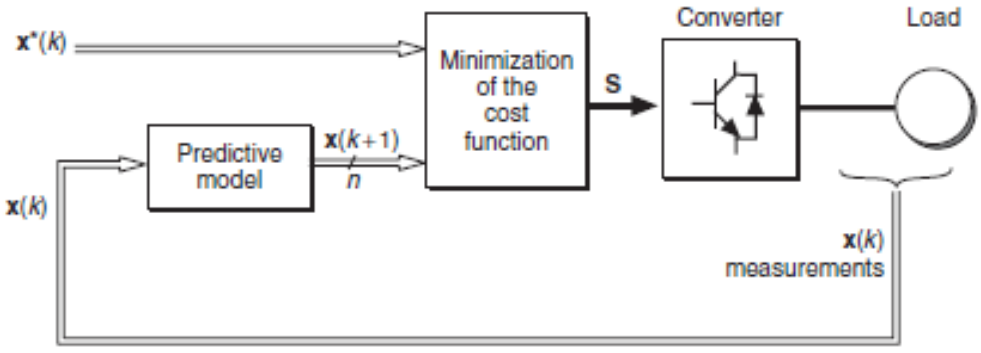

Figure 38. MPC control scheme for power inverter

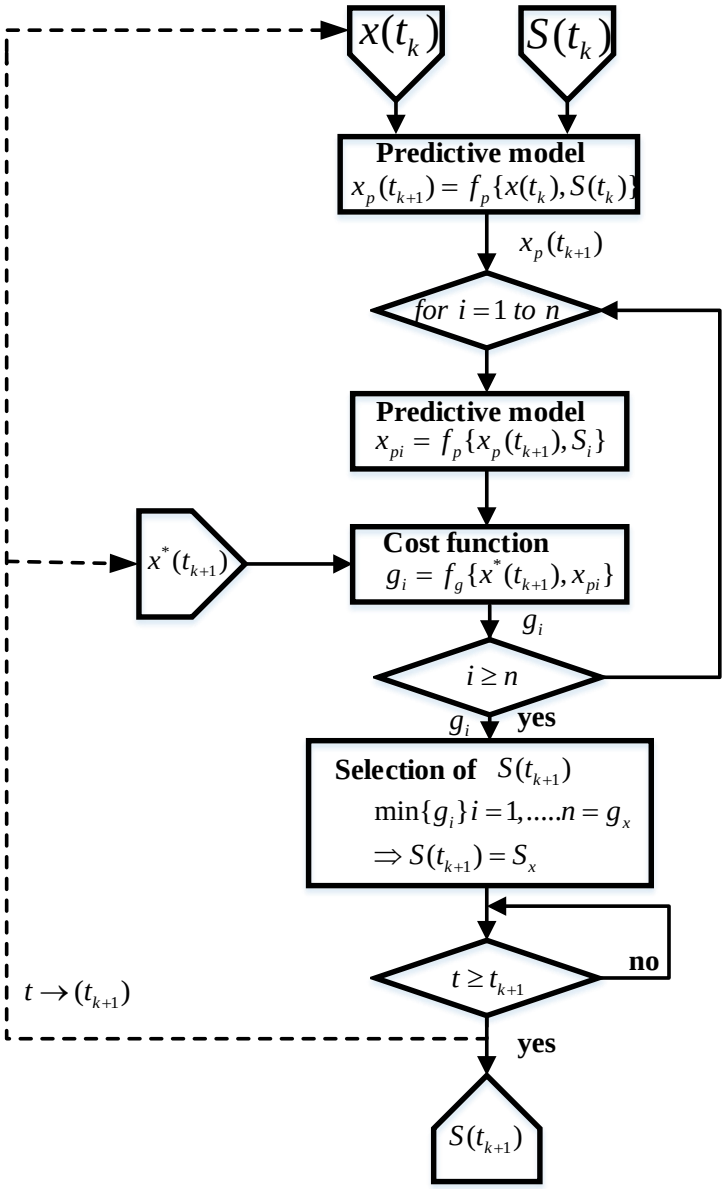

Figure 39. MPC generic algorithm

Considering the generic MPC algorithm in figure, the system controllable variable x which is controlled by MPC algorithm via a control action S which is switches gating signals in this case. The measured variable $x(tk)$ is fed back to calculate a discrete predictive model of the systemf_p, to achieve the predicted future values of the system $x_i^p(t_k + 1)$ for each possible control action S_i [31].

3.5 MPC for Grid-Connected PV system based on Quasi-Z-Source Inverter

This section presents a digital model predictive control technique based on finite control set of grid connected q-ZSI where the grid current is controlled , the q-ZSI inductor current and the capacitor voltage are considered in the cost function as well.

The model predictive control (MPC) for the q-ZSI shown in Figure 40 by which finding the optimized switching states of this three-phase grid connected inverter. The total number of the possible switching states are shown in table 2. For the sake of easiness, the three-phase (a,b,c) components will be converted to two phase (α, β) .In order to reduce the number of calculations for the optimal voltages vectors, this proposed control is counting for 6 active states, one state for zero and shoot-through states. The inverter output voltage vectors are generated according to the following equation.

$$V_{inv} = \frac{2}{3}(V_{aN} + aV_{aN} + a^2V_{cN}) \tag{3.14}$$

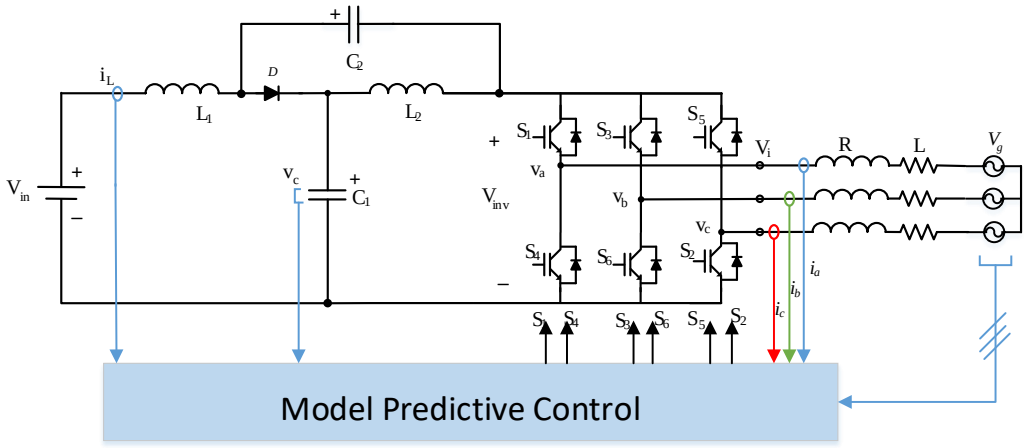

Figure 40. Schematic diagram for the power circuit

Output voltage	S_{a1}	S_{a2}	S_{b1}	S_{b2}	S_{c1}	S_{c2}
V_0 (null)	1	0	1	0	1	0
V_1	1	1	0	1	0	1
V_2	1	0	1	0	0	1
V_3	0	1	1	0	0	1
V_4	0	1	1	0	1	0
V_5	0	1	0	1	1	0
V_6	1	0	0	1	1	0
	1	1	0	0	0	0
	0	0	1	1	0	0
V_7	0	0	0	0	1	1
Shoot	1	1	1	1	0	0
Through	0	0	1	1	1	1
	1	1	0	0	1	1
	1	1	1	1	1	1

From Figure 40, the inverter voltage can be rewritten a follows:

$$V_{inv} = L\frac{di_{out}}{dt} + i_{out}R + V_g \tag{3.15}$$

Where L is the filter inductance, R is the filter resistance, i_{out} is the grid injected current and V_g is the grid voltage.

As mentioned in section (2.4) equations (2.1-2.5), and from the equivalent circuits Figure 23-Figure 24 and Figure 25 , considering the three modes and using Euler forward approximation, the predictive equations of the q-Z source inverter for injected grid current, can be expressed as follows:

$$i_{out}(k+1) = \frac{T_s}{L}(V_{int}(k) - V_g(k) - i_{out}(k)R) \tag{3.16}$$

The inductor current and capacitor voltage for active state can be expressed as follows:

$$V_{c1}(k+1) = V_{c1}(k) + \frac{T_s}{C_1}(i_{L1}(k+1) - i_{inv}(k+1)) \tag{3.17}$$

$$i_{L1}(k+1) = \frac{L_1 i_{L1}(k) + T_s(V_{inv} - V_{c1}(k+1))}{L_1 + R_{L1}T_s} \tag{3.18}$$

The inductor current and capacitor voltage for null state can be expressed as follows:

$$V_{c1}(k+1) = V_{c1}(k) + \frac{T_s}{C_1}(i_{L1}(k+1)) \tag{3.19}$$

$$i_{L1}(k+1) = \frac{L_1 i_{L1}(k) + T_s(V_{inv} - V_{c1}(k+1))}{L_1 + R_{L1}T_s} \tag{3.20}$$

The inductor current and capacitor voltage for shoot-through state can be expressed as follows:

$$V_{c1}(k+1) = V_{c1}(k) - \frac{T_s}{C_1}(i_{L1}(k+1)) \tag{3.21}$$

$$i_{L1}(k+1) = \frac{L_1 i_{L1}(k) + T_s(V_{c1}(k+1))}{L_1 + R_{L1}T_s} \tag{3.22}$$

3.5.1 Qusai-Z-Source MPC Control Implementation

In this section, the model predictive control is applied to the q-ZSI. Figure 42 shows the power stage system that is simulated in PLECS, power electronics simulation tool. The system is a grid connected. The three phase $V_{RMS} = 208V$ line to line voltage. The grid side components and the Z-impedance passive components are described in the table below. The control system is divided into two part, namely, PLL-based grid synchronization for generating the grid injected current reference shown in Figure 43 and MPC to achieve the generated reference. The latter is needed for the optimization of the cost function. As mentioned early, MPC is multi-objective controller, in general for q-ZSI, the capacitor voltage V_{c1}, the inductor current i_{L1} , and the injected grid current. The V_{c1} reference is set to be 600V to have the active power transferred easy. The implemented MPC algorithm doesn't include the V_{c1} in the cost function to provide simpler requirements for weight factors tuning [32].

Parameter	Value
C1	1000 µF
C2	1000 µF
L1	0.7 mH
L2	0.7 mH
T_s	60 µs
Lgrid	1 mH

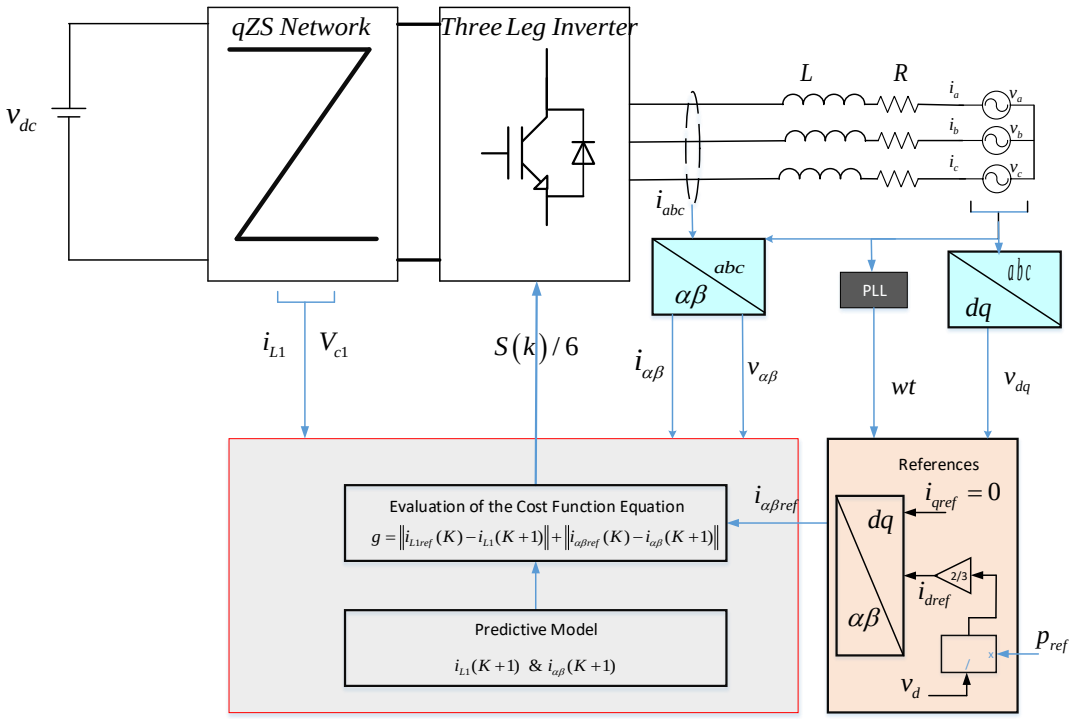

Figure 41.MPC schematic for q-ZSI grid connected

It's worth to be mentioned, a finite set control MPC approach is presented in this proposed system. This approach is capable to generate a unity factor and deliver low THD current to the utility grid. In the main time, it can also compensate for reactive power requirement of the grid which either can be achieved by providing the Q_{ref} or estimated based on the connected local loads reactive power requirements.

The MPC current control algorithm part is shown in Figure 45 is executed for 9 vectors which are including 6 active sates, 2 zero or null states and 1 shoot through state. The generated voltage vector from the 9 cases which minimizes the cost function g is applied to the inverter. From the control algorithm flow chart, the phase-locked loop (PLL) senses the phase angle of the grid voltage to ensure the grid synchronization for unity power factor operation.

For generating the current grid reference, depending on the active power available or set by the user, it's obtained through $i_{dref} = \frac{2}{3}(P_{ref}/v_d)$. Also, the three phase actual grid voltage v_{abc} and the grid-tie current i_{abc} are transformed to the two-phase rotating coordinates in d and q components, respectively and to the two-phase α and β as well to reduce the amount of calculation. Another method to obtain the i_{dref} is presented in [32] can be used as well, a PI controller is used for regulating the voltage capacitor V_{c1} to generate the real power component reference to be

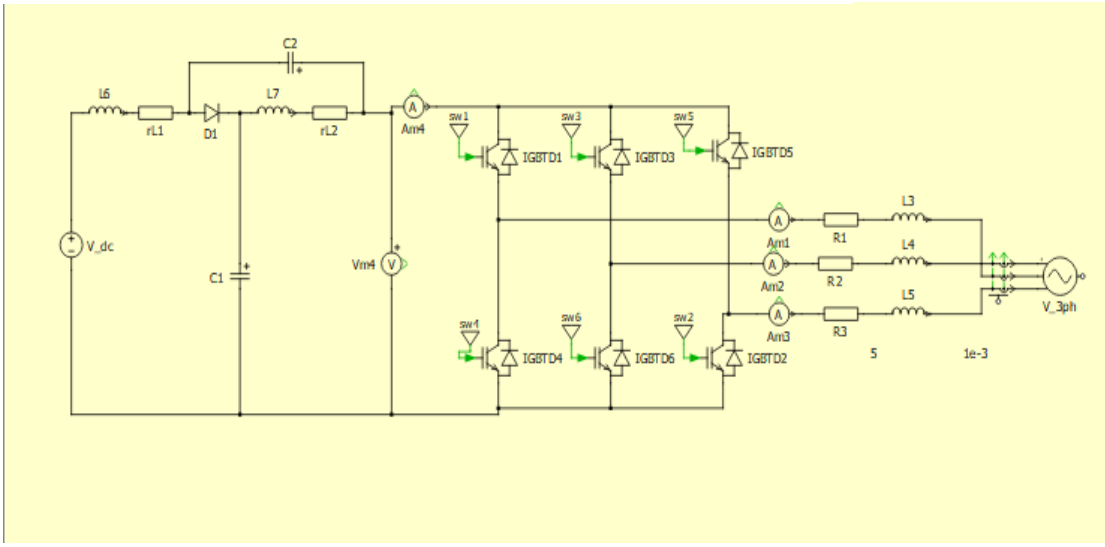

Figure 42.Power stage for q-ZSI grid connected in PLECS

injected into the grid.

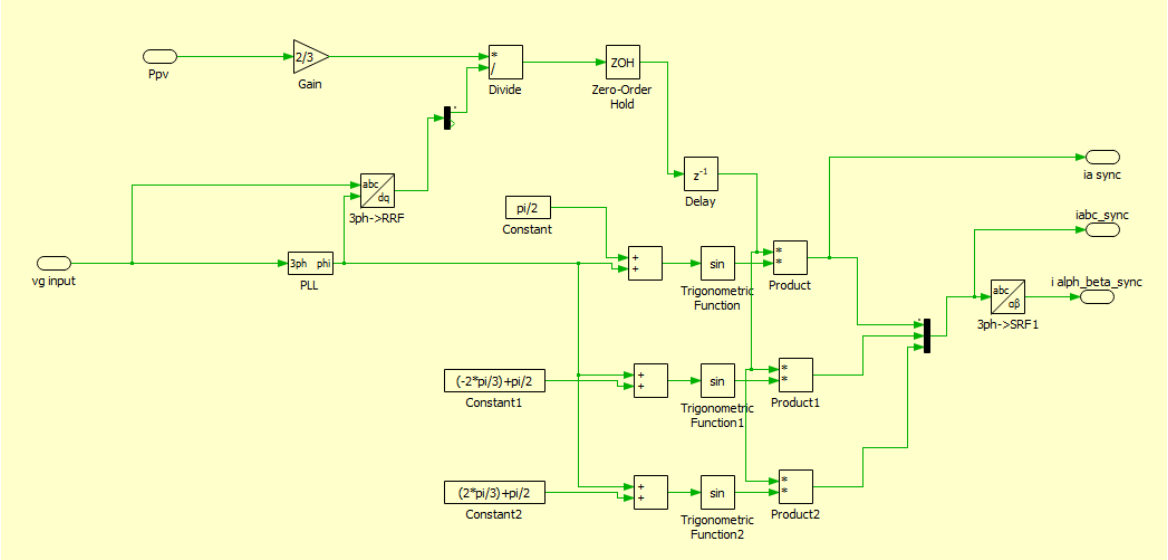

Figure 43.MPC reference generator for q-ZSI grid connected in PLECS

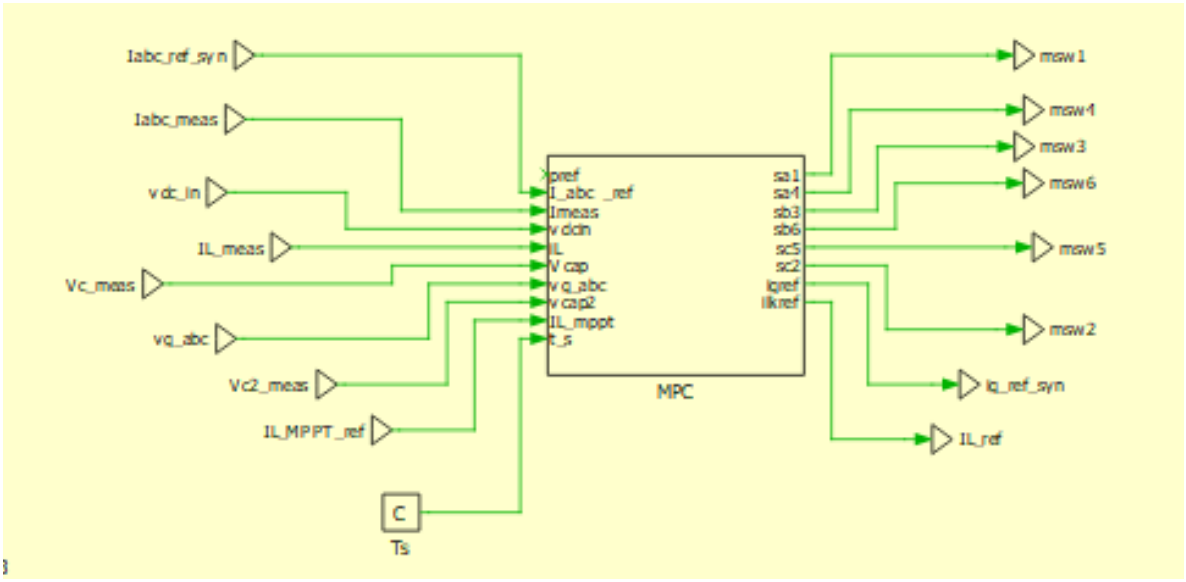

Figure 44.MPC block for q-ZSI grid connected in PLECS

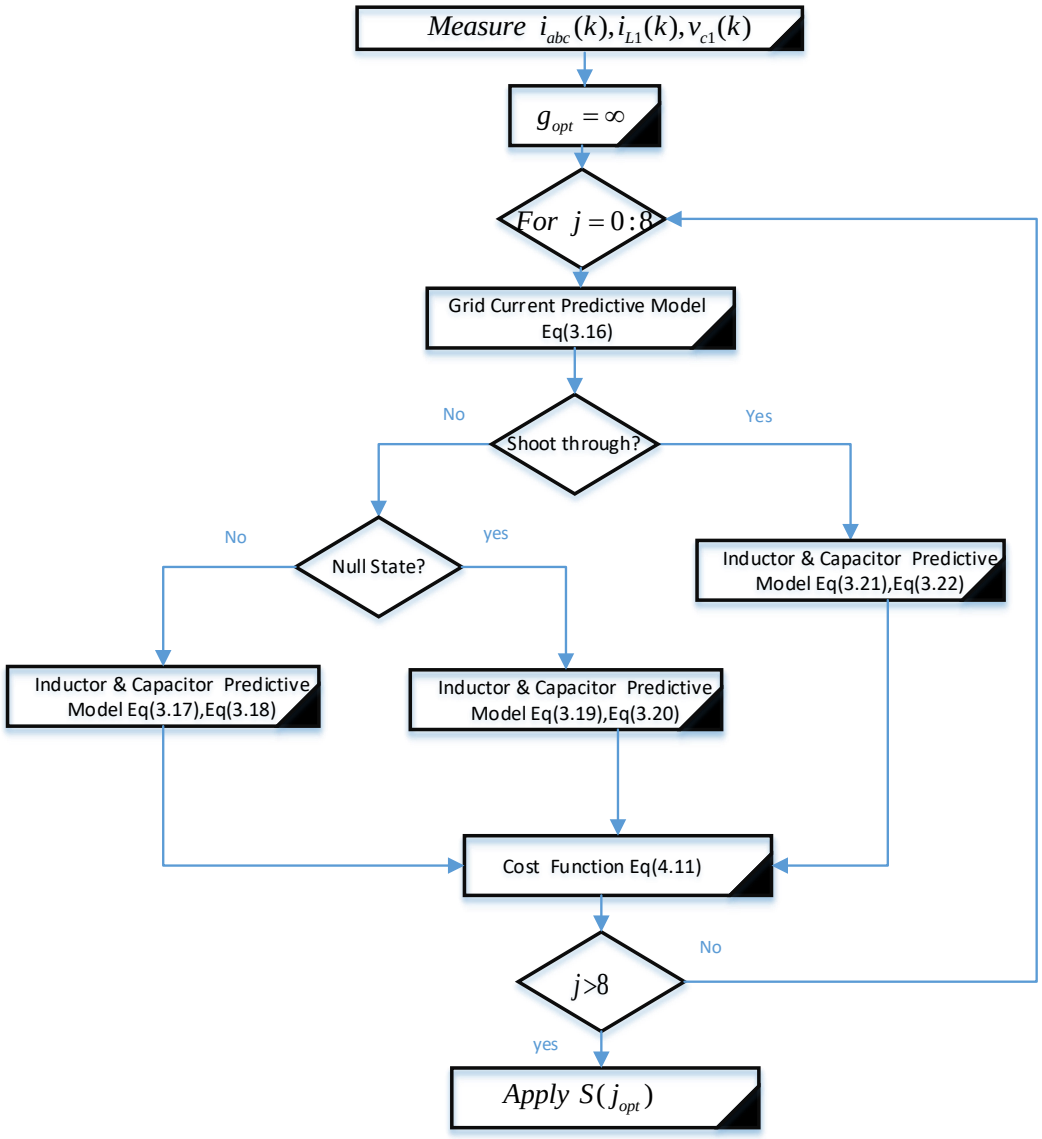

Figure 45. MPC prediction algorithm

Chapter 4

4 Maximum Power Point Tracking "MPPT"[4]

4.1 Literature Review

An effective MPPT algorithm should be able to track the MPP of the PV panel under natural dynamic ambient conditions throughout an ordinary day. To achieve stable, effective, and economically viable MPPT methods, numerous optimization algorithms have been explored over the past few years [33-61].

The authors in [62] try to classify a number of the proposed methods in the literature based on factors such as ease of implementation, effectiveness, and convergence speed. In a very broad sense, the MPPT methods in the literature can be classified into a few general categories. Several proposed methods are based on engineering intuition, such as simple hill-climbing algorithms, perturb and observe (P&O), Incremental Conductance (Inc.Cond), and their derivations [33-39]. Many other methods are proposed based on artificial intelligence algorithms such as Fuzzy Logic Control and Artificial Neural Networks [40-42]. A number of methods use complex mathematical calculations for MPPT, such as dP/dV or dP/dI Feedback Control, state-based MPPT, and sliding mode control [43-46]. There are also a few proposed methods that do not directly track the MPP but either approximate it from the PV panel parameters or identify it by a current or voltage sweep procedure [47].

[4] Part of this section is reprinted with permission from A. A. Abushaiba, S. M. M. Eshtaiwi, and R. Ahmadi, "Comparative analysis of dynamic performance of four prominent Maximum Power Point Tracking algorithms in photovoltaic systems using realistic experimental implementation," in 2016 IEEE International Conference on Electro Information Technology (EIT), 2016, pp. 0576-0579. A. A. Abushaiba, S. M. M. Eshtaiwi, and R. Ahmadi, "Dynamic performance analysis of a PV charger system," in IECON 2014 - 40th Annual Conference of the IEEE Industrial Electronics Society, 2014, pp. 2069-2074. R. Ahmadi and H. Zargarzadeh, "A new discrete-in-time extremum seeking based technique for maximum power point tracking of photovoltaic systems," in Applied Power Electronics Conference and Exposition (APEC), 2015 IEEE, 2015, pp. 1751-1756.

Although MPPT algorithms have been investigated broadly in the literature lately, not many MPPT methods based on the concept of Extremum Seeking (ES) have been proposed thus far. Extremum Seeking is a non-model based real-time optimization approach for dynamic problems where only limited knowledge of a system is available; such as when the system has a nonlinear equilibrium map that has a local minimum or maximum. The ES-based techniques in the area of applied control have proven their effectiveness in a variety of applications such as soft landing of electromagnetic actuators [63], PID tuning [64], thermo-acoustic coolers [65], and engine control [66]. The simplicity and the rigorous supporting mathematics of ES-based control methods are the main reason for their popularity in applied control [67].

Recently, a few ES-based MPPT techniques with applications to PV systems have been proposed [68-70]. Commonly, these approaches are based on continuous-in-time formulations. The work in [69] proposes a simple ES-based MPPT system based on the P&O method that identifies the PV's MPPT using an analog controller. The work in [70] proposes some modifications to the standard P&O so the converter's natural ripple can be used instead of a fixed perturbation. Continuous-in-time solutions need analog realization [59] or high speed processors to guarantee the continuity and convergence of the controller [69].

4.2 Conventional MPPT Methods

This section presents an experimental comparative analysis of four very well-known Maximum Power Point Tracking algorithms in terms of their response to dynamic environmental conditions. In this section, the four algorithms are discussed briefly and the performed experiments are presented.

Several MPPT algorithms have been proposed in the literature [71], [62] throughout the last decade. Each method has its own set of advantageous and disadvantageous. Several papers have compared different MPPT techniques [72] from many aspects such as ease of implementation, cost, and convergence performance. However, not many scholars have looked into the problem of dynamic response of MPPT algorithms to dynamical environmental conditions such as sudden temperature or irradiation variations.

The purpose of this section is to implement and experimentally compare four well-known MPPT algorithms in terms of their response to environmental condition variations. When comparing the four methods, to perform a fair comparison, all of the implementation parameters such as the sampling time, voltage step, etc. are set to the same values. It is worth mentioning that the four algorithms perform very well on the paper and in simulations, however, the goal here has been to compare them in actual experimental system to gain a real understanding of the merits of each algorithm.

4.2.1 Experimental System Setup

The block diagram of the experimental setup for evaluation of the MPPT algorithms is illustrated in Figure 46. As visualized, the experimental setup is comprised of a PV module, a dc-dc power converter, a digital controller, and a 24 V battery. The actual lab setup of

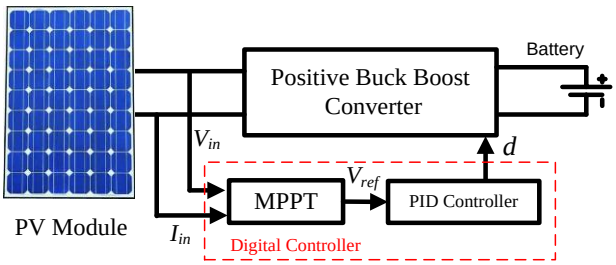

Figure 46. Block diagram of the experimental setup

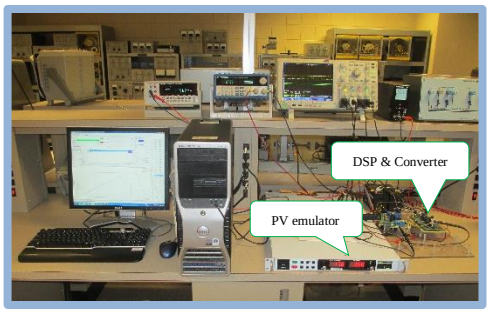

Figure 47. Actual experimental setup in lab

the system is shown in Figure 47. A brief description of each component in the system is as follows,

A. DC-DC Converter: A dc-dc converter is used to interface the PV module to the battery. The converter topology utilized in this paper is a pulse-width modulated (PWM) positive buck-boost topology as shown in Figure 48. This topology is picked because of its flexible input-output voltage transfer ratio. The output terminal of this converter is connected to the battery and thus the output voltage is always fixed at 24 V battery voltage. The input terminal is connected to the PV module and the input voltage can be controlled by altering the duty cycle of the switching signals. As a result, the MPPT algorithm can vary the input voltage to track the MPP. The parameters of the designed converter are as follows:

$L = 50\mu H, C_{in} = 560\mu F, P_{out} = 300W, V_{in} = 0 - 24V, f_{sw} = 100KHZ, \Delta iL = 20\%\ iL, \Delta V_c = 0.01V.$

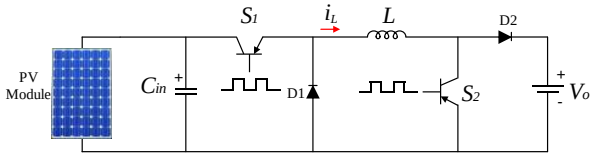

Figure 48. Positive buck-boost topology.

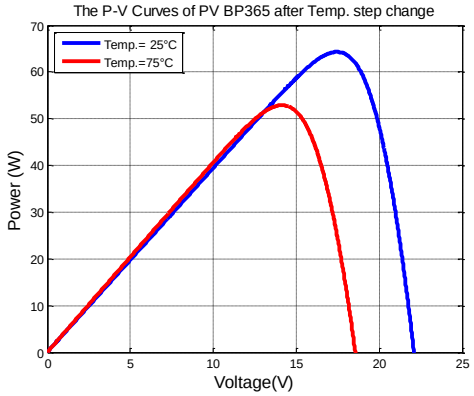

Figure 49. P-V curves of BP365 at different Temp.

B. PV Panel: The PV panel chosen is a silicon nitride multi-crystalline 65W PV-module by BP solar technology (BP365). The parameters of the PV panel are as follows: Pmax = 65W, Voc = 22.1V, Vmp = 17.6V, Imp = 3.69A, Isc = 3.99. In this work a solar array emulator is used to emulate the behavior of the chosen PV panel in the laboratory. The solar array emulator is comprised of a SL100 programmable DC power supply and a companying windows based software called Photovoltaic Power Profile Emulator (PPPE), by Magna-Power electronics. The PPPE reads in the parameters of the PV panel and controls the DC power supply such that it imitates the I-V characteristics of the panel. The variation of the I-V curve of the PV panel as a function of irradiance or temperature can be emulated with this software as well.

C. Digital Controller: A TMS320f28335 digital signal processor (DSP) from Texas Instruments (TI) is employed to implement the MPPT algorithm and low level voltage regulation loops. An I/O board containing the input voltage and current sensors and gate driver circuits is designed to accompany the DSP.

4.2.2 MPPT Algorithms

Four widely recognized MPPT algorithms are studied and compared in this work. A brief description of the four algorithms are as follows,

Perturb and Observe (P&O) Method: P&O is one of the simplest and very well-known MPPT algorithms in the literature [73], [72], [62].It perturbs the input voltage in each step and observes the resulting difference in power. Then, it decides on the direction of the voltage change for the next step.

Incremental Conductance (INC) Method: It uses the fact that the slope of the P-V curve is equal to zero at the MPP, negative on the right of MPP, and positive on the left of the MPP. Therefore, it uses a PI controller to regulate the calculated slope to zero by altering the input voltage of the converter [73], [72], [62].

Estimated Perturb-Perturb (EPP) Method: This method is introduced in [74] with the goal to improve the tracking speed and dynamic response to environmental conditions. This method is based on the P&O method with the exception that it implements one estimate process for every two perturb processes while searching for MPP. The details and a block diagram representation of this method can be found in [4].

Optimized P&O (OPO) Method: This method is introduced in [73]. In conventional P&O method the perturbation step size has a fixed magnitude, however, in OPO an average of different samples of the PV power is used to dynamically alter the size of perturbation steps. The idea behind altering the step size is to reduce the oscillations around the MPP when using a conventional P&O. The details and a block diagram representation of this method can be found in [73].

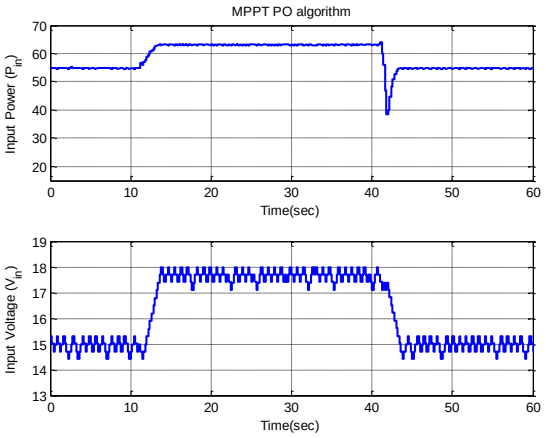

Figure 50. Response of the P&O algorithm to temperature step change.

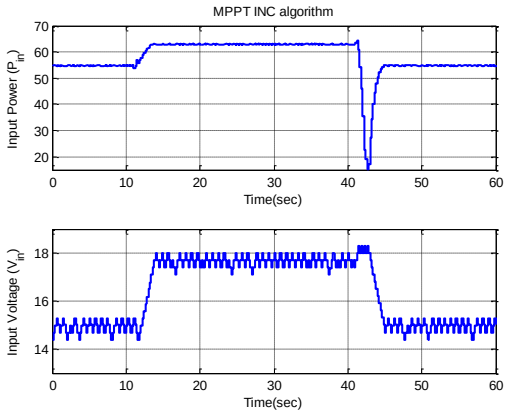

Figure 51. Response of the INC algorithm to temperature step change.

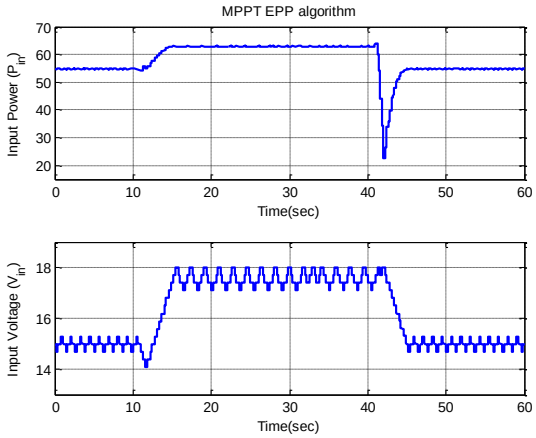

Figure 52. Response of the EPP algorithm to temperature step change.

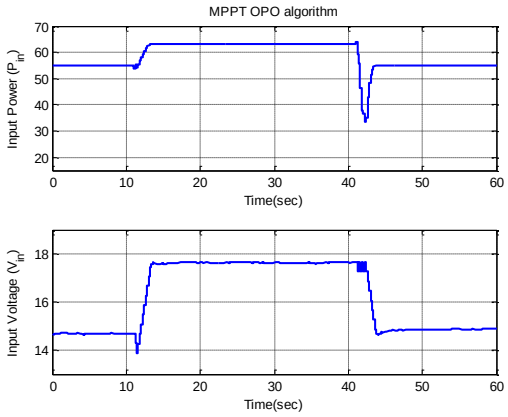

Figure 53. Response of the OPO algorithm to temperature step change.

4.2.3 Experimental Results

The experimental results for the four MPPT algorithms under study are shown in Figure 50-Figure 53. It is possible to compare the generated results in several different aspects. However, due to the page limit, in this digest the results are compared only in terms of the speed of convergence and oscillations around MPP.

According to Figure 50- Figure 53. The P&O algorithm converges to MPP in 3 seconds in step-up direction and 3.6 sec in step-down direction. The same time intervals for the INC algorithm are 3.2 seconds and 4.6 seconds. However, it takes nearly 4.8 Sec for the EPP algorithm to converge in either direction, in addition to the power drop is twice which is a huge performance degradation in comparison to conventional P&O. The OPO algorithm has, 4 seconds, convergence time, in the step-down direction, however, surprisingly it has a fast response, 2.8 seconds, in the step-up direction.

In terms of oscillations around the MPP, the OPO algorithm seems to have an advantage over all the other algorithms, while the INC algorithm seems to be the worst of the four in terms of the power drop. The oscillations of the INC, EPP and PO seem to be in the same order of magnitude, however, the OPO seems to have a slight advantage over the INC.

4.2.4 Conclusions

An experimental comparison of the dynamic response of four well-known MPPT algorithms were provided in this paper. The experiments were performed by stepping the panel surface temperature and recording the response of the MPPT algorithms. The speed of convergence and oscillations for the four algorithms proved to be different.

4.3 Proposed MPPT for Stand-alone PV System

The objective of this section is to propose a discrete-in-time (DT) ES-based MPPT method that can be implemented with reasonable processing effort on an inexpensive digital controller. The approach is to study the stability analysis of the proposed method by Lyapunov's Theorem, which should guarantee the convergence of the algorithm to the MPP as long as the sampling rate is slower than the converter's dynamic response. The proposed method should exhibit better performance in comparison to conventional hill-

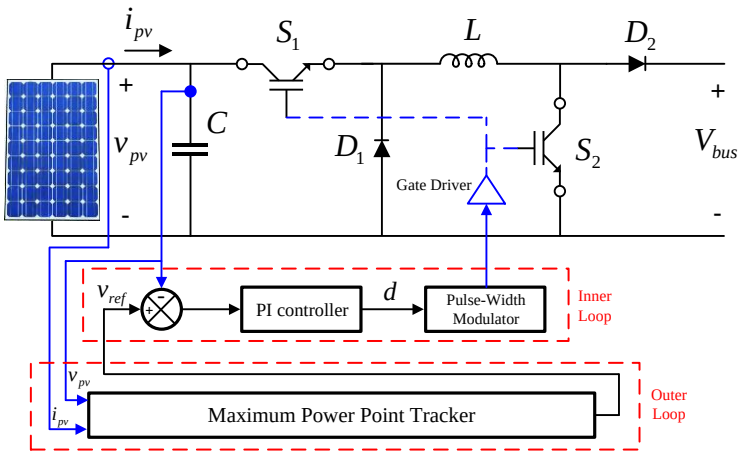

Figure 54. The positive buck-boost converter with the inner voltage control loop and outer MPP tracker.

climbing methods and requires less computational effort than artificial intelligence-based and complex mathematical methods. Figure 54, illustrates a typical positive buck-boost type power converter interfacing a PV panel to a dc bus. The results of this study will be based on the use of a positive buck-boost converter for MPPT [75].

The MPP voltage can be tracked either directly by the controller algorithm through controlling the duty cycle of the active switches of the converter, or indirectly by generating reference voltage set points by an outer MPP tracker loop and regulating the PV voltage to the generated reference points by an inner controller loop.

The aim of this work is to design the outer loop in Figure 54 in a way that it can always track the MPP voltage. The dynamic model of the converter used for PI controller design can be obtained by employing state-space averaging method [31].

4.3.1 System description and modeling

The block diagram of the proposed MPPT system is introduced in Figure 55. The Converter Dynamics block in this figure represents the general dynamic model of the converter as in (4.1).

The PV Panel block represents the P-V characteristic of the panel based on (4.2). The states of the converter (x_k) are inputs to this block.

$$\dot{x} = f(x) + g(x)u \tag{4.1}$$

$$y = h(x) \tag{4.2}$$

The output of this block is the amount of power generated by the PV panel (y_k). For the converter system of Figure 29, the state being fed to this block is the PV voltage (v_{pv}) and the output is the PV power(p_{pv}). The two Sample/Hold and Memory blocks sample the states and the PV power and form Y_k and $\bar{S}_k$ in (4.3)-(4.4).

$$Y_k \left[y_k \ \ \ldots \ \ y_{k-j} \right]^T \tag{4.3}$$

$$\bar{S}_k = \left[S(x_k) \ \ \ldots \ \ S(x_{k-J-1}) \right]^T \tag{4.4}$$

where the $S(x_k)$ is the regression vector which is represented as in (4.5)

$$S(x_k) = \left[x_k \ \ \ldots \ \ x_k^2 \right]^T \tag{4.5}$$

These matrices are then fed to the Parameter Estimator block that realizes (4.6) to generate $\hat{\gamma}_k$. The estimated parameter vector ($\hat{\gamma}_k$) is then transferred to the Maximum Power Point Tracker block to generate the desired state trajectory (x_k^d) based on (4.7).

$$\hat{\gamma}_{k+1} = (\bar{S}_k^T \bar{S}_k)^{-1} \bar{S}_k^T Y_k \tag{4.6}$$

$$x_{k+1}^d = x_k + \frac{\eta_k \hat{\gamma}_k^T \frac{\partial S(x_k)}{\partial x_k}}{\left| \hat{\gamma}_k^T \frac{\partial S(x_k)}{\partial x_k} \right|} \tag{4.7}$$

Where η_k is an adaption parameter that will be discussed further in the final analysis.

The final step is to make the PV voltage follow the desired state trajectory (x_k^d). This can be accomplished by feeding the desired trajectory (x_k^d) to the inner loop in Figure 54 as the reference points. The PV voltage regulator block in Figure 55 represents the inner

$$x_{k+1}^* = x_k^* = f(x_k^*) + g(x_k^*) u_k^* \tag{4.8}$$

voltage control loop. The inner control loop can be designed based on classical control schemes such as a simple PI controller as in section 3.2 in conjunction with a Pulse Width Modulator (PWM) that regulates the PV voltage to the desired voltage by controlling the duty cycle of the active switches of the converter. By tracking the desired trajectory (x_k^d), the states of the system of (4.1) will converge to the equilibrium point at x_k^* that coincides with the MPP,

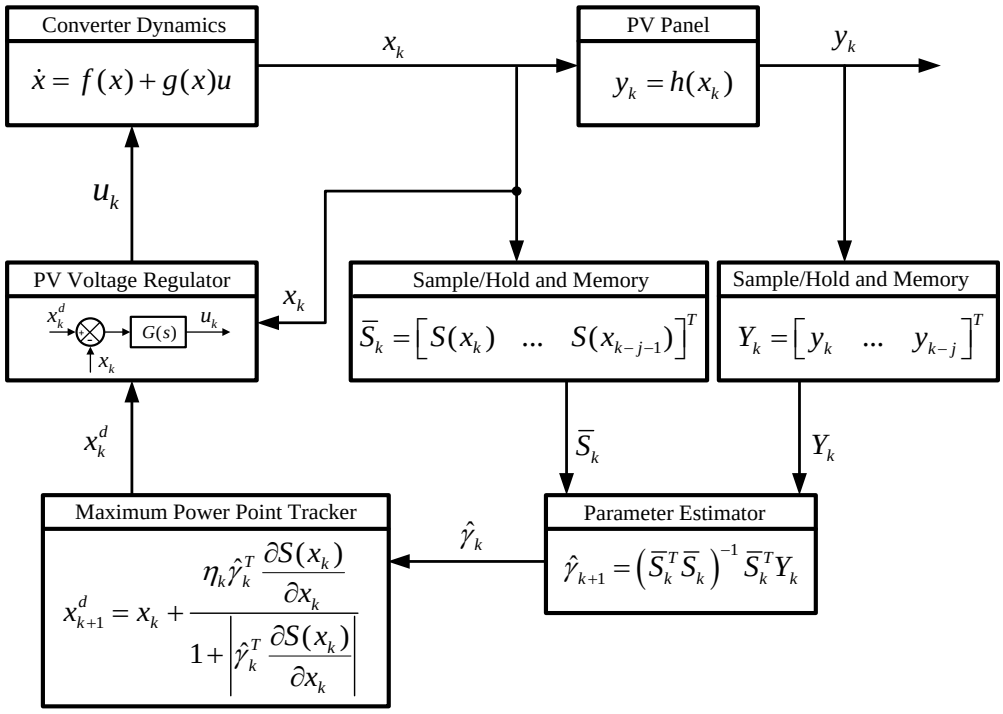

Figure 55. The block diagram of the proposed MPPT method.

4.3.2 Simulation results of the proposed MPPT method.

This section presents a preliminarily simulation results with the proposed MPPT to validate the proposed method in terms of their response to dynamic environmental conditions. Typically, the merit of a new MPPT algorithm is evaluated based on three important factors: The accuracy of tracking the MPP, extent of oscillations around the MPP, and the dynamic response to the varying temperature and irradiance conditions. Several simulations are carried-out with the proposed MPPT method to evaluate the performance of the method according to the three mentioned factors.

In the first simulation, the PV panel is set to emulate the I-V characteristics of the BP365 in STC. In STC the local irradiation is equal to 1 kW/m^2 and temperature is equal to 25℃. The converter is started with the proposed MPPT method to track the MPP. The resulting waveforms

are reported in Figure 56. This figure shows the climb of the voltage to the MPP voltage and convergence of the current to the MPP current. According to this figure, the PV voltage, current, and power are converged to 17.6 V, 3.7 A and 65W in 1 seconds after starting the simulation. Based on the BP365 parameters in STC listed above, this point is the actual MPP of the panel in STC. This verifies the effectiveness of the proposed method for tracking the MPP of the PV panel.

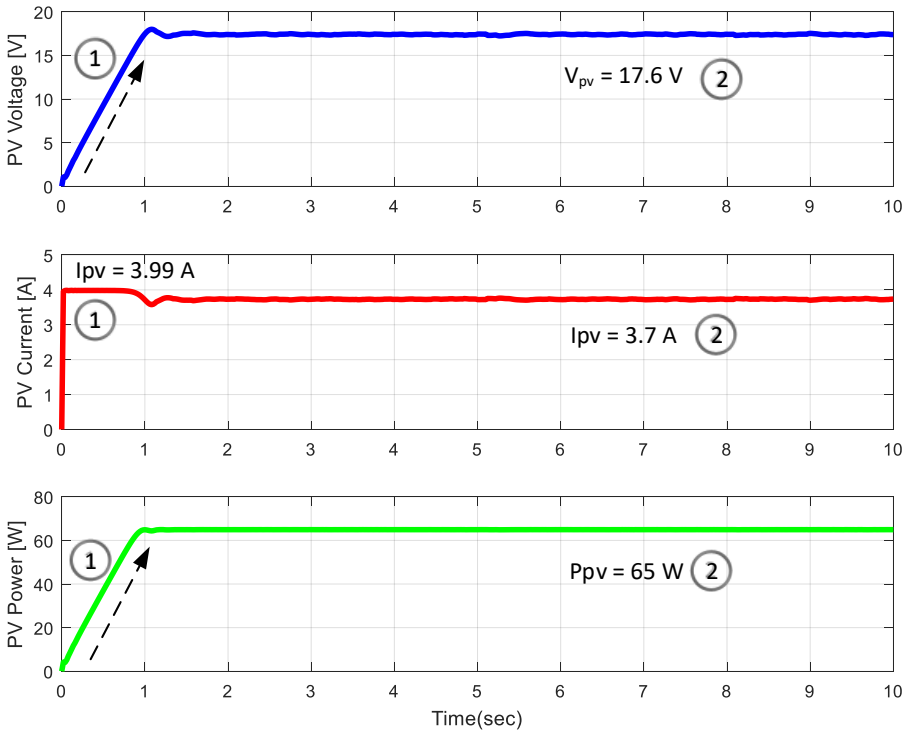

Figure 56. The resulting waveforms for the first simulation of the proposed MPPT.

The second simulation is designed to investigate the dynamic response of the proposed MPPT method to the variations in solar irradiance. In this simulation, the temperature is fixed at 25℃, however the PV panel is set the irradiance to 0.8 kW/m^2 initially, switch to 1 kW/m^2 after 3 seconds, and finally switch back to 0.8 kW/m^2. This scenario replicates a real-world situation

were the solar irradiance delivered to a PV panel is suddenly varied as a result of a passing cloud blocking the sun for a short period of time.

The resulting waveforms for this experiment are reported in Figure 57, according to this figure, initially the MPP tracker has managed to converge to 3 A and 52.8 W. Subsequent to the upsurge in irradiance it shifts the PV current and power to the MPP values in STC at 3.7 A and 65 W, and upon switching back to 0.8 kW/m^2 it recovers the current and power to 3 A and 52.8 W. The PV voltage is nearly constant at 17.6 V throughout this experiment. This confirms the effectiveness of the proposed MPPT method in dealing with varying irradiance conditions.

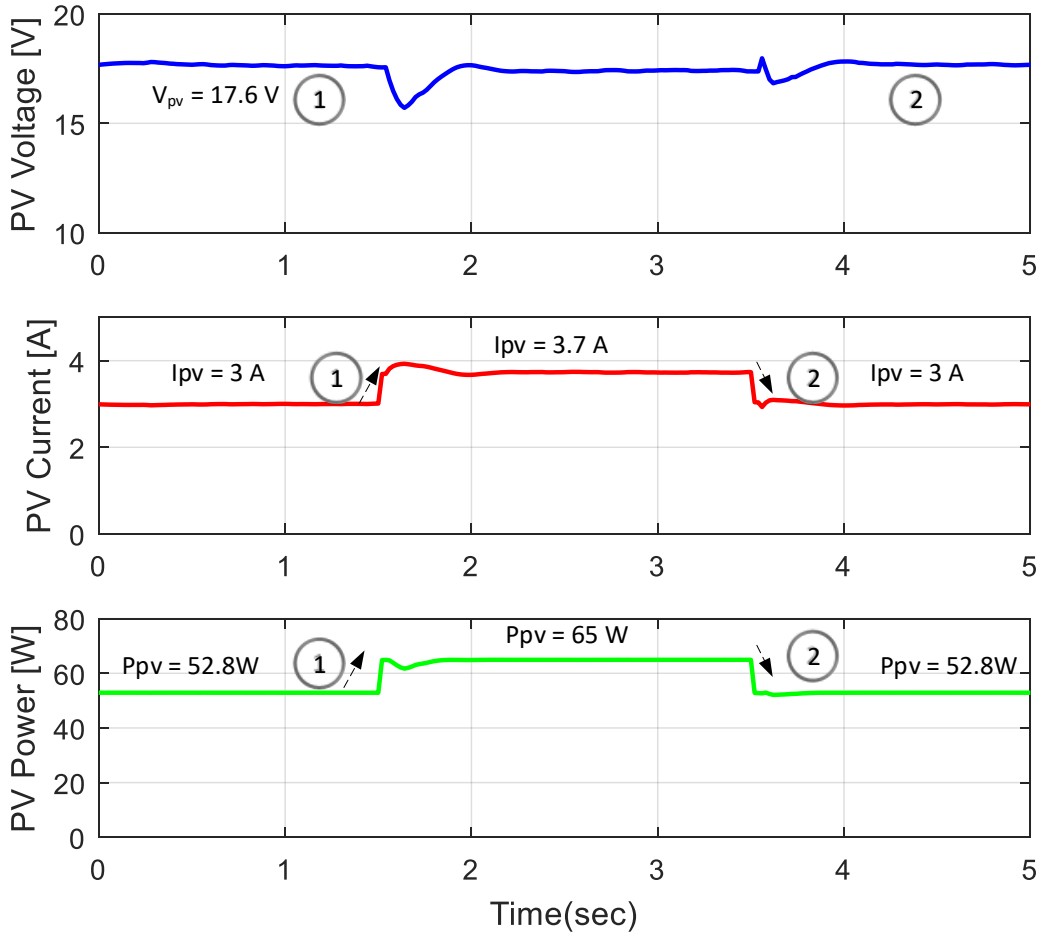

Figure 57. The resulting waveforms for the second simulation, response to irradiance step change.

The third simulation is designed to inspect the response of the proposed MPPT technique to the temperature fluctuations. In this simulation, the PV panel is set to the level of delivered irradiance fixed at 1 kW/m2 while the temperature is switched from 35℃ to 25℃ and back to 35℃

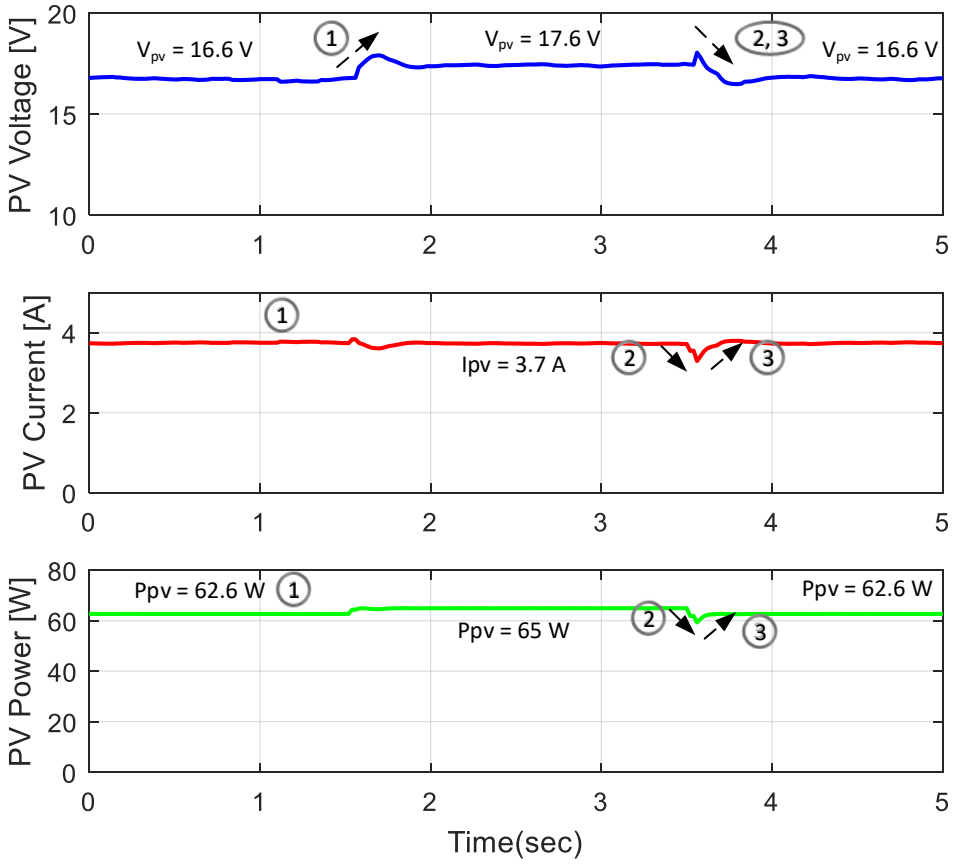

Figure 58. The resulting waveforms for the third simulation, response to temp change.

after 3 seconds. This simulation replicates the fluctuating ambient temperatures throughout a day. The resulting waveforms for this simulations are reported in Figure 58.

According to Figure 58, when temperature is equal to 35℃ the PV voltage and power are converged to 16.6 V and 62.6 W. Following the step change in temperature from 35℃ to 25℃ the proposed MPPT method shifts the PV voltage and power to the MPP in STC at 17.6 V and 65 W and then shifts it back to 16.6 V and 62.6 W subsequent to the temperature rise to 35℃. This confirms the effectiveness of the proposed MPPT method in handling of fluctuating temperature conditions. Similar to the previous experiment, the transitions happen relatively fast (in fraction of seconds), with no undesirable effects. This further illustrates the superiority of the proposed MPPT method.

4.4 Proposed MPPT for Three Phase Grid-Connected PV System

The purpose of this section is to implement the proposed MPPT method for a grid-tied q-Z-Source inverter that interfaces photovoltaic (PV) system to a three-phase utility grid. The concept of model predictive control method is used in combining with the proposed MPPT extremum seeking (ES) optimization to maximize the energy harvest form the PV system. The maximum harvested power from the PV system will be injected to the grid which will controlled based on the power factor control. The MPC controller will determine the optimal switching signals that minimizes the defined cost function to be applied to q-ZSI. The proposed method with MPC control can be implemented on inexpensive digital controller and guarantee true convergence to MPP and feature fast dynamic response in the steady sate and transient operation.

4.4.1 Description of the Proposed MPPT for q-Z-Source inverter

The purpose of this section is to propose a discrete-in-time ES based Predictive MPPT (referred to as ESP-MPPT hereinafter) method without a modulator for a q-ZSI acting as a PEI. The predictive controllers can be used for implementation of ES based MPPT algorithms on q-ZSIs

with multi-objective control functionality. Comparing to classical control schemes, MPC techniques deliver fast dynamic response with high stability marking, making them well suited for PV systems in harsh ambient condition and abnormal grid condition. Also, for the q-ZSIs, the MPC eliminates the complex modulation stage required to implement the shoot through state [76], [77]. In addition, the proposed approach features fast dynamic response and negligible oscillations around the MPP at steady state, which results in size reduction of passive components in the impedance network of ZSI which is a challenge in ZSI design [78]. The one-line block diagram of the proposed system is illustrated in Figure 59.

4.4.2 System Model

In section (3.5), the predictive modeling of the grid side that the injected current and the DC input side impedance network that the inductor current and capacitor voltage was presented. As it was mentioned early in section 3, one of the main characteristics of ZSI is its shoot-through mode for

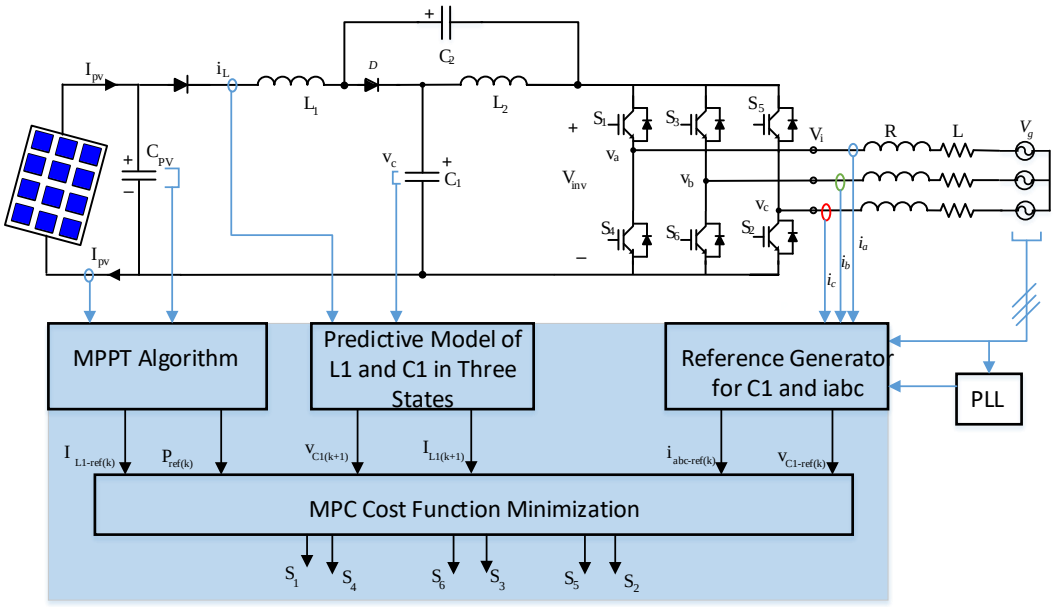

Figure 59. General schematic of the proposed power electronics interface based on grid-tied z-source inverter for photovoltaic application.

flexible boosting of the input (PV) voltage. In this mode, both switches in one leg of the inverter are simultaneously turned ON.

4.4.2.1 Photovoltaic Side

The Extremum Seeking Maximum Power Point Tracking Algorithm block in Figure 59 is responsible for determining a desirable trajectory for the L1 current that leads to MPP. The trajectory provided by this block is tracked using the MPC. The MPC approach for determination of optimal switching state at each iteration are commonly formulated in discrete-time with fixed sampling intervals. . This concept fits well with the proposed discrete-in-time ES based predictive MPPT algorithm. The general model of the ZSI impedance network can be represented as a nonlinear system in discrete-time state space form as,

$$x_{k+1} = f(x_k, u_k) \tag{4.9}$$

Where $x \in \mathbb{R}^n$ and $u \in \mathbb{R}^m$ are the states and the inputs of the inverter. For q-ZSI of Figure 59, for instance, one of the controller inputs for MPC is the reference signal generated by the Extremum Seeking-MPPT block and the states are the PV panel voltage (V_{pv}) and current (I_{pv}). The states (x) are inputs of a function that represents the P-V characteristic of the PV panel.

The MPPT algorithm is responsible for the accurate tracking of x_k^* in presence of ambient and parameter variations. It also should be able to make the system globally asymptotically stable, and be easy and economical to implement. The proposed MPPT method introduces the following iterative hill-climbing formula based on the derivative of a Linear-In-Parameter (LIP) form [] that generates a desired trajectory x_k^d for the states to climb to the MPP,

$$x_{k+1}^{d} = x_k + \frac{\eta_k \hat{\gamma}_k^T \dfrac{\partial S(x_k)}{\partial x_k}}{1 + \left| \hat{\gamma}_k^T \dfrac{\partial S(x_k)}{\partial x_k} \right|} \tag{4.10}$$

The estimated parameter vector ($\hat{\gamma}_k$) is then transferred to the *Desired Trajectory Determination* block to generate the desired state trajectory (x_k^d) based on the above mentioned equation. Thus two of the reference signals ($I_{L1-\text{ref}}(k), P_{\text{ref}}(k)$) for the MPC cost function formulation are determined as shown in Figure 59. The MPC cost function, which will be developed at the end of this section, will track the desired trajectory (x_k^d) by operating in the shoot through and non-shoot through states.The optimization of the MPC cost function is performed with a sampling time at least two times smaller than the sampling time of the Extremum Seeking-MPPT algorithm (desirable trajectory determination algorithm.

4.4.2.2 Grid Side

At the grid side, the controller should inject the maximum power harvested from the PV panel and control the ratio of active/reactive power injected to the grid (power factor control). For the ZSI nine vectors are considered including six active states, two null states, and one shoot through state. Then the MPC cost function evaluates and compare these resulting indictor current and capacitor voltage values with the desired active and reactive power to be injected to the grid. The active power reference ($P_{\text{ref}}(k)$) can be determined from the proposed ESP-MPPT method explained earlier in this section. The reactive power reference ($Q_{\text{ref}}(k)$) can be zero for unity p.f.

operation or can be set by the grid operator according to grid requirement as an ancillary service [79].

4.4.2.3 MPC Cost Function and Optimization

The control objectives for the q-ZSI are the inductor (L1) current (I_{L1}), the capacitor (C1) voltage (V_{C1}), the grid side active power (P), and the grid side reactive power (Q). The desired reference signal for each of these control objectives were explained earlier in this section. In summary, the reference signal for inductor (L1) current (I_{L1}) and active power (P) are determined from the ESP-MPPT. The reference signal for reactive power (Q) is set according to grid requirement by the grid operator. The capacitor (C1) voltage (V_{C1}) reference signal is assumed to be 600 V which is more than double the grid voltage of 208 V_{RMS} to transfer the active power easily. The reference value for (V_{C1}) can be different according to active/reactive power requirement of the grid.

Finally, in order to determine the optimal switching signal for the ZSI, a single cost function g is developed with all these control objectives and their corresponding desired values. The designed cost function g subject to minimization is given by,

$$g = \lambda \left\| i_{L1ref}(k) - i_{L1ref}(k+1) \right\| + \lambda \left\| i_{\alpha\beta ref}(k) - i_{\alpha\beta ref}(k+1) \right\| \qquad (4.11)$$

4.4.3 Simulation Results

The proposed controller is implemented and simulation results are provided that validate the operation of the method. The proposed system has negligible current and voltage ripple in the impedance network, thus smaller impedance network elements can be used for the ZSI. One of the challenges of employing impedance source inverters is the size of the passive elements in the impedance network.

To start the analysis, the operation of system with solar irradiance of 1000 W/m^2 is evaluated. The results for simulation are shown in Figure 60, Figure 61 and Figure 62.The three phase grid side current and the inductor L1 current of the impedance network at the PV side are shown in Figure 61. As it is shown, the injected current to grid has negligible harmonic distortions. Figure 61 validates the unity power factor operation of the system. The pulsating dc-link voltage demonstrates the operation of q-ZSI in shoot through (when the dc-link voltage is zero) and non-shoot through (when the dc-link voltage is non-zero) sates.

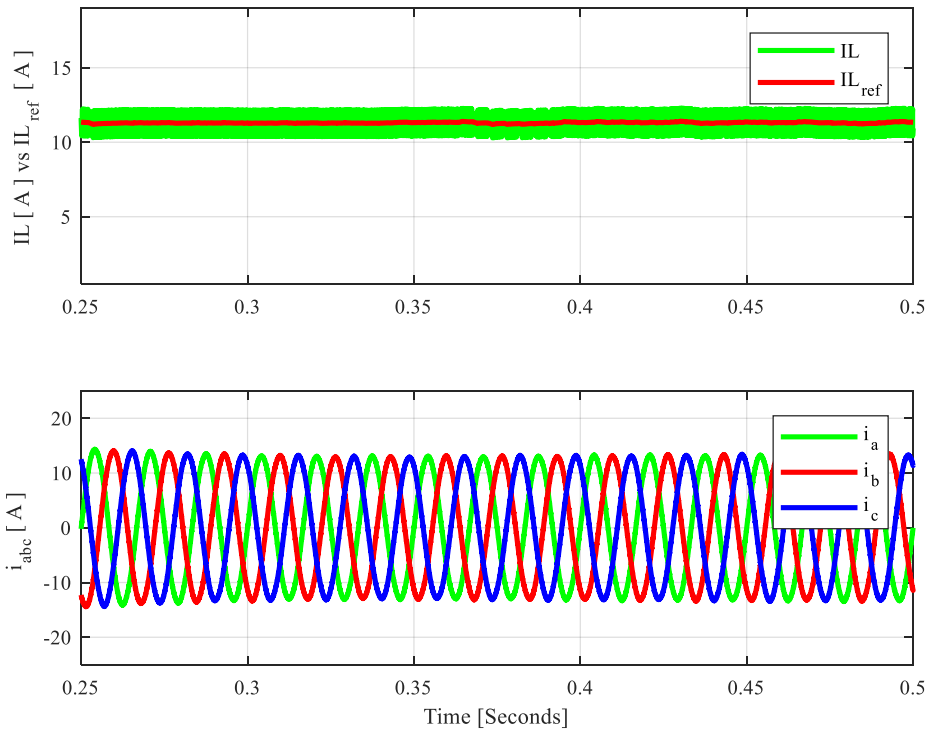

Figure 60. System operation in steady state solar irradiance at 1000W/m^2, the inductor current, the three phase grid side current.

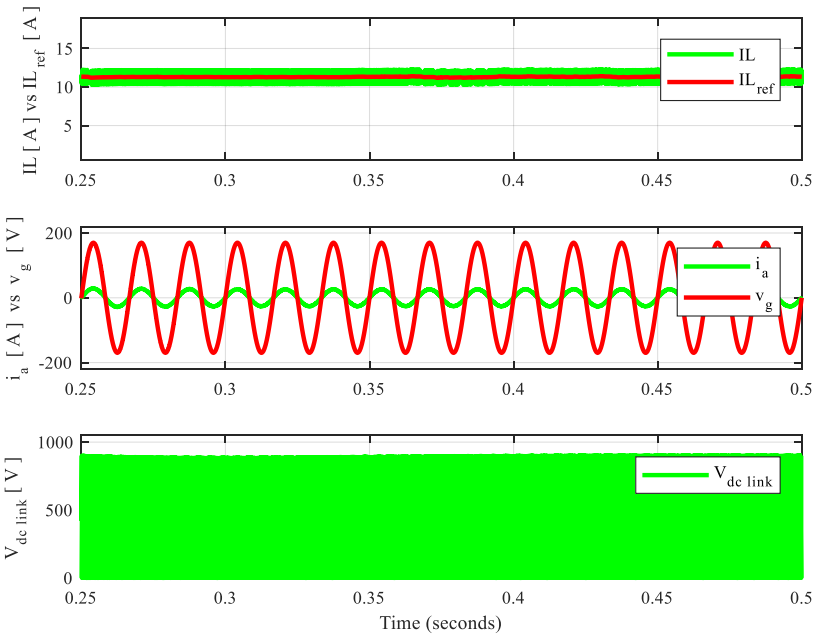

Figure 61. System operation in steady state solar irradiance at 1000W/m^2, the inductor current, phase (a) of the grid voltage and the current, the dc-link voltage

In Figure 62 , The reference q-ZSI capacitor voltage is set to be 600V and the reference output peak value of the injected grid current and the inductor current are calculated from the reference output power. In addition, the output injected current i_a tracks the reference current with high dynamic performance. Moreover, the DC-Link voltage is witched and constant. An important fact it worth to be mentioned from all the provided result so far, the inductor current is continuous which is in favour of PV application. Since the discontinuous input current is not easy to be controlled and can shorten the life time of the PV panel. For the mentioned one reason above, the q-ZSI with a continuous current was chosen over the ZSI which has discontinues current.

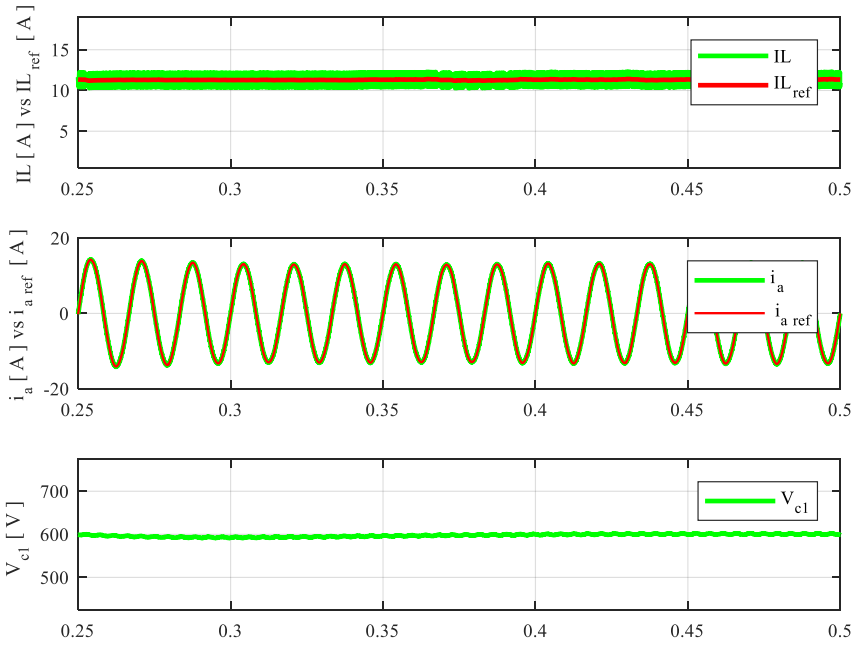

Figure 62. System operation in steady state solar irradiance at 1000W/m^2, the inductor current, phase (a) of the current, the capacitor voltage

4.5 Results of experimental implementation for the proposed MPPT for the stand-alone system

The block diagram of the experimental setup for evaluation of the proposed MPPT algorithm is illustrated in Figure 63. As visualized, the experimental setup is comprised of a PV module emulator, a positive buck-boost power converter, a digital controller, and a 24 V battery. The actual lab setup of the system is shown in Figure 64.

The merits of the new MPPT algorithm are evaluated based on three factors: the accuracy of tracking the MPP, the extent of oscillations around the MPP, and the dynamic response to the varying temperature and irradiance conditions. Several experiments are carried out on the experimental system with the proposed MPPT method to evaluate its performance.

In the first experiment, the PV emulator is set to emulate the I-V characteristics of the BP365 in STC. In STC, the local irradiation is equal to 1.0kW/m$_2$ and temperature is equal to 25^{o}C. The converter is started with the proposed MPPT method to track the MPP. The resulting waveforms for this experiment are reported. The data from this experiment are recorded using the DSP directly

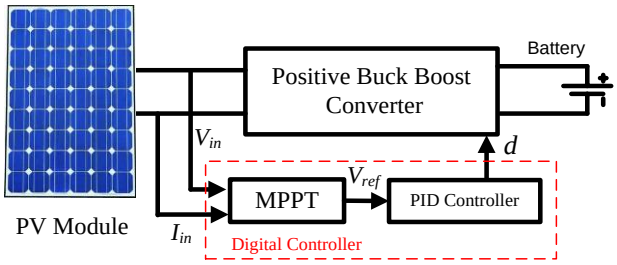

Figure 63. Block diagram of the experimental setup

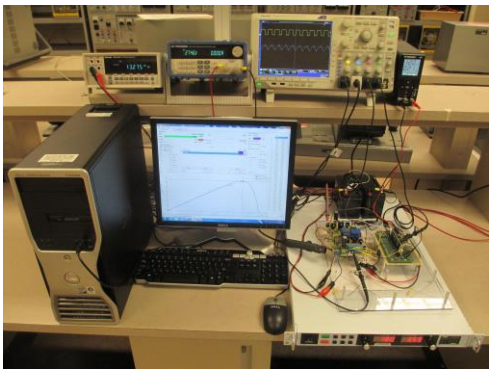

Figure 64. Actual experimental setup in lab

and plotted using MATLAB for better visualization. The resulting waveforms are shown in Figure 65 and Figure 66.

Figure 65 displays the waveforms for PV voltage, current, and power vs. time. According to this figure, the PV voltage, current, and power are converged to 17.6 V, 3.7 A, and 65 W in 12 seconds. Based on the BP365 parameters in STC listed above, this point is the actual MPP of the panel in STC. This verifies the effectiveness of the proposed method for tracking the MPP of the PV panel. To further validate the operation of the proposed method, the power vs. voltage data points for this experiment are plotted on top of the P-V characteristic curve of the BP365 in Figure 66. This figure clearly shows the climb of the proposed algorithm to the MPP.

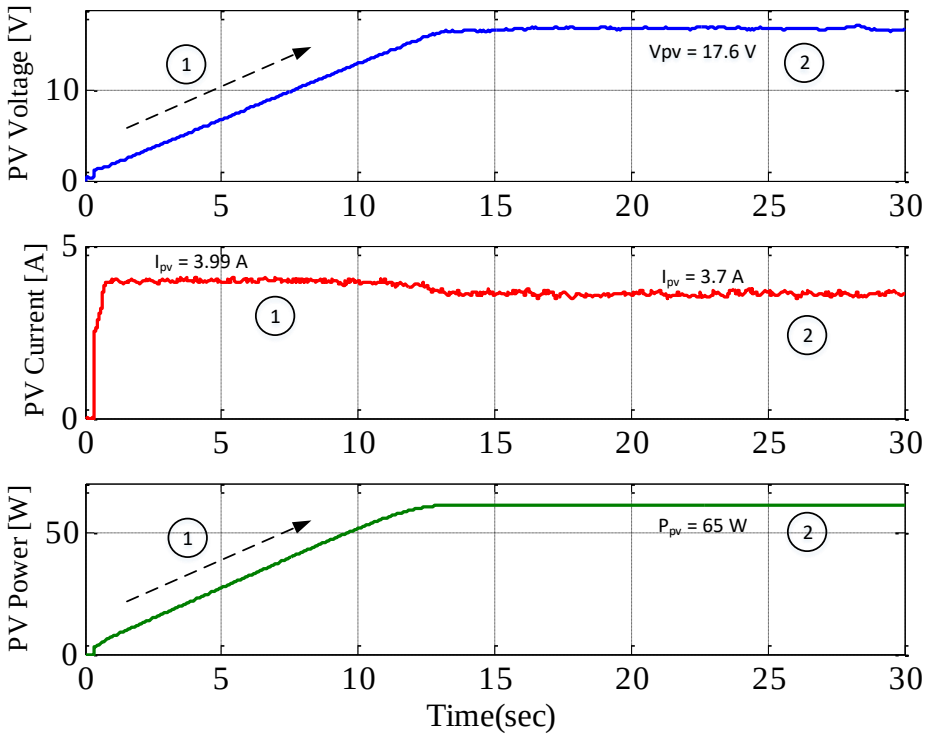

Figure 65. The resulting waveforms for the first experiment. The PV voltage, current, and power waveforms vs. time.

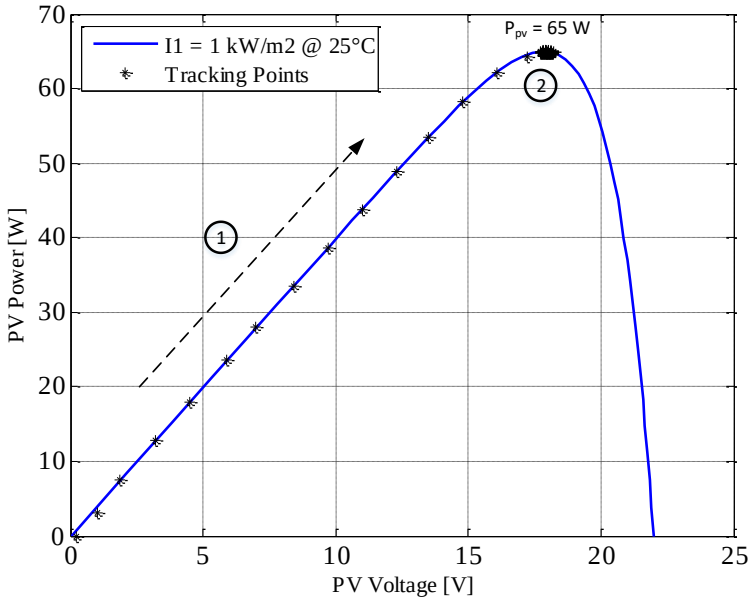

Figure 66. The power vs. voltage data points (black stars) plotted on top of the BP 365 P-V curve (blue curve).

The second experiment is designed to investigate the dynamic response of the proposed MPPT method to the variations in solar irradiance. In this experiment the temperature is fixed at 25℃, however the PV emulator is programmed to set the irradiance to 0.7 kW/m^2 initially, switch to 1 kW/m^2 after 30 seconds, and finally switch back to 0.7 kW/m^2. This scenario replicates a real-world situation were the solar irradiance delivered to a PV panel is suddenly varied as a result of a passing cloud blocking the sun for a short period of time. The resulting waveforms for this experiment are reported in Figure 67 and Figure 68. Similar to the previous experiment, the waveforms for PV voltage, current, and power vs. time are illustrated in Figure 67. According to this figure, initially the MPP tracker has managed to converge to 2.56 A and 46.1 W.

Subsequent to the upsurge in irradiance it shifts the PV current and power to the MPP values in STC at 3.7 A and 65 W, and upon switching back to 0.7 kW/m^2 it recovers the current and power to 2.56 A and 46.1 W. The PV voltage is nearly constant at 17.6 V throughout this experiment.

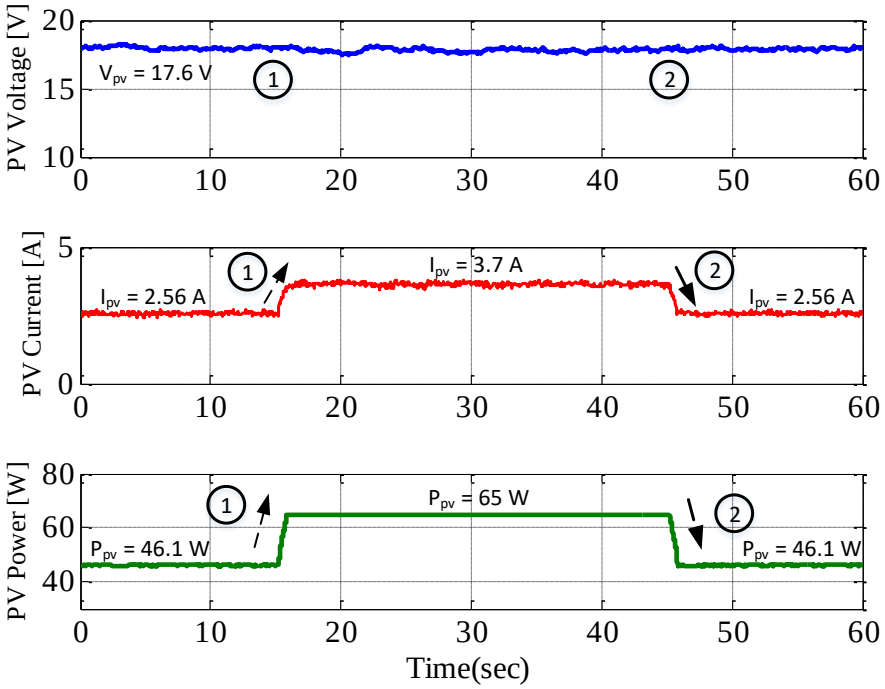

Figure 67. The resulting waveforms for the second experiment. The PV voltage, current, and power waveforms vs. time.

The power vs. voltage data points for this experiment are plotted on top of the two P-V characteristic curves of the BP365 for 1 kW/m^2 and 0.7 kW/m^2 irradiation in Figure 68. According to this figure, the convergence point at 17.6 V and 46.1 W is the true MPP of the BP365 when the

received irradiance is equal to 0.7 kW/m^2. This confirms the effectiveness of the proposed MPPT method in dealing with varying irradiance conditions.

Moreover, according to Figure 67 the transition from the MPP in STC to the new MPP and reverse takes place in less than 2 seconds with no overshoot and no additional oscillations. Comparing with the traditional MPPT methods, the dynamic response of the proposed method is far more superior in terms of speed and shape of response [80].

The third experiment is designed to inspect the response of the proposed MPPT technique to the temperature fluctuations. In this experiment using the PV emulator the level of delivered irradiance to the panel is fixed at 1 kW/m^2 while the temperature is switched from 75℃ to 25℃

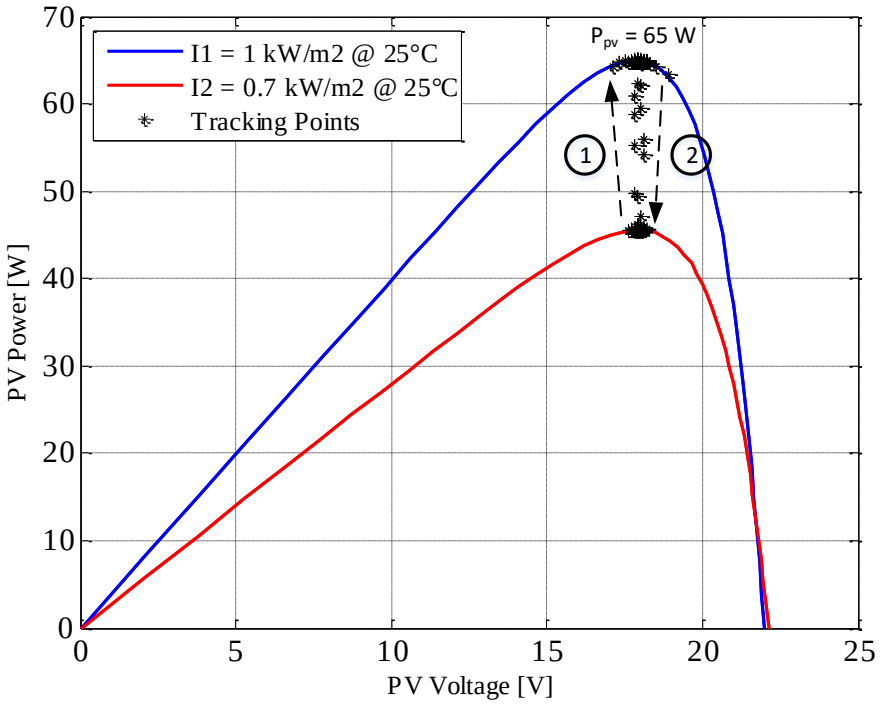

Figure 68. The power vs. voltage data points (black stars) plotted on top of the BP 365 P-V curves for 1 kW/m2 (blue curve) and 0.7 kW/m2 (red curve) irradiance.

and back to 75℃ after a short period of time. This experiment replicates the fluctuating ambient temperatures throughout a day. The resulting waveforms for this experiment are reported in Figure 69 and Figure 70. According to Figure 69, when temperature is equal to 75℃ the PV voltage and power are converged to 15.1 V and 56.6 W. Following the step change in temperature from 75℃ to 25℃ the proposed MPPT method shifts the PV voltage and power to the MPP in STC at 17.6 V and 65 W and then shifts it back to 15.1 V and 56.6 W subsequent to the temperature rise to 75℃.

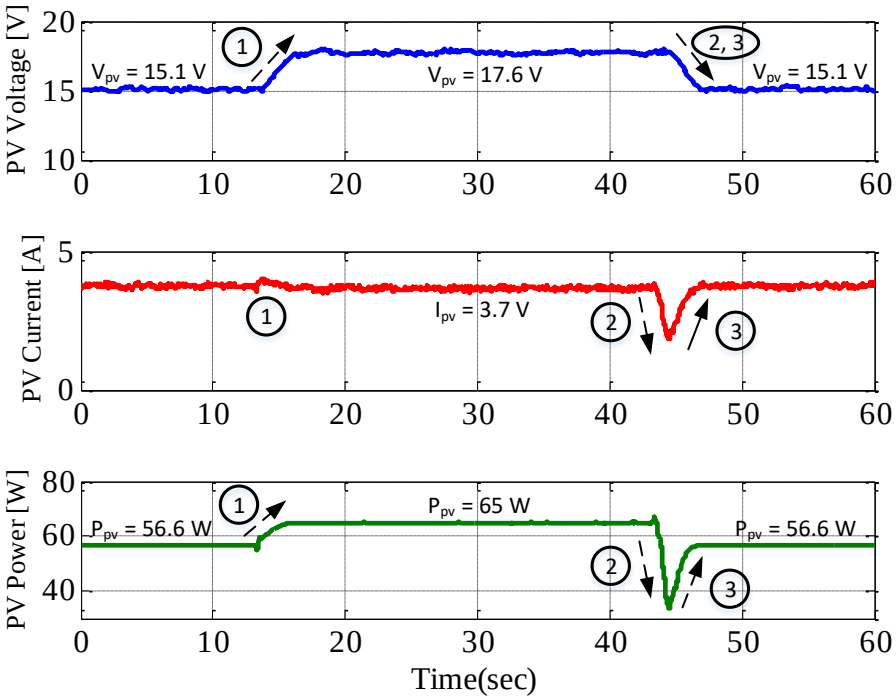

Figure 69. The resulting waveforms for the third experiment. The PV voltage, current, and power waveforms vs. time.

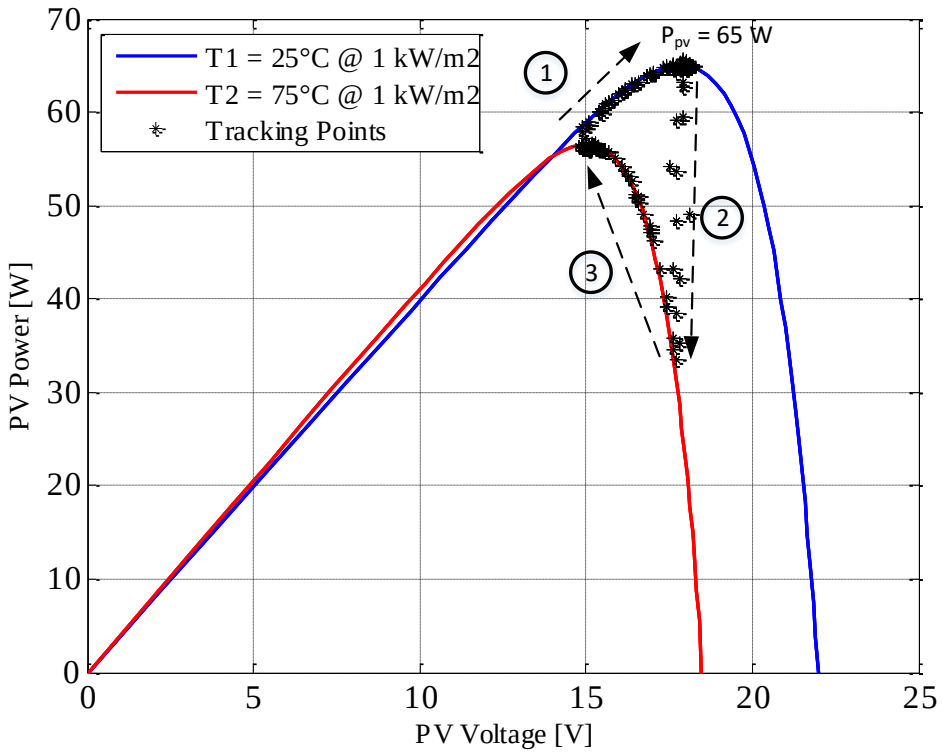

Figure 70. The power vs. voltage data points (black stars) plotted on top of the BP 365 P-V curves for 25°C (blue curve) and 75°C (red curve) temperature.

Similar to before, the power vs. voltage data points for this experiment are plotted on top of the two P-V characteristic curves of the BP365 for 25℃ and 75℃ in Figure 70. According to this figure, the convergence point at 15.1 V and 56.6 W is the true MPP of the BP365 when the panel temperature is equal to 75℃. This confirms the effectiveness of the proposed MPPT method in handling of fluctuating temperature conditions. Similar to the previous experiment, the transitions happen relatively fast (less than 2 seconds), with no undesirable effects. This further illustrates the superiority of the proposed MPPT method over the traditional MPPT methods [80].

4.5.1 Experimental comparison of proposed MPPT to P&O MPPT

In this section, the performance of the proposed method is compared to P&O MPPT algorithm experimentally. The P&O method is designed to perform at their best in terms of dynamic response and oscillations around MPP. Figure 71, Figure 72 and Figure 73 compares the performance of the proposed method vs. the P&O method.

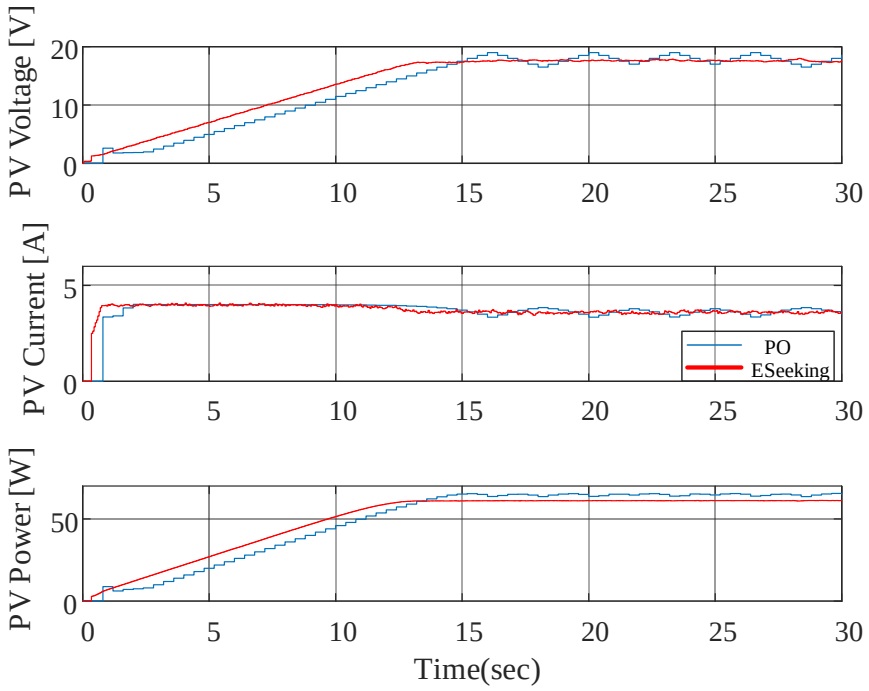

Figure 71. Comparing performance of the proposed ESP-MPPT method for startup.

Figure 71 illustrates the tracking performance at the startup and the oscillations of the two methods. According to this figure, the startup time of the two methods are comparable, while the amplitude of oscillations of the proposed method is much less than the P&O method.

Figure 72 demonstrates the performance of the two methods when the temperature is stepped down from 25ºC to 75ºC. According to this figure the proposed method performs well by tracking the new MPP voltage in a few seconds while the P&O algorithm struggles and takes much longer to converge.

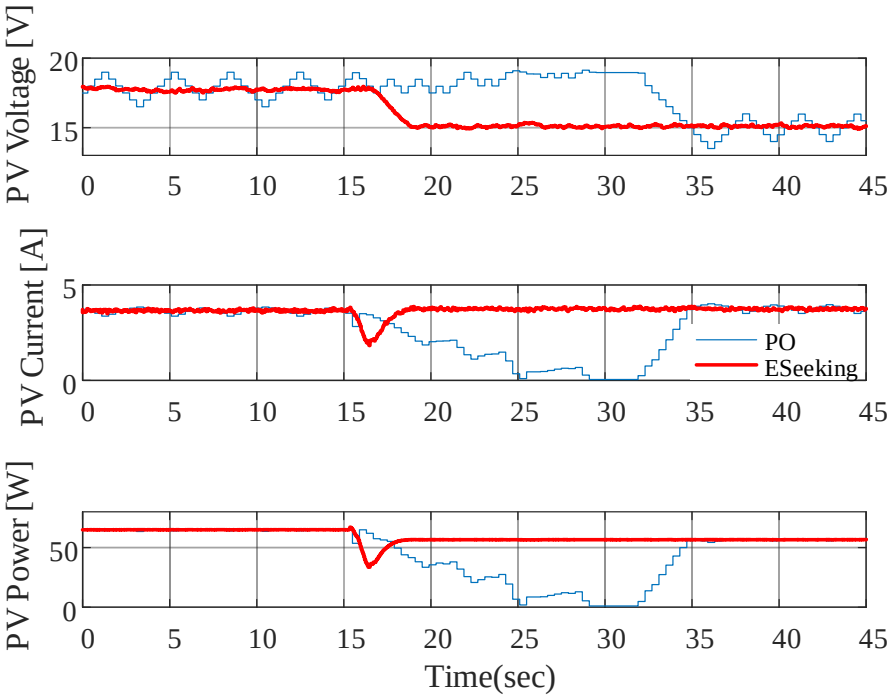

Figure 72. Comparing performance of the proposed ES to PO-MPPT method for a step change in temperature.

Figure 73 compares the performance of the two methods when irradiance is stepped up from 0.7kW/m2 to 1kW/m2. According to this figure, the proposed method maintains the voltage very close to the MPP voltage during the transient and regulates the current to the MPP current in a few seconds. However, the P&O algorithm is tricked into decreasing the voltage which leads to much longer convergence time.

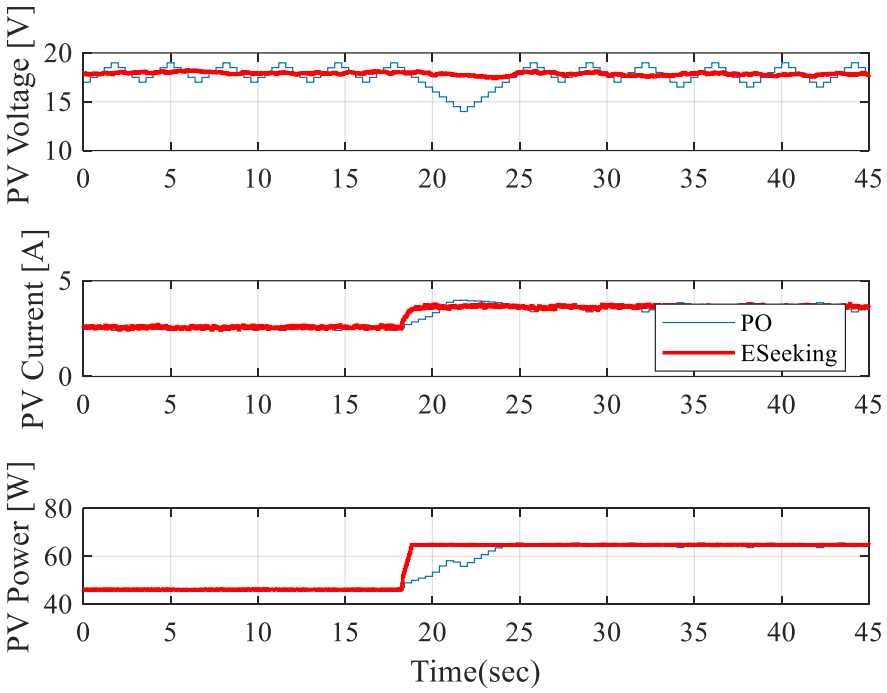

Figure 73. Comparing performance of the proposed ES to PO -MPPT method for a step change in irradiance.

4.6 Simulation results for q-ZSI grid-connected for a step change

This section evaluates the dynamic response of the system to a step change in solar irradiance from 1000 W/m^2 to 750 W/m^2. Figure 74, Figure 75, and Figure 76 demonstrate the system performance for this experiment. The system is initially operating at solar irradiance of 1000 W/m^2, then at instant t_1=0.34s the solar irradiance is step changed from 1000 W/m^2 to 750 W/m^2. Figure 74 shows the dynamic response of the inductor L1 current and the three phase injected current to the grid. At the PV side, as it is shown by inductor L1 current, the controller tracks the new MPP fast, without significant overshoot/undershoot. At the grid side, the system reaches to

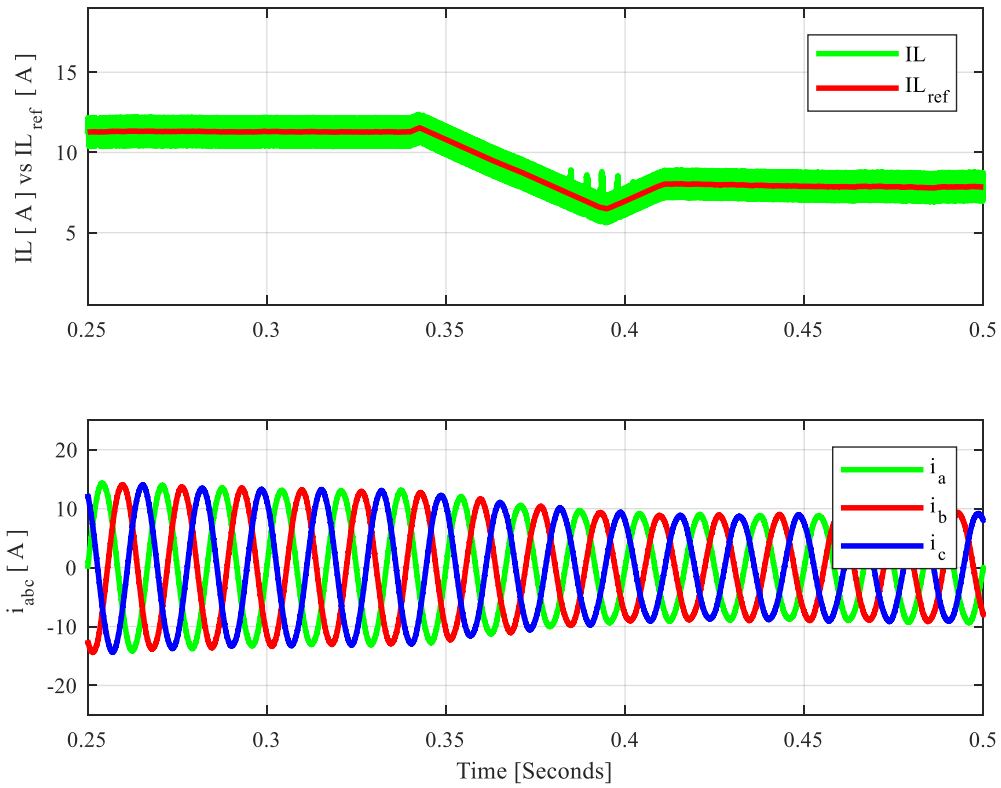

Figure 74. Dynamic response of the system to step change in solar irradiance from 1000 W/m^2 to 750 W/m^2, the three phase grid side current and the inductor L1 current in the impedance network.

its new operating point around 70ms after the step change occurred at instant t_1. The injected currents to the grid do not show any inrush effect due to step change in solar irradiance.

Figure 75 illustrates the effect of solar irradiance change on unity power factor operation of the system. As it is captured in Figure 75, the system is injecting the current into the grid with smooth reduction in the grid peak current without change in its phase to maintain unity power factor operation. The effect of this step change in solar irradiance on capacitor C1 voltage in the impedance network is shown in Figure 76. As it is captured, the change in solar irradiance has

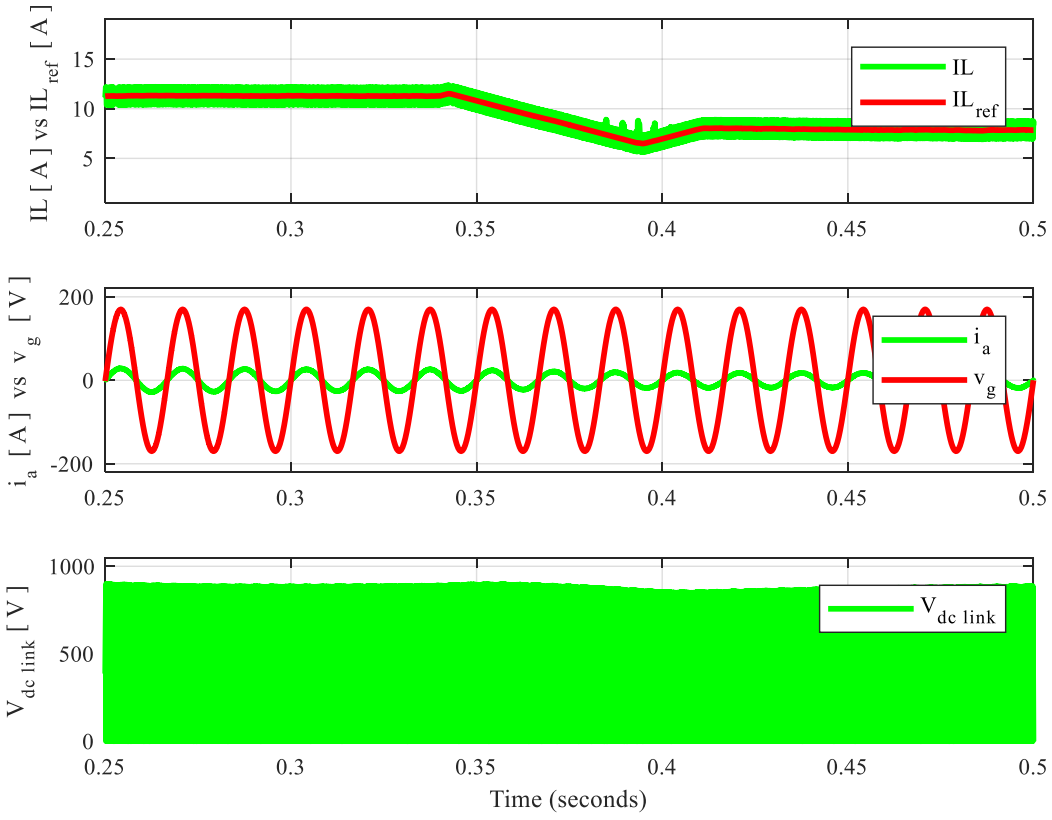

Figure 75. Dynamic response of the system to step change in solar irradiance from 1000 W/m^2 to 750 W/m^2, phase (a) of grid voltage and current, pulsating dc-link voltage, and inductor L1 current in the impedance network.

minor effects on the C1 voltage as it is expected according to the PV characteristics curve when there is a change in solar irradiance.

Moreover, the response of the system to a step change in the ambient temperature of the PV panel is evaluated for a step of 25 deg C to 50 deg C. The system performance for this experiment is shown in Figure 77. As it is captured, after the step change at instant t2, the inductor L1 current moves to its new MPP operation and coordinates very fast to extract the maximum available power from the PV array. This will results in lower peak current at grid side. The grid side current is changed smoothly without experiencing inrush current.

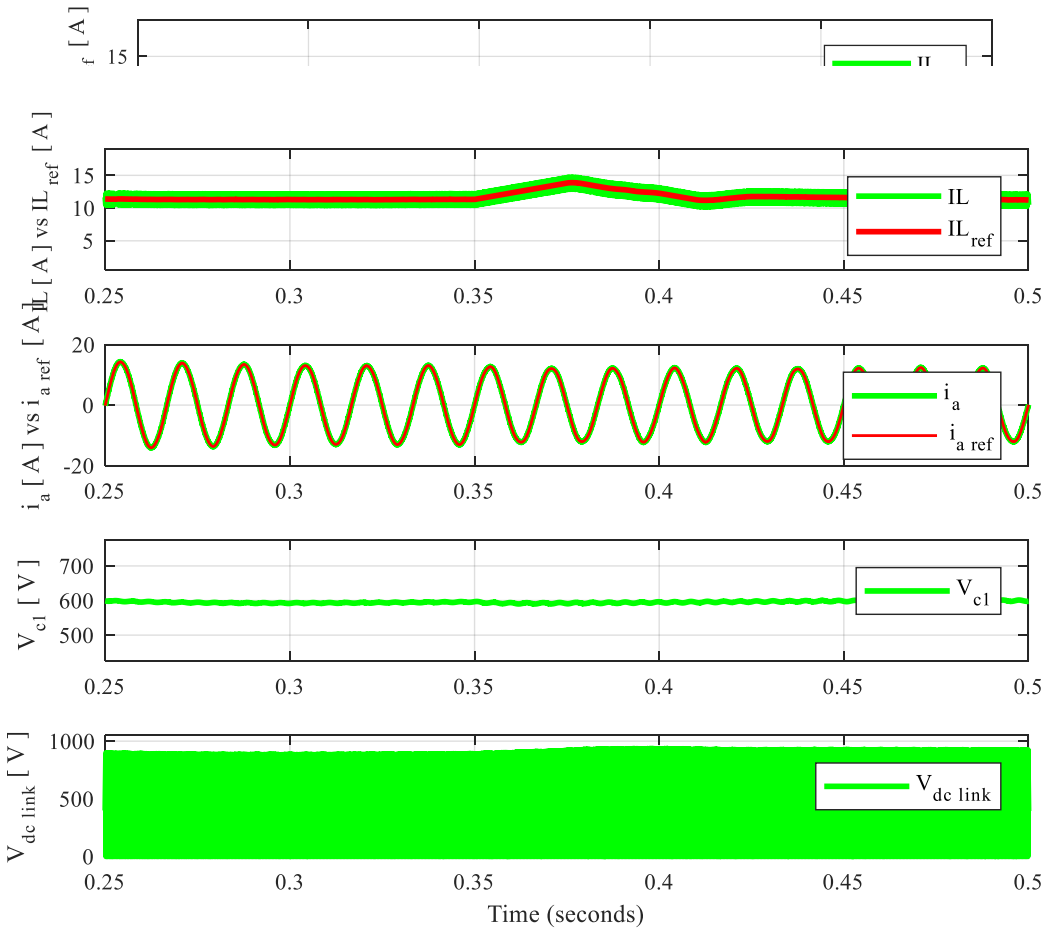

Figure 77. Dynamic response of the system to step change in ambient temperature of the PV panel from 25 deg C to 50 deg C, capacitor C1 voltage and inductor L1 current in the impedance network, pulsating dc-link voltage, and phase (a) of grid current.

Finally, Figure 78 shows the dynamic response of active power, the MPP voltage and MPP current to step change in solar irradiance from 1000 W/m2 to 750 W/m2 at instant t1. As it is shown, the system response to this step change is fast without significant overshoot/undershoot. Although a step change in solar irradiance is not happening in realistic conditions, but this scenario is considered as the worst case situation for the proposed system evaluation in this work.

To conclude Figure 79 compares the performance of the proposed method (ES) with improved or optimized incremental conductance (OPINC) method when irradiance is stepped down from 1kW/m2 to 0.7kW/m2. According to this figure, the proposed method maintains the voltage very close to the MPP voltage during the transient and regulates the current to the MPP current in a few seconds. However, the OPINC algorithm is trapped into decreasing the voltage which leads to much slower convergence time.

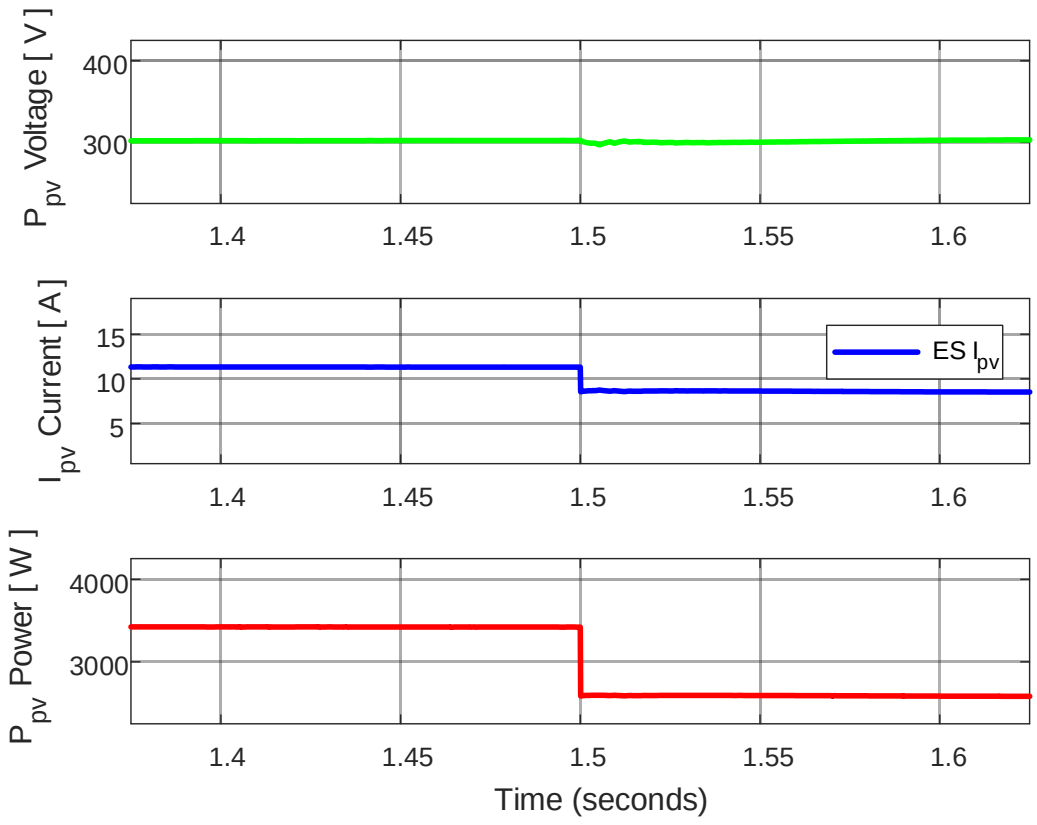

Figure 78. System response to step change in solar irradiance from 1000 W/m^2 to 750 W/m^2, the active power, MPP voltage and MPP current.

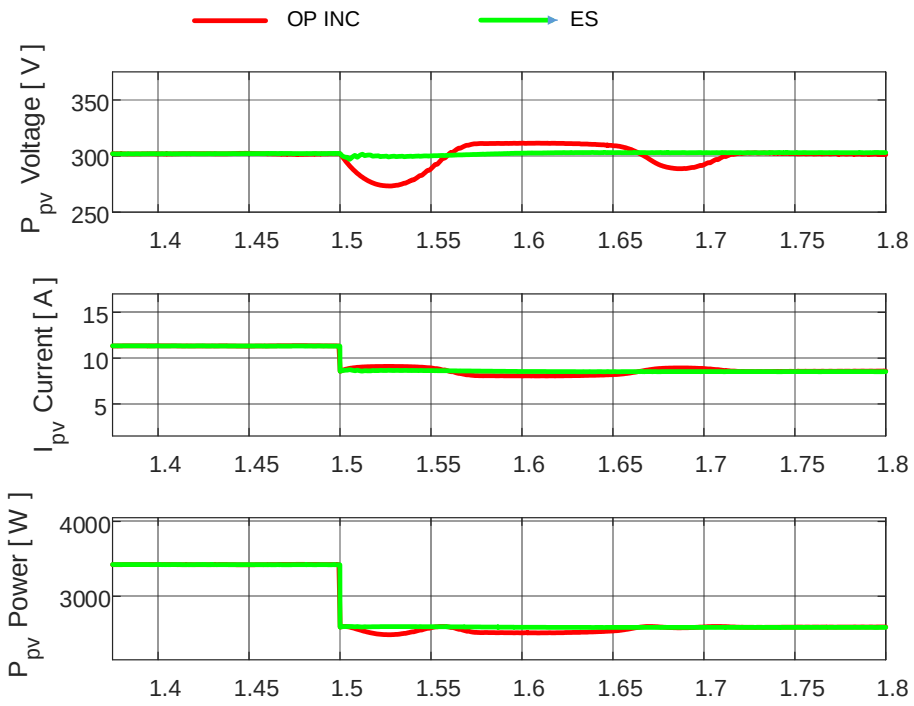

Figure 79. Comparing performance of the proposed ES to OPINC-MPPT method for a step change in irradiance.

Chapter 5

5 Conclusion and Future work

5.1 Conclusion

Photovoltaic systems are one of the most promising renewable electric power generation systems due to their low environment impact and high availability of solar irradiation in most geographical locations [81]. However, the downside to the PV power systems is the cost of the required equipment. To compensate for the high initial cost of the PV infrastructure, it is imperative that a solar-generation system always operates near its most efficient operating point, thus Maximum Power Point Tracking (MPPT) for PV systems is essential [21].

In this work, a comprehensive framework for control and MPPT for two-types of PV systems, a stand-alone system and a three-phase grid connected system, was proposed. The design objective for each case was to offer more efficiency, better performance, increased reliability, simplified implementation, and to reduce the costs associated with the power electronic stage. The proposed controller satisfies a key criteria for PV systems, i.e. controlling the stand-alone converter input voltage or the inverter input current of the grid-tied system, to extract the maximum available power from the connected PV modules.

The standalone system under study was a conventional Buck-Boost convertor interfacing a PV module to a battery. A classical PI controller was designed to regulate the input voltage of the converter according to the stability criteria. The reference values for the PI controller were generated by the proposed Maximum Power Point Tracking (MPPT) algorithm. Simulation and experimental results were provided to validate the design performance under different environmental conditions.

Grid-tied PV systems commonly use a two-stage power electronics interface [81]: an upstream dc/dc power conversion stage from the PV module to a dc link energy buffer element, and a downstream dc/ac power conversion stage from the energy buffer element to the grid. Commonly, in these PV systems architectures, the MPPT is implemented in the upstream dc/dc conversion stage and is only responsible for transferring the maximum available energy from the PV panel to the intermediate energy buffer. The responsibility of the downstream stage is to control the flow of energy to the grid by generating controllable ac voltages synchronized with the grid voltage.

The use of a two-stage topology is necessitated due to the inherent limitation of the dc/ac inverters for stepping up/down the voltage freely. Commonly, the conventional inverters classified as Voltage-Source Inverters (VSI) can only step-down the voltage while the Current-Source Inverters (CSI) can only step-up the voltage (the VSIs can have a boost factor of almost 1.15 which is not enough for most applications) [82, 83]. Therefore, a conventional dc/ac inverter in general, cannot both step-down and step-up the voltage freely. As mentioned above, the MPP voltage of a PV module is not constant and needs to be tracked by the PV harvesting system. This voltage can be higher/lower than the grid voltage based on the environmental conditions, necessitating a power conversion system that can step up/down the voltage freely to track the MPP accurately. Hence, the dc/dc stage in the conventional systems is used to step up/down the dc link voltage freely when necessary.

Due to this limitation of conventional VSIs and CSIs, this author decided to design the grid-tied system based on a newly introduced converter topology, denoted as the impedance-source converter, that undermines the limitations with the conventional VSIs and CSIs [84]. As mentioned previously, these new converters provide several advantages for a variety of

applications with different input-output requirements [85-88]. In particular, a class of dc/ac inverters designed based on the concept of impedance-source conversion, denoted as a Quasi-Impedance source power inverter (q-ZSI), can step up/down the voltage freely, and thus are very well suited for designing single-stage PV harvesting systems. Moreover, the q-ZSIs feature several additional advantages over the conventional inverters that makes them even more appealing for energy harvesting systems [24]. Although very resourceful, the q-ZSIs operate differently than conventional inverters due to incorporation of energy storage elements in their input port and thus require new and innovative control strategies to boost their performance.

This dissertation has presented a new MPPT method that maximizes the amount of power extracted by the q-ZSI from the PV panel based on the concept of Model Predictive Control (MPC) [89] in conjunction with Extremum Seeking (ES) optimization algorithm. Due to promising performance of MPC methods for MPPT of PV systems, there have been works in the literature that explore the possibility of using MPC for MPPT [90, 91]. However, as mentioned previously, these works each come with some shortcomings such as indirect use of predictions for MPPT, not addressing the use of MPC for q-ZSI converters, and inadequate performance of the designed system. However in the presented work in this dissertation, decisions on the trajectory of the PV voltage and current of the q-ZSI are directly made through a predictive control approach by taking advantage of ES optimization algorithm and the provided experimental results clearly demonstrate superior performance compared to classical MPPT algorithms. Additionally, at the grid-side, the proposed controller for q-ZSI injects the maximum available power determined by the MPPT algorithm to grid with adjustable power factor (p.f.) by minimizing the MPC cost function to determine the switching signals for the inverter.

To achieve stable, effective, and economically viable MPPT methods, numerous optimization algorithms have been explored over the past few years. As mentioned previously, the authors in

[92] classify a large number of the proposed methods in the literature very nicely into the two categories of simple to implement but with limited performance [91, 93-96], and high performance but with taxing computational burden for implementation [97, 98]. Although MPPT algorithms have been investigated extensively in the literature for various applications lately [63-66], not many MPPT methods based on the concept of Extremum Seeking (ES) have been proposed so far. The simplicity and the rigorous supporting mathematics of ES-based control methods are the main motivation for the authors to pursue design of an ES-based MPPT algorithm [67]. The proposed ES-based MPPT in this dissertation strikes a balance between simplicity of implementation and performance which makes it particularly useful for PV applications that require high performance with limited available computational resources of small-scale embedded controllers. On the other hand, as mentioned previously, although there are a number of ES-based MPPT methods proposed in the literature lately [68, 99, 100], all the available methods are based on continuous-in-time formulations which need analog realization or high speed processors to guarantee the continuity and convergence of the controller [99]. The proposed MPPT algorithm in this work, however, was designed based on a new discrete-in-time Extremum-Seeking (ES) technique for tracking the maximum power point of the PV modules using the two discussed PV systems. This proposed MPPT method has introduced a new iterative formula that generates the desired trajectory for the states to climb to the MPP. As it proven in chapter 4, the generated desired trajectory will direct the system toward the MPP. As result, the designed estimator can grantee the convergence to the equilibrium point that coincides with the MPP.

The main features of the proposed MPPT and control system are:

(a) True maximum power point tracking under dynamic ambient condition with fast dynamic response and negligible oscillation around MPP,

(b) A predictive optimal controller based on ES algorithm is proposed without needing a modulator that can be implemented with reasonable processing effort on an inexpensive digital controller,

(c) High efficiency and reliable operation due to the single power conversion q-ZSI,

(d) Minimizing the required size of passive component in the impedance network of q-ZSI due to negligible oscillation around MPP by the proposed MPPT algorithm; it is well-known in literature that smaller current ripple reduces the size of passive component required in the PEI [101, 102]. This is especially important because according to [103], one of the challenges of employing impedance source inverters is the large size of the passive elements in the impedance network. Consequently, by using the proposed method, the footprint area of a q-ZSI converter can be reduced significantly. Although the proposed method can be used in conjunction with other converters, its benefits will signify when used with a q-ZSI,

(e) Simple control architecture without needing many cascaded loops as in classical linear control methods for q-ZSIs,

(f) The proposed method can also be applied to a wide range of PV systems aside from the two systems discussed in this work.

The operation of the proposed MPPT method was experimentally verified using both the stand-alone and the grid tied systems. The merits of the new MPPT algorithm were evaluated based on three factors: the accuracy of tracking the MPP, the extent of oscillations around the MPP, and the dynamic response to the varying temperature and irradiance conditions. According to the provided

experimental results, the proposed method demonstrated a better performance in both systems and faster dynamic behavior compared to the well-known conventional P&O method for a step change in irradiance or temperature. In addition, it was shown that the proposed method has almost negligible oscillations and higher efficiency at the MPP compared to P&O method.

5.2 Future Work

The future work pursuant to this dissertation opened new challenges that require further studies and analysis can be listed as the following:

- Implementing measures into the proposed MPPT to incorporate partial shading
- Exploring more various isolated and non-isolated DC-DC convertors topology for the stand-alone PV system
- Considering model predictive control methods with different constraints can be added to incorporate the advantages of MPC
- Adapting important safety requirements can be addressed in grid connected power electronics systems
- Using of Wide Gap Devices in order to maximize the performance and reduce the overall cost of the power conversion system

References

[1] RENEWABLES 2017 GLOBAL STATUS REPORT. (2017). *RENEWABLES 2017 GLOBAL STATUS REPORT*. Available: http://www.ren21.net/gsr-2017/

[2] Solar Energy Industries Association. (2017). *Solar Energy*. Available: http://www.seia.org/about/solar-energy

[3] national laboratory of the U.S. Department of Energy. (2017). *Wind Energy Basics*. Available: https://www.nrel.gov/about/

[4] Wikipedia. (2017). *Photovoltaic system*. Available: https://en.wikipedia.org/wiki/Photovoltaic_system

[5] T. Burton, N. Jenkins, D. Sharpe, and E. Bossanyi, *Wind energy handbook*: John Wiley & Sons, 2011.

[6] O. Hasnaoui, J. Belhadj, and M. Elleuch, "Direct Drive Permanent Magnet Synchronous Generator Wind Turbine investigation (Low Voltage Ride Through capability, Dynamic behaviour in presence of grid disturbance)," *http\\: journal. esrgroups. org/jes/papers/4,* vol. 3, 2008.

[7] OFFICE of ENERGY EFFICIENCY & RENEWABLE ENERGY. (2017). *Types of Hydropower Plants*. Available: https://energy.gov/eere/water/types-hydropower-plants

[8] A. Goetzberger and V. U. Hoffmann, *Photovoltaic solar energy generation* vol. 112: Springer Science & Business Media, 2005.

[9] A. Khaligh and O. C. Onar, *Energy harvesting: solar, wind, and ocean energy conversion systems*: CRC press, 2010.

[10] D. P. Hohm and M. E. Ropp, "Comparative study of maximum power point tracking algorithms," *Progress in Photovoltaics: Research and Applications,* vol. 11, pp. 47-62, 2003.

[11] M. B. Shadmand, R. S. Balog, and H. Abu-Rub, "Model Predictive Control of PV Sources in a Smart DC Distribution System: Maximum Power Point Tracking and Droop Control," *Energy Conversion, IEEE Transactions on,* vol. PP, pp. 1-9, 2014.

[12] J. W. Kimball and P. T. Krein, "Discrete-Time Ripple Correlation Control for Maximum Power Point Tracking," *Power Electronics, IEEE Transactions on,* vol. 23, pp. 2353-2362, 2008.

[13] A. A. Abushaiba, S. M. M. Eshtaiwi, and R. Ahmadi, "Comparative analysis of dynamic performance of four prominent Maximum Power Point Tracking algorithms in photovoltaic systems using realistic experimental implementation," in *2016 IEEE International Conference on Electro Information Technology (EIT)*, 2016, pp. 0576-0579.

[14] C.-C. Liu, K.-H. Ding, J. R. Young, and J. F. Beutler, "A systematic method for the stability analysis of multiple-output converters," *IEEE transactions on power electronics,* pp. 343-353, 1987.

[15] J. Liu, X. Feng, F. C. Lee, and D. Borojevich, "Stability margin monitoring for DC distributed power systems via perturbation approaches," *IEEE transactions on power electronics,* vol. 18, pp. 1254-1261, 2003.

[16] K. Mehran, D. Giaouris, and B. Zahawi, "Stability analysis and control of nonlinear phenomena in boost converters using model-based Takagi–Sugeno fuzzy approach," *IEEE Transactions on Circuits and Systems I: Regular Papers,* vol. 57, pp. 200-212, 2010.

[17] A. Urtasun, P. Sanchis, and L. Marroyo, "Adaptive Voltage Control of the DC/DC Boost Stage in PV Converters With Small Input Capacitor," *IEEE Transactions on Power Electronics,* vol. 28, pp. 5038-5048, 2013.

[18] S. J. Chiang, H. J. Shieh, and M. C. Chen, "Modeling and Control of PV Charger System With SEPIC Converter," *IEEE Transactions on Industrial Electronics,* vol. 56, pp. 4344-4353, 2009.

[19] F. Z. Peng, "Z-source inverter," *IEEE Transactions on industry applications,* vol. 39, pp. 504-510, 2003.

[20] P. Loh, M. Vilathgamuwa, Y. Lai, G. Chua, and Y. Li, "Pulse-Width Modulation of Z-Source Inverters," *IEEE Transactions on Power Electronics,* vol. 20, pp. 1346-1355, 2005.

[21] M. Shen, A. Joseph, J. Wang, F. Z. Peng, and D. J. Adams, "Comparison of traditional inverters and $ Z $-source inverter for fuel cell vehicles," *IEEE Transactions on Power Electronics,* vol. 22, pp. 1453-1463, 2007.

[22] Y. Li, J. Anderson, F. Z. Peng, and D. Liu, "Quasi-Z-source inverter for photovoltaic power generation systems," in *Applied Power Electronics Conference and Exposition, 2009. APEC 2009. Twenty-Fourth Annual IEEE*, 2009, pp. 918-924.

[23] M. Mosa, H. Abu-Rub, and J. Rodriguez, "High performance predictive control applied to three phase grid connected Quasi-Z-Source Inverter," in *Industrial Electronics Society, IECON 2013-39th Annual Conference of the IEEE*, 2013, pp. 5812-5817.

[24] Y. Liu, H. Abu-Rub, B. Ge, and O. Ellabban, *Impedance source power electronic converters*: John Wiley & Sons, 2016.

[25] M. Trabelsi and L. Ben-Brahim, "Development of a grid connected photovoltaic power conditioning system based on flying capacitors inverter," in *Systems, Signals and Devices (SSD), 2011 8th International Multi-Conference on*, 2011, pp. 1-6.

[26] Y. Huang, M. Shen, F. Z. Peng, and J. Wang, " Z -Source Inverter for Residential Photovoltaic Systems," *IEEE Transactions on Power Electronics,* vol. 21, pp. 1776-1782, 2006.

[27] J. Rodriguez and P. Cortes, *Predictive control of power converters and electrical drives* vol. 40: John Wiley & Sons, 2012.

[28] A. Ioinovici, *Fundamentals and hard-switching converters*: John Wiley & Sons, 2013.

[29] P. T. Krein, *Elements of power electronics* vol. 126: Oxford University Press New York, 1998.

[30] A. A. Abushaiba, S. M. M. Eshtaiwi, and R. Ahmadi, "Dynamic performance analysis of a PV charger system," in *IECON 2014 - 40th Annual Conference of the IEEE Industrial Electronics Society*, 2014, pp. 2069-2074.

[31] O. Ellabban, M. Mosa, H. Abu-Rub, and J. Rodriguez, "Model predictive control of a grid connected quasi-Z-source inverter," in *Industrial Technology (ICIT), 2013 IEEE International Conference on*, 2013, pp. 1591-1596.

[32] S. Jain, S. P. Nanduri, M. B. Shadmand, R. S. Balog, and H. Abu-Rub, "Direct decoupled active and reactive predictive power control of grid-tied quasi-Z-source inverter for photovoltaic applications," in *Energy Conversion Congress and Exposition (ECCE), 2017 IEEE*, 2017, pp. 4582-4588.

[33] E. Koutroulis, K. Kalaitzakis, and N. C. Voulgaris, "Development of a microcontroller-based, photovoltaic maximum power point tracking control system," *Power Electronics, IEEE Transactions on,* vol. 16, pp. 46-54, 2001.

[34] O. Wasynezuk, "Dynamic Behavior of a Class of Photovoltaic Power Systems," *Power Apparatus and Systems, IEEE Transactions on,* vol. PAS-102, pp. 3031-3037, 1983.

[35] S. Jain and V. Agarwal, "A new algorithm for rapid tracking of approximate maximum power point in photovoltaic systems," *Power Electronics Letters, IEEE,* vol. 2, pp. 16-19, 2004.

[36] N. Femia, G. Petrone, G. Spagnuolo, and M. Vitelli, "Optimization of perturb and observe maximum power point tracking method," *Power Electronics, IEEE Transactions on,* vol. 20, pp. 963-973, 2005.

[37] N. Kasa, T. Iida, and C. Liang, "Flyback Inverter Controlled by Sensorless Current MPPT for Photovoltaic Power System," *Industrial Electronics, IEEE Transactions on,* vol. 52, pp. 1145-1152, 2005.

[38] A. F. Boehringer, "Self-Adapting dc Converter for Solar Spacecraft Power Supply Selbstanpassender Gleichstromwandler fÃ¿r die Energieversorgung eines Sonnensatelliten," *Aerospace and Electronic Systems, IEEE Transactions on,* vol. AES-4, pp. 102-111, 1968.

[39] K. Yeong-Chan, L. Tsorng-Juu, and C. Jiann-Fuh, "Novel maximum-power-point-tracking controller for photovoltaic energy conversion system," *Industrial Electronics, IEEE Transactions on,* vol. 48, pp. 594-601, 2001.

[40] M. Veerachary, T. Senjyu, and K. Uezato, "Neural-network-based maximum-power-point tracking of coupled-inductor interleaved-boost-converter-supplied PV system using fuzzy controller," *Industrial Electronics, IEEE Transactions on,* vol. 50, pp. 749-758, 2003.

[41] T. Hiyama, S. Kouzuma, and T. Imakubo, "Identification of optimal operating point of PV modules using neural network for real time maximum power tracking control," *Energy Conversion, IEEE Transactions on,* vol. 10, pp. 360-367, 1995.

[42] R. Kyoungsoo and S. Rahman, "Two-loop controller for maximizing performance of a grid-connected photovoltaic-fuel cell hybrid power plant," *Energy Conversion, IEEE Transactions on,* vol. 13, pp. 276-281, 1998.

[43] S. J. Chiang, K. T. Chang, and C. Y. Yen, "Residential photovoltaic energy storage system," *Industrial Electronics, IEEE Transactions on,* vol. 45, pp. 385-394, 1998.

[44] J. A. M. Bleijs and J. A. Gow, "Fast maximum power point control of current-fed DC-DC converter for photovoltaic arrays," *Electronics Letters,* vol. 37, pp. 5-6, 2001.

[45] E. V. Solodovnik, S. Liu, and R. A. Dougal, "Power controller design for maximum power tracking in solar installations," *Power Electronics, IEEE Transactions on,* vol. 19, pp. 1295-1304, 2004.

[46] C. Yang and K. M. Smedley, "A cost-effective single-stage inverter with maximum power point tracking," *Power Electronics, IEEE Transactions on,* vol. 19, pp. 1289-1294, 2004.

[47] M. A. Masoum, H. Dehbonei, and E. F. Fuchs, "Theoretical and Experimental Analyses of Photovoltaic Systems with Voltage and Current-Based Maximum Power Point Tracking," *Power Engineering Review, IEEE,* vol. 22, pp. 62-62, 2002.

[48] M. B. Shadmand, M. Mosa, R. S. Balog, and H. A. Rub, "An improved MPPT technique for high gain DC-DC converter using model predictive control for photovoltaic applications," in *2014 IEEE Applied Power Electronics Conference and Exposition - APEC 2014*, 2014, pp. 2993-2999.

[49] R. Khanna, Q. Zhang, W. E. Stanchina, G. F. Reed, and Z. H. Mao, "Maximum Power Point Tracking Using Model Reference Adaptive Control," *IEEE Transactions on Power Electronics,* vol. 29, pp. 1490-1499, 2014.

[50] C. Konstantopoulos and E. Koutroulis, "Global Maximum Power Point Tracking of Flexible Photovoltaic Modules," *IEEE Transactions on Power Electronics,* vol. 29, pp. 2817-2828, 2014.

[51] P. Sharma and V. Agarwal, "Exact Maximum Power Point Tracking of Grid-Connected Partially Shaded PV Source Using Current Compensation Concept," *IEEE Transactions on Power Electronics,* vol. 29, pp. 4684-4692, 2014.

[52] R. C. N. Pilawa-Podgurski and D. J. Perreault, "Submodule Integrated Distributed Maximum Power Point Tracking for Solar Photovoltaic Applications," *IEEE Transactions on Power Electronics,* vol. 28, pp. 2957-2967, 2013.

[53] M. Sokolov and D. Shmilovitz, "A Modified MPPT Scheme for Accelerated Convergence," *IEEE Transactions on Energy Conversion,* vol. 23, pp. 1105-1107, 2008.

[54] Y. Levron and D. Shmilovitz, "Maximum Power Point Tracking Employing Sliding Mode Control," *IEEE Transactions on Circuits and Systems I: Regular Papers,* vol. 60, pp. 724-732, 2013.

[55] R. Haroun, A. E. Aroudi, A. Cid-Pastor, G. Garcia, C. Olalla, and L. Martínez-Salamero, "Impedance Matching in Photovoltaic Systems Using Cascaded Boost Converters and Sliding-Mode Control," *IEEE Transactions on Power Electronics,* vol. 30, pp. 3185-3199, 2015.

[56] J. M. Blanes, F. J. Toledo, S. Montero, and A. Garrigós, "In-Site Real-Time Photovoltaic I–V Curves and Maximum Power Point Estimator," *IEEE Transactions on Power Electronics,* vol. 28, pp. 1234-1240, 2013.

[57] Y. C. Chang, C. L. Kuo, K. H. Sun, and T. C. Li, "Development and Operational Control of Two-String Maximum Power Point Trackers in DC Distribution Systems," *IEEE Transactions on Power Electronics,* vol. 28, pp. 1852-1861, 2013.

[58] L. V. Hartmann, M. A. Vitorino, M. B. d. R. Correa, and A. M. N. Lima, "Combining Model-Based and Heuristic Techniques for Fast Tracking the Maximum-Power Point of Photovoltaic Systems," *IEEE Transactions on Power Electronics,* vol. 28, pp. 2875-2885, 2013.

[59] R. C. N. Pilawa-Podgurski and D. J. Perreault, "Sub-module integrated distributed maximum power point tracking for solar photovoltaic applications," in *2012 IEEE Energy Conversion Congress and Exposition (ECCE)*, 2012, pp. 4776-4783.

[60] B. Somaiah and V. Agarwal, "Recursive Estimation-Based Maximum Power Extraction Technique for a Fuel Cell Power Source Used in Vehicular Applications," *IEEE Transactions on Power Electronics,* vol. 28, pp. 4636-4643, 2013.

[61] S. Qin, S. T. Cady, A. D. Domínguez-García, and R. C. N. Pilawa-Podgurski, "A distributed approach to MPPT for PV sub-module differential power processing," in *2013 IEEE Energy Conversion Congress and Exposition*, 2013, pp. 2778-2785.

[62] T. Esram and P. L. Chapman, "Comparison of Photovoltaic Array Maximum Power Point Tracking Techniques," *Energy Conversion, IEEE Transactions on,* vol. 22, pp. 439-449, 2007.

[63] K. S. Peterson and A. G. Stefanopoulou, "Extremum seeking control for soft landing of an electromechanical valve actuator," *Automatica,* vol. 40, pp. 1063-1069, 6// 2004.

[64] N. J. Killingsworth and M. Krstic, "PID tuning using extremum seeking: online, model-free performance optimization," *Control Systems, IEEE,* vol. 26, pp. 70-79, 2006.

[65] L. Yaoyu, M. A. Rotea, G. T. C. Chiu, L. G. Mongeau, and P. In-Su, "Extremum seeking control of a tunable thermoacoustic cooler," *Control Systems Technology, IEEE Transactions on,* vol. 13, pp. 527-536, 2005.

[66] H. Zargarzadeh, S. Jagannathan, and J. A. Drallmeier, "Extremum-seeking for nonlinear discrete-time systems with application to HCCI engines," in *American Control Conference (ACC), 2014*, 2014, pp. 861-866.

[67] K. B. Ariyur and M. Krstic, *Real-Time Optimization by Extremum-Seeking Control* Wiley-Interscience, 2003.

[68] L. Xiao, L. Yaoyu, and J. E. Seem, "Maximum Power Point Tracking for Photovoltaic System Using Adaptive Extremum Seeking Control," *Control Systems Technology, IEEE Transactions on,* vol. 21, pp. 2315-2322, 2013.

[69] R. Leyva, C. Alonso, I. Queinnec, A. Cid-Pastor, D. Lagrange, and L. Martinez-Salamero, "MPPT of photovoltaic systems using extremum - seeking control," *IEEE Transactions on Aerospace and Electronic Systems,* vol. 42, pp. 249-258, 2006.

[70] S. L. Brunton, C. W. Rowley, S. R. Kulkarni, and C. Clarkson, "Maximum Power Point Tracking for Photovoltaic Optimization Using Ripple-Based Extremum Seeking Control," *IEEE Transactions on Power Electronics,* vol. 25, pp. 2531-2540, 2010.

[71] A. R. Reisi, M. H. Moradi, and S. Jamasb, "Classification and comparison of maximum power point tracking techniques for photovoltaic system: A review," *Renewable and Sustainable Energy Reviews,* vol. 19, pp. 433-443, 2013.

[72] B. Subudhi and R. Pradhan, "A Comparative Study on Maximum Power Point Tracking Techniques for Photovoltaic Power Systems," *IEEE Transactions on Sustainable Energy,* vol. 4, pp. 89-98, 2013.

[73] A. Dolara, R. Faranda, and S. Leva, "Energy Comparison of Seven MPPT Techniques for PV Systems," *Journal of Electromagnetic Analysis and Applications,* vol. 01, pp. 152-162, 2009.

[74] C. Liu, B. Wu, and R. Cheung, "Advanced algorithm for MPPT control of photovoltaic systems," in *Canadian Solar Buildings Conference, Montreal*, 2004, pp. 20-24.

[75] R. Ahmadi and H. Zargarzadeh, "A new discrete-in-time extremum seeking based technique for maximum power point tracking of photovoltaic systems," in *Applied Power Electronics Conference and Exposition (APEC), 2015 IEEE*, 2015, pp. 1751-1756.

[76] S. Bayhan, H. Abu-Rub, and R. S. Balog, "Model predictive control of quasi-z-source four-leg inverter," *IEEE Transactions on Industrial Electronics,* vol. 63, pp. 4506-4516, 2016.

[77] S. Bayhan, M. Trabelsi, H. Abu-Rub, and M. Malinowski, "Finite-control-set model-predictive control for a quasi-Z-source four-leg inverter under unbalanced load condition," *IEEE Transactions on Industrial Electronics,* vol. 64, pp. 2560-2569, 2017.

[78] B. Ge, Y. Liu, H. Abu-Rub, R. S. Balog, F. Z. Peng, S. McConnell*, et al.*, "Current Ripple Damping Control to Minimize Impedance Network for Single-Phase Quasi-Z Source Inverter System," *IEEE Transactions on Industrial Informatics,* vol. 12, pp. 1043-1054, 2016.

[79] B. Olek and M. Wierzbowski, "Local energy balancing and ancillary services in low-voltage networks with distributed generation, energy storage, and active loads," *IEEE Transactions on Industrial Electronics,* vol. 62, pp. 2499-2508, 2015.

[80] M. A. G. de Brito, L. Galotto, L. P. Sampaio, G. de Azevedo e Melo, and C. A. Canesin, "Evaluation of the Main MPPT Techniques for Photovoltaic Applications," *Industrial Electronics, IEEE Transactions on,* vol. 60, pp. 1156-1167, 2013.

[81] C. Jain and B. Singh, "An Adjustable DC Link Voltage-Based Control of Multifunctional Grid Interfaced Solar PV System," *IEEE Journal of Emerging and Selected Topics in Power Electronics,* vol. 5, pp. 651-660, 2017.

[82] S. Miaosen, A. Joseph, W. Jin, F. Z. Peng, and D. J. Adams, "Comparison of Traditional Inverters and Z -Source Inverter for Fuel Cell Vehicles," *IEEE Transactions on Power Electronics,* vol. 22, pp. 1453-1463, 2007.

[83] M. S. Diab, A. A. Elserougi, A. M. Massoud, A. S. Abdel-Khalik, and S. Ahmed, "A Pulsewidth Modulation Technique for High-Voltage Gain Operation of Three-Phase Z-Source Inverters," *IEEE Journal of Emerging and Selected Topics in Power Electronics,* vol. 4, pp. 521-533, 2016.

[84] P. Fang Zheng, "Z-source inverter," *IEEE Transactions on Industry Applications, ,* vol. 39, pp. 504-510, 2003.

[85] A. Battiston, J.-P. Martin, E.-H. Miliani, B. Nahid-Mobarakeh, S. Pierfederici, and F. Meibody-Tabar, "Comparison criteria for electric traction system using Z-source/quasi Z-source inverter and conventional architectures," *IEEE Journal of Emerging and Selected Topics in Power Electronics,* vol. 2, pp. 467-476, 2014.

[86] H. Liu, Y. Ji, and P. Wheeler, "Coupled-inductor L-source inverter," *IEEE Journal of Emerging and Selected Topics in Power Electronics,* 2017.

[87] S. Jain, S. P. Nanduri, M. B. Shadmand, R. S. Balog, and H. Abu-Rub, "Direct decoupled active and reactive predictive power control of grid-tied quasi-Z-source inverter for photovoltaic applications," in *IEEE Energy Conversion Congress and Exposition (ECCE),*, 2017, pp. 4582-4588.

[88] Y. Liu, W. Liang, B. Ge, H. Abu-Rub, and N. Nie, "Quasi-Z-Source Three-to-Single-Phase Matrix Converter and Ripple Power Compensation Based on Model Predictive Control," *IEEE Transactions on Industrial Electronics,* 2017.

[89] J. Rodriguez, M. P. Kazmierkowski, J. R. Espinoza, P. Zanchetta, H. Abu-Rub, H. A. Young*, et al.*, "State of the Art of Finite Control Set Model Predictive Control in Power Electronics," *IEEE Transactions on Industrial Informatics,* vol. 9, pp. 1003-1016, 2013.

[90] S. Sajadian and R. Ahmadi, "Model Predictive-Based Maximum Power Point Tracking for Grid-Tied Photovoltaic Applications Using a Z-Source Inverter," *IEEE Transactions on Power Electronics,* vol. 31, pp. 7611-7620, 2016.

[91] M. B. Shadmand, R. S. Balog, and H. Abu-Rub, "Model Predictive Control of PV Sources in a Smart DC Distribution System: Maximum Power Point Tracking and Droop Control," *IEEE Transactions on Energy Conversion,* vol. 29, pp. 913-921, 2014.

[92] T. Esram and P. L. Chapman, "Comparison of Photovoltaic Array Maximum Power Point Tracking Techniques," *IEEE Transactions on Energy Conversion,* vol. 22, pp. 439-449, 2007.

[93] J. Kivimäki, S. Kolesnik, M. Sitbon, T. Suntio, and A. Kuperman, "Revisited Perturbation Frequency Design Guideline for Direct Fixed-Step Maximum Power Point Tracking Algorithms," *IEEE Transactions on Industrial Electronics,* vol. 64, pp. 4601-4609, 2017.

[94] M. A. Elgendy, B. Zahawi, and D. J. Atkinson, "Operating Characteristics of the P&O Algorithm at High Perturbation Frequencies for Standalone PV Systems," *Energy Conversion, IEEE Transactions on,* vol. 30, pp. 189-198, 2015.

[95] S. B. Kjaer, "Evaluation of the "Hill Climbing" and the "Incremental Conductance" Maximum Power Point Trackers for Photovoltaic Power Systems," *Energy Conversion, IEEE Transactions on,* vol. 27, pp. 922-929, 2012.

[96] M. Metry, M. B. Shadmand, R. S. Balog, and H. Abu-Rub, "MPPT of Photovoltaic Systems Using Sensorless Current-Based Model Predictive Control," *IEEE Transactions on Industry Applications,* vol. 53, pp. 1157-1167, 2017.

[97] W.-M. Lin, C.-M. Hong, and C.-H. Chen, "Neural-network-based MPPT control of a stand-alone hybrid power generation system," *IEEE transactions on power electronics,* vol. 26, pp. 3571-3581, 2011.

[98] L. M. Elobaid, A. K. Abdelsalam, and E. E. Zakzouk, "Artificial neural network-based photovoltaic maximum power point tracking techniques: a survey," *IET Renewable Power Generation,* vol. 9, pp. 1043-1063, 2015.

[99] R. Leyva, C. Alonso, I. Queinnec, A. Cid-Pastor, D. Lagrange, and L. Martinez-Salamero, "MPPT of photovoltaic systems using extremum - seeking control," *Aerospace and Electronic Systems, IEEE Transactions on,* vol. 42, pp. 249-258, 2006.

[100] S. L. Brunton, C. W. Rowley, S. R. Kulkarni, and C. Clarkson, "Maximum Power Point Tracking for Photovoltaic Optimization Using Ripple-Based Extremum Seeking Control," *Power Electronics, IEEE Transactions on,* vol. 25, pp. 2531-2540, 2010.

[101] L. Zhang, W. G. Hurley, and W. H. Wölfle, "A new approach to achieve maximum power point tracking for PV system with a variable inductor," *IEEE Transactions on Power Electronics,* vol. 26, pp. 1031-1037, 2011.

[102] J. Yang, D. Yu, H. Cheng, X. Zan, and H. Wen, "Dual-coupled inductors-based high step-up DC/DC converter without input electrolytic capacitor for PV application," *IET Power Electronics,* vol. 10, pp. 646-656, 2016.

[103] B. Ge, H. Abu-Rub, Y. Liu, and R. S. Balog, "Minimized quasi-Z source network for single-phase inverter," in *Applied Power Electronics Conference and Exposition (APEC), 2015 IEEE*, 2015, pp. 806-811.